


This item was submitted to Loughborough University as an MPhil thesis by the author and is made available in the Institutional Repository (<https://dspace.lboro.ac.uk/>) under the following Creative Commons Licence conditions.




creative
commons
C O M M O N S D E E D


Attribution-NonCommercial-NoDerivs 2.5


You are free:

- to copy, distribute, display, and perform the work

Under the following conditions:

 **BY:** **Attribution.** You must attribute the work in the manner specified by the author or licensor.


 **Noncommercial.** You may not use this work for commercial purposes.

 **No Derivative Works.** You may not alter, transform, or build upon this work.

- For any reuse or distribution, you must make clear to others the license terms of this work.
- Any of these conditions can be waived if you get permission from the copyright holder.

Your fair use and other rights are in no way affected by the above.

This is a human-readable summary of the [Legal Code \(the full license\)](#).

[Disclaimer](#) 

For the full text of this licence, please go to:
<http://creativecommons.org/licenses/by-nc-nd/2.5/>

**LOUGHBOROUGH
UNIVERSITY OF TECHNOLOGY
LIBRARY**

AUTHOR/FILING TITLE	
NASHAN, Y	
ACCESSION/COPY NO.	
102473/02	
VOL. NO.	CLASS MARK
	<p>LOAN COPY</p> <p>- 3 JUL 1987</p> <p>- 1 JUL 1988</p> <p>- 6 JUL 1989 30 JUN 1989</p> <p>- 6 JUL 1990</p> <p>- 2 JUL 1993</p>
	<p>- 1 JUL 1994</p> <p>17 MAR 1995</p> <p>25 JUN 1999</p>

019 2473 02



PULSED GAS LASER

by

YAREB NABHAN B.Sc., M.Sc.

A MASTER OF PHILOSOPHY THESIS

Submitted in partial fulfillment of
the requirements for the award of M.Phil.
of the Loughborough University of Technology, 1981

Supervisor: Dr. D.C. Emmony

Department of Physics

© by Y. Nabham, 1981.

↑
?

Loughborough University of Technology Library	
Date	May 82
Class	
Acc. No.	192473/02

TO MY
Mother

ABSTRACT

A review of pulsed laser discharge systems based on CO_2 , N_2 and excimer gas mixtures is given. The design of a double discharge self-preionized TE laser system is described.

Two pulsed laser systems were operated at atmospheric pressure using the same design, a carbon dioxide laser giving an output at 10.6 μm , and a nitrogen laser giving an output in the ultraviolet region of the spectrum (337nm).

Several parameters which affect the output energy of the laser were investigated. The effect of varying the peaking capacitors across the discharge electrodes was studied and results showed that a maximum output energy (1.45J) was obtained at 17nF corresponding to a ratio peaking to main capacitance of 0.3 in a good agreement with other workers. The effect of preionizer arc length on the output energy was also investigated and a maximum energy of 1.5J for a preionizer gap of 6mm was achieved. The effect of gas flow and mixture composition was investigated. The laser pulse width was also measured as a function of gas parameters. The same excitation circuit was used to operate the laser with N_2 gas and the output energy studied for different operating conditions of flow rate and mirror configuration.

The N_2 laser energy output was 2.8mJ at 40cc/min N_2 flow rate with a two mirror cavity. A reduction of 60% was observed when the laser was operated with only one mirror.

ACKNOWLEDGEMENTS

I am greatly indebted to my supervisor, Dr. D.C. Emmony, for his encouragement, his kind advice and many helpful suggestions during the experimental work and discussion during the preparation of the thesis.

I am grateful to the Syrian Government for the grant that made the work possible. I would also like to thank the work shop staff for their help and in particular to M.F. Hartley, for the help in constructing the system.

CONTENTS:

	<u>Page:</u>
Title Page	i
Abstract	ii
Acknowledgements	iii
Contents	iv
Symbols used	v
<u>CHAPTER 1:</u>	1
1.1 Introduction	4
1.2 The present work	4
1.3 Thesis structure	4
<u>CHAPTER 2:</u> CARBON DIOXIDE LASER	6
2.1 Introduction and the initial discovery	6
2.2 Industrial application of CO ₂ laser	10
2.3 Vibrational energy levels of CO ₂	17
2.3.1 Rotational energy levels of CO ₂	21
2.3.2 Vibrational energy levels of N ₂	23
2.4 Excitation mechanism of the CO ₂ laser	24
2.4.1 Direct electron impact excitation	24
2.4.2 Excitation by resonant energy transfer	27
2.5 Relaxation mechanisms of the CO ₂ laser	27
2.6 CO ₂ laser requirements	29
2.7 CO ₂ laser cavity	30
2.7.1 Mode configurations	30
2.7.2 Optical resonance and the resonant stability	39

	<u>Page:</u>	
2.8	Review of the published work on TEA CO ₂ laser	43
2.8.1	Background and original	43
2.8.2	TEA laser electrode configuration	46
2.9	Conclusion to the Chapter	53
<u>CHAPTER 3:</u>	NITROGEN LASER	
3.1	Introduction	54
3.2	Nitrogen molecule spectra	55
3.2.1	Band system of nitrogen	55
3.2.1.1	The first positive system	55
3.2.1.2	The second positive system	58
3.2.1.3	The fourth positive system	62
3.2.1.4	Vigard-Kaplan Bands	62
3.2.1.5	The fifth positive system	62
3.2.1.6	Herman Kaplan system	62
3.3	Population inversion requirements in the N ₂ laser	63
3.4	Excitation criterion circuits	64
3.5	Practical electrodes configurations	69
3.6	Review of published work on N ₂ lasers	71
3.6.1	Nitrogen low pressure triplet systems	71
3.6.2	Nitrogen high pressure laser (TEA)	78
3.7	Summary	81
<u>CHAPTER 4:</u>	RARE GAS HALIDE EXCIMER LASERS	
4.1	Introduction and background	83
4.2	Rare gas halides spectroscopy	86
4.3	Rare gas halide kinetic reactions	91
4.4	Excimer quenching processors	91

		95
4.5	Excitation schemes	95
4.5.1	Electron-beam excitation	100
4.5.2	Discharge pumped rare gas halide excimer lasers	100
4.5.2.1	Electron-beam sustained/stabilized discharge lasers	110
4.5.2.2	Avalanche discharge	104
4.6	Summary	

CHAPTER 5: THE LASER CONSTRUCTION

		108
5.1	Introduction	108
5.2	The operating requirements	108
5.2.1	Spark gap design	110
5.2.2	Trigger circuit unit	110
5.2.3	The operating test of the spark gap	115
5.2.4	The laser chamber	115
5.2.5	The preionizer electrode	115
5.2.6	The saw blade holder	116
5.2.7	The main discharge electrodes	116
5.2.8	The storage and the peaking capacitor	119
5.2.9	The power supply	119
5.2.10	The operating principle of the electrical discharge circuit	120
5.2.11	The mirror mounting construction	120
5.3	The preliminary test of the discharge uniformity	122
5.4	The modification of the discharge circuit	123
5.5	The gas flow system and observation of the discharge uniformity	127
5.6	Conclusion to the Chapter	

<u>CHAPTER 6:</u>	THE OPERATION AND RESULTS OF THE LASER SYSTEM	130
6.1	Introduction	130
6.2	Single pulse measurements	132
6.3	The TEA CO ₂ (flow rate) laser results	132
6.3.1	Gas flow rate effect	137
6.3.2	Peaking capacitors effect	138
6.3.3	The preionizer arc length effect	138
6.3.4	Electrodes separation effect	143
6.3.5	The effect of the main storage capacitor on the output energy	143
6.3.6	The charging voltage effect	143
6.4	Pulse shape measurement	146
6.5	The N ₂ laser	146
6.5.1	Variations of the output energy with N ₂ flow rate and input energy	150
6.5.2	N ₂ pulse shape measurements	150
6.6	Rare gas halide excimer laser	154
6.7	Summary of the results	
<u>CHAPTER 7:</u>	THE COMPUTATION MODELLING OF THE ELECTRICAL DISCHARGE CIRCUIT OF THE LASER SYSTEM	155
<u>CHAPTER 8:</u>	CONCLUSIONS AND RECOMMENDATIONS	170
	Appendix (I)	172
	References	174

LIST OF FIGURES

	<u>Page:</u>
<u>Chapter 2</u>	
2.1 Reaction of metals and non-metals to CO ₂ laser energy (after Allen 1979).	13
2.2 Vibrational modes of carbon-dioxide molecule.	18
2.3 Vibrational energy levels of the CO ₂ , N ₂ molecules and laser transitions.	20
2.4 Details of rotational substructure of CO ₂ vibrational levels (after Ready 1978).	22
2.5 Gain distribution in CO ₂ as a function of wavelength and the quantum number J of the lower rotational level L (from Oppenheim 1968).	22
2.6 Fractional electron power transfer to CO ₂ and N ₂ in a (1% CO ₂ , 1% N ₂ , 8% He) gas mixture, (after Nighan 1974).	26
2.7 Typical mode configurations of a gas laser oscillator (after Kogehnic and Li 1966).	35
2.8 Some laser resonator geometries (after Ready 1978).	40
2.9 Stability diagram. Unstable resonators lie in shaded region (Kogehnic 1966).	42
2.10 Original TEA CO ₂ laser configuration (after Beaulieu 1970).	44
2.11 (a) Resistively stabilised pin rod electrodes (after Fortin 1971).	47
(b) Capacitively stabilised pin rod electrodes (after Johnson 1971).	47

2.11	(c)	Multiple pin two dimensional cathode (after Robinson 1971).	49
	(d)	Helical pin to pin electrodes (after Fortin et al 1971).	49
2.12	(a)	Double discharge electrode config- uration with parallel blade cathode (Dumanchin et al 1969).	50
	(b)	Double discharge electrode config- uration with mesh cathode (after Laflamme 1970).	50
	(c)	Double discharge electrode config- uration with Rogouski profile electrodes (after Pearson et al 1972).	52
	(d)	UV preionised double discharge electrode configuration with pin mesh cathode (after Richardson et al 1973).	52

Chapter 3

3.1		Energy level diagram and electronic transition of the N_2 molecule.	56
3.2		Potential energy diagram of N_2 molecule (after Young 1964).	57
3.3		Simple energy level to explain spontaneous and stimulated transitions.	64
3.4	(a)	Capacitor discharge type.	68
	(b)	Blumlein circuit discharge type.	
3.5	(a)	Channelized discharge	68
	(b)	Unchannelized discharge	70
3.6		Nitrogen energy levels diagram with the laser transitions.	73

		<u>Page:</u>
3.7	(a) Schematic of apparatus in which the electric field is perpendicular to the stimulated emission (after Leonard 1965).	75
	(b) Coaxial transmission line nitrogen laser (after Geller 1960).	75
	(c) Schematic of the Blumlein generator with flat plate transmission (after Shipman 1967).	77
	(d) The modified Blumlein excitation method in which the discharge is pressure confined and does not touch the vacuum enclosure (after Small et al 1972).	77
	(e) Perspective view and partial cross section of the laser (after Basting et al 1972).	79
3.8	Blumlein type discharge TEA N ₂ laser (after Bergmann 1976).	80

Chapter 4

4.1	Basic molecular structure for abouund-free excimer.	83
4.2	Potential energy diagram of rare gas halide molecule showing laser and self-absorption transitions (after Brau 1978).	87
4.3	(a) Electron-beam pumping excitation method (after Burnham 1979).	97
	(b) Schematic diagram of a transverse e-beam pumping geometry (after Brau 1978).	97

4.4	(a) Schematic diagram of a laser pumped by an electron beam stabilized discharge.	102
	(b) Schematic diagram of a laser pumped by a transverse discharge using uv radiation.	102
4.5	Some electrical circuits have been used for exciting excimer lasers.	105
4.6	The different types of preionization (after Tallman 1980).	105

Chapter 5

5.1	The spark gap used with the laser.	109
5.2	Laser trigger circuit (Thyratron).	112
5.3	A photography of the car-coil pulse voltage output.	113
5.4	A photography of the trigger electrode gap voltage breakdown.	114
5.5	Cross section of the original laser changer.	117
5.6	The electrode structure of the laser discharge model.	117
5.7	The electrical connections of the capacitor.	119
5.8	Cross section of the mirror mounting.	121
5.9	The system after modification.	124
5.10	A photograph of the laser.	125
5.11	Gas flow system.	126
5.12	A photograph of the CO ₂ laser discharge.	128
5.13	A photograph of the N ₂ laser discharge.	129

Chapter 6

6.1	Single pulse energy measurement arrangement.	131
6.2	Gas flow rates effect on the output energy.	133
6.3	Peaking capacitors effect on the output energy.	139
6.4	The preionizer arc length effect on the output energy.	140
6.5	A photograph of the 3 meshes which were used in the laser system.	141
6.6	Storage capacitors effect on the output energy.	144
6.7	Charging voltage effect on the output energy.	145
6.8	CO ₂ pulse shape measurement as a function of CO ₂ concentration in the mixture.	147
6.9	CO ₂ pulse shape measurement as a function of N ₂ concentration in the mixture.	147
6.10	CO ₂ pulse shape when the laser was operated without N ₂ .	148
6.11	The output energy as a function of the N ₂ flow rate.	149
6.12	The output energy as a function of stored energy.	151
6.13	N ₂ pulse shape measurement.	152

Chapter 7

		156
7.1	The discharge circuit model	
7.2	The discharge circuit model without a preionizer impedance	156
7.3	Fast and slow voltage photographs	161
7.4	Computing result of the discharge voltage	164
7.5	The fast circuit voltage as a function of peaking capacitor and inductance	165

LIST OF TABLES

	<u>Page:</u>
<u>Chapter 1</u>	
1.1 Characteristics of common gas laser	2
<u>Chapter 2</u>	
2.1 Some of commercial CO ₂ lasers suitable for materials processing.	11
2.2 Cutting rates for non-metals using CO ₂ laser with gas jet assistance (after Saleh 1981).	15
2.3 Cutting rate for metal sheets using CO ₂ laser with gas jet assistance (after Saleh 1981).	16
<u>Chapter 3</u>	
3.1 Absolute transition probabilities for bands of the N ₂ first positive system (after Nicholls 1964).	59
3.2 Absolute transition probabilities for bands of the N ₂ second positive system (after Nicholls 1964).	61
3.3 Nitrogen Triplet Systems.	72
<u>Chapter 4</u>	
4.1 Rare gas halide laser wavelength.	85
4.2 Showing the different wavelengths of each noble gas halogen lasers with respect of different halogens.	90
<u>Chapter 5</u>	
5.1 The different value of the trigger gap volt- 104 age breakdown at different N ₂ pressure.	

SYMBOLS USED

<u>Symbol:</u>	<u>Description:</u>
a_i	gas constant
A_{21}	Spontaneous emission probability from the upper laser level to the lower laser level
B_i	Rotational constant of the vibrational levels.
B	Einstein coefficient for stimulated transition
C	Velocity of light
CW	Continuous wave
d	Resonant mirrors separation
D	Spectroscopic constant of the molecule
E	Electric field
E_{ij}	Molecular energy J^{th} rotational level
f	Mode frequency
f_{21}	Oscillation strength of the transition from level 2 to level 1
F_N	Fresnel number
h	Planck's constant
I	Moment of inertia
j	Current density
J	Rotational quantum number
k	Boltzmann constant
L	Loss per pass
N	Population density of the energy used
W	Pumping rate of laser energy level
α	Absorption coefficient of a laser medium
ν	Vibrational quantum number
$\tilde{\tau}_1$	Lifetime of the lower laser levels
$\tilde{\tau}_2$	Lifetime of the upper laser levels

CHAPTER 1

INTRODUCTION

1.1 Introduction

Gas lasers are sources of coherent radiation which operate at different wavelengths in the spectral range from the ultra violet to the far infrared (Table 1.1).

The laser cavity is normally electrically excited, and comprises of a tube which contains the laser medium. Amplification occurs in a direction along the tube's axis using two mirrors, one at each end of the tube, facing each other, to form the optical resonator required for oscillation. The laser radiation at the frequency of oscillation is coupled from the resonator by making one of the mirrors partially transmitting.

Neutral atom laser transitions occur in the 1000-10000 nm in infrared region of the spectrum, with doppler width of the order of 500 MHz. Helium-Neon lasers are an example of this type, which operate in three distinct spectral ranges; in the red at 632.8nm, in the near-infrared around 1150nm, and farther in the infrared at 7390nm. It has been estimated that over 100,000 He-Ne lasers have been manufactured and sold commercially, with a lifetime of 10,000 hr, and with output powers ranging from a few tenths of mw up to 50 mw.

The neutral atom lasers have a lower laser level of approximately 0.1 ev to 1 ev, so the plasma temperature should not be higher than 500k to avoid thermal population of these levels.

Ion lasers such as Argon, Krypton, and Xenon, usually operate in the visible and near ultra violet part of the spectrum. The high values of energy of the lower laser levels (2 ev - 5 ev) enables this type of laser to be operated with high excitation intensity with a plasma temperature in the region of 3000k. The spontaneous line width is wide at these temperatures, due to

Gas Nature	Type	Wave Lengths (nm)	Mode of Operation	Pulse Width	Repetition rate p/s .	Average Power
Neutral	He-Ne	632.8	CW	-	-	0.5 - 50 mw
Ionised	Argon	514.5) 488)	CW	-	-	10 w
Ionised	Krypton	350.7 to 799.3	CW	-	-	20 w
Ionised	He-Cl	441.6) 325)	CW	-	-	6 w
Molecular	N ₂	337.1	Pulsed	0.01	to 500	up to 1 mw
Molecular	CO ₂	10600) 9600)	CW	-	-	up to 100 kw
Molecular	CO ₂	10600) 9600)	Pulsed	100	2500	up to 4 kw
Molecular	CO ₂ TEA	10600) 9600)	Pulsed	10	400	10 mw
Excimer	RGH	200 to 350	Pulsed	10	100	up to 20 w

Table 1.1 Characteristic of Common Gas Lasers

doppler and collision broadening. The argon ion laser line width is typically 3500 MHz.

Ion and neutral atom lasers are operating with electronic energy levels, molecular lasers such as CO₂ lasers usually operated with vibrational and rotational energy levels. The CO₂ lasers are operated at 10.6 μ m with a line width of the order of 100 MHz. The transitions between the vibrational-rotational levels can provide large CW or pulsed power, with relatively high efficiency (up to 30%) at these wavelengths.

The nitrogen laser is another type of molecular laser, in which the transitions occur between two vibrational levels. The N₂ lasers are operated at 337 nm wavelength of the spectrum. Due to the lower laser level being close to the ground state of the molecule, the molecular lasers are more efficient than neutral atom or ion lasers.

Another version of molecular gas lasers is the excimer laser in which the laser transition occurs between a stable bound state and unbound state which in turn is followed rapidly by dissociation of the ground state which gives an automatic population inversion. The excimer lasers are operated over a wide range of the spectrum between 170 nm - 400 nm. The rare gas halides excimer lasers are commercially available with a repetition rate of 100 pps, Table 1.1.

1.2 The Present Work

Since the discovery of the double discharge CO_2 laser in 1970, attention has been concentrated on designing the electrical circuit of the laser and efficient sources of preionization in order to achieve a good discharge and high efficiency.

The object of the present work is to apply the principles of double discharge TEA lasers to develop a laser which can operate with various gas mixtures, CO_2 , N_2 , rare gas halides. The development of the laser included the preionization technique and the study of the various parameters which affect the laser operation such as the peaking capacitors and the preionizing arc length.

1.3 The Thesis Structure

The overall structure of the thesis is as follows:

The spectroscopy of the CO_2 molecule and the theory of the CO_2 laser, with a review of the published materials which are discussed in Chapter 2. The spectroscopy of the N_2 molecule and the excitation circuits, with a review of TEA N_2 laser which are discussed in Chapter 3. The spectroscopy of rare gas halide excimer lasers, the kinetic reaction, and the excitation methods such as e-beam and avalanche discharges are discussed in Chapter 4.

The construction of the laser, the laser chamber, preionizer electrode, spark gap, trigger unit, and the preliminary test of the discharge with the modification of the electrical circuit are discussed in Chapter 5.

Investigation of the gas flow rates, the peaking capacitors, the preionization arc length, the storage capacitor effects on the output energy of CO_2 and N_2 lasers are described in Chapter 6.

The variation of pulse shape as a function of the gas flow rate is also discussed in this chapter.

A theoretical model of the electrical discharge circuit using computer programs is described in Chapter 7.

The results of the investigations and recommendation for further research are summarised in Chapter 8.

Chapter 2

CARBON DIOXIDE LASER

2.1 Introduction and the Initial Discovery

The possibility of using rotational-vibrational transitions for laser action was suggested by (Polanyi 1961). The vibrational excitation of a molecule by energy transfer from another vibrationally excited molecule was noted as enabling a fast and efficient process (Schwrat et al 1952). When CO₂ gas mixed with vibrationally excited nitrogen, strong infrared emission was observed, and interpreted as an indication of collisional transfer (Legay et al 1963).

The first laser action in pure CO₂ at 10.6 μ m was observed by (Patel 1964 a,b). Output powers of 1mw cw with dc excitation and 10mw peak with 1000 nsec excitation pulses was obtained from the 5m laser tube. This laser action was followed by the lasing from a Fabry-perot resonator full of CO₂, N₂ mixture. An output of over 1mw was observed with a 200 mm long interaction region (Patel 1964 c). Further work led to the direct excitation of the gas within a mixture of CO₂ and air, (Patel 1965). 10 w/m from a sealed tube of CO₂-He mixture has been reported (Moeller et al 1965). 50 w/m was obtained using a water cooled tube with flowing CO₂-N₂-He mixture (1965).

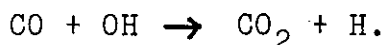
Since its discovery, various forms of CO₂ lasers have been achieved. CW powers up to 60kw, operating efficiencies approaching 30%, pulse energies of 2×10^3 J/pulse with pulse widths less than 1 ns and peak pulse powers in excess of 10^9 w, and Q-switched mode of operation at pulse repetition rate of 500s^{-1} , because lifetime of upper laser level is around one millisecond. The laser has been pumped electrically, optically, thermally, chemically and by electron-beam. The CO₂ laser is established as one of the most important among the numerous

lasers presently known. Carbon dioxide lasers can be divided into several types from their construction point of view.

- (a) Axial flow lasers
- (b) Sealed-tube lasers
- (c) Transverse flow lasers
- (d) Transversely Excited Atmospheric lasers (TEA)
- (e) Gas Dynamic Lasers
- (f) Electron-beam controlled lasers

The axial flow lasers are simply constructed and most efficient of the different types of CO₂ lasers, and more often used in industrial applications. The laser consists of a glass tube which contains the gas mixture. The advantage of the axial flow of gas through the tube is to replenish the gas molecules and to remove heat and the dissociation products in particular, CO, which would contaminate the laser. Two mirrors are located at each end of the tube to form the optical cavity.

Another type of the CO₂ laser is the sealed tube, which uses a self-contained supply of gas for the lasing medium. There is no need for a gas flow or a vacuum pump during operation. The major problem involved in the operation of sealed CO₂ lasers is to provide a chemical reaction path for the products of dissociation of CO₂ (mainly CO, and O₂) to be regenerated to form CO₂. The problem can be overcome by adding a small amount of H₂O, H₂ or H₂ and O₂ to the gas mixture. These species reduce the amount of CO present in the discharge through the following reaction:



Sealed operation of several thousands of hours is now possible with output powers of around 60 w/m discharge length. Since the heat removal is effected by diffusion from the centre of the tube towards the water sealed walls as well as by gas flow through the tube in the axial flow and sealed tube lasers, there is another effective cooling method in which the gas passes perpendicularly to the optical axis. Several different configurations have been developed to provide fast transverse flow of the gas mixture. Powers of 27 kw with 17% efficiency are now possible with transverse discharge CO₂ laser. It is not easy to achieve operation at gas pressures above 7-13 kpa (50-100 torr) in axial discharge lasers, since an increase in pressure requires a corresponding increase in the discharge breakdown voltage. But this problem can be avoided by using a discharge perpendicular to the optical axis and it has been used at atmospheric pressures (TEA). This simple and inexpensive technique has made possible to assemble multimegawatt pulsed CO₂ gas lasers. Various configurations of TEA CO₂ lasers have been used. (Section 2.8). Excitation in the gas dynamic CO₂ laser is not produced by an electrical discharge, but by rapid expansion of a gas medium through a nozzle. The gas is heated to high temperature and pressure and allowed to expand through a supersonic nozzle. During the expansion, the gas turned into a laser medium (i.e. a population inversion is created), and then passes into the laser cavity where, if mirrors are placed on each side of the cavity, the laser radiation can be coupled perpendicularly to the gas flow. The gas flow is then choked down to subsonic speeds and exhausted. Such CO₂ lasers have the capability of continuous operation at levels up to 100kw. These power

levels far exceed those of other continuous gas lasers. One pulsed gas dynamic laser has been described (Christiansen 1973) produced 450kw for a period up to 4 m sec of multimode CO₂ laser.

Another version of CO₂ laser is the electron-beam controlled CO₂ lasers in which the discharge uses a high energy (100-200 kev) electron-beam to ionize the gas. A field across the gap accelerates the resulting electrons and provides electrical excitation of the laser molecules. The discharge is non-self-sustaining without the electron beam. One such system used injection of a 130 kev electron-beam into 110 litres of CO₂, He, N₂ gas mixture at 1 atm pressure, produces TEM₀₀ output plus up to 1200J/pulse (a peak power of 50Mw in a pulse of 50000 nsec duration) and multimode outputs of up to 2000J/pulse. (Ready 1978).

2.2 Industrial Applications of CO₂ Laser

Carbon dioxide lasers are of interest because they give a higher CW or pulsed output power and higher efficiency (wall-plug, 10 - 30%) than any other lasers. The CO₂ lasers have been developed from laboratory instrument to a rugged industrial tool. They have been used widely in materials processing (metal and non metallic), medical, surgical treatments, metrology and holography. The repetitively pulsed TEA CO₂ lasers with 100 pulse/second and capable of producing a typical output energy of 1J/pulse, and pulse durations with range of 10 - 100 μs. CW CO₂ lasers are capable of generating several kilowatts in the far infrared (at 10600 nm). Table 2.1 shows some of the commercial CO₂ lasers for materials processing. At this wavelength, many different materials including ceramic, glass, plastic, most metal oxides and dielectric materials have high absorption at the wavelength of 10600 nm.

High power lasers have been used in both conduction limited, and deep penetration weldings. The repetitively pulsed TEA CO₂, and CW CO₂ lasers (with few hundreds of watts) have been used for conduction limited welding where the depth of the zone is limited by the thermal conduction (Harry, 1974). The energy from CW and TEA CO₂ lasers is absorbed at the surface of the workpieces and the penetration of laser energy is absorbed into the sample (after reaching the boiling point) by thermal conduction. The weld depth in this case is small. But the use of multikilowatt CW CO₂ allows welding with much deeper penetration. Such lasers can produce narrow, deep welds much like electron beam welds (Ready, 1978), without the need of a vacuum or magnetic chuck. Since the laser beam can be transmitted through the atmosphere without attenuation, the use of a mirror can deflect the beam close to the desired area, allowing

Laser	Wavelength (nm)	Type of Operation	Typical Power (W)	Pulse rep. rate (pps)	Pulse length	Typical Use
CO ₂	10600	CW	100 - several thousand	-	-	Welding
CO ₂	10600	Repetitively pulsed	100 (average)	100	100 μ s	Welding, hole drilling
CO ₂	10600	TEA	10 ⁷ -	up to 100	10 μ s	Hole drilling, marking, welding

Table 2.1: Some of Commercial CO₂ Lasers Suitable for Materials Processing.

otherwise inaccessible joints to be welded. CW CO₂ lasers have been used for deep penetration welding in which heat is transferred along the depth of the weld producing a weld bead that is deeper than it is wide (Harry, 1974).

CO₂ laser has been used to drill high quality holes by vaporisation of the materials at the focus of the beam. Since a large number of metallic and non metallic materials have a high absorption at CO₂ laser wavelength (Fig. 2.1), the CO₂ laser (CW, pulsed) have been used to drill holes in stainless steel, plastic, rubber, sapphire and ceramics. The advantage of laser drilling is the high speed and the ability to drill small holes.

Another industrial application of the CO₂ laser is cutting the materials in a number of different processes:

1. Vaporisation process, in which the material is in the path of the laser beam, and heated up to the plasma boiling point, and leaves the cut regions a vapour.
2. The use of a gas jet co-axial with the beam, in which the material is brought to the melting point by direct heating from the laser radiation, and the jet of the gas is used to blow the molten metal out of the cut region in order to produce a clean, unscratched edge cut.
3. Reactive gas is used when a high level of power is needed. Most of the energy which is needed for the cut is supplied by an exothermic chemical reaction between the metal and the gas (usually oxygen). The laser heats the material to its ignition point, then the actual cutting occurs by the interaction with oxygen. The oxygen gas also serves to blow the liquid metal away from the cut region. The oxygen jet can increase the cutting rate by approximately 40% over the rate when an inert gas is present (Ready, 1978). With multikilowatts CO₂ laser oxygen jet gas may no longer be necessary.

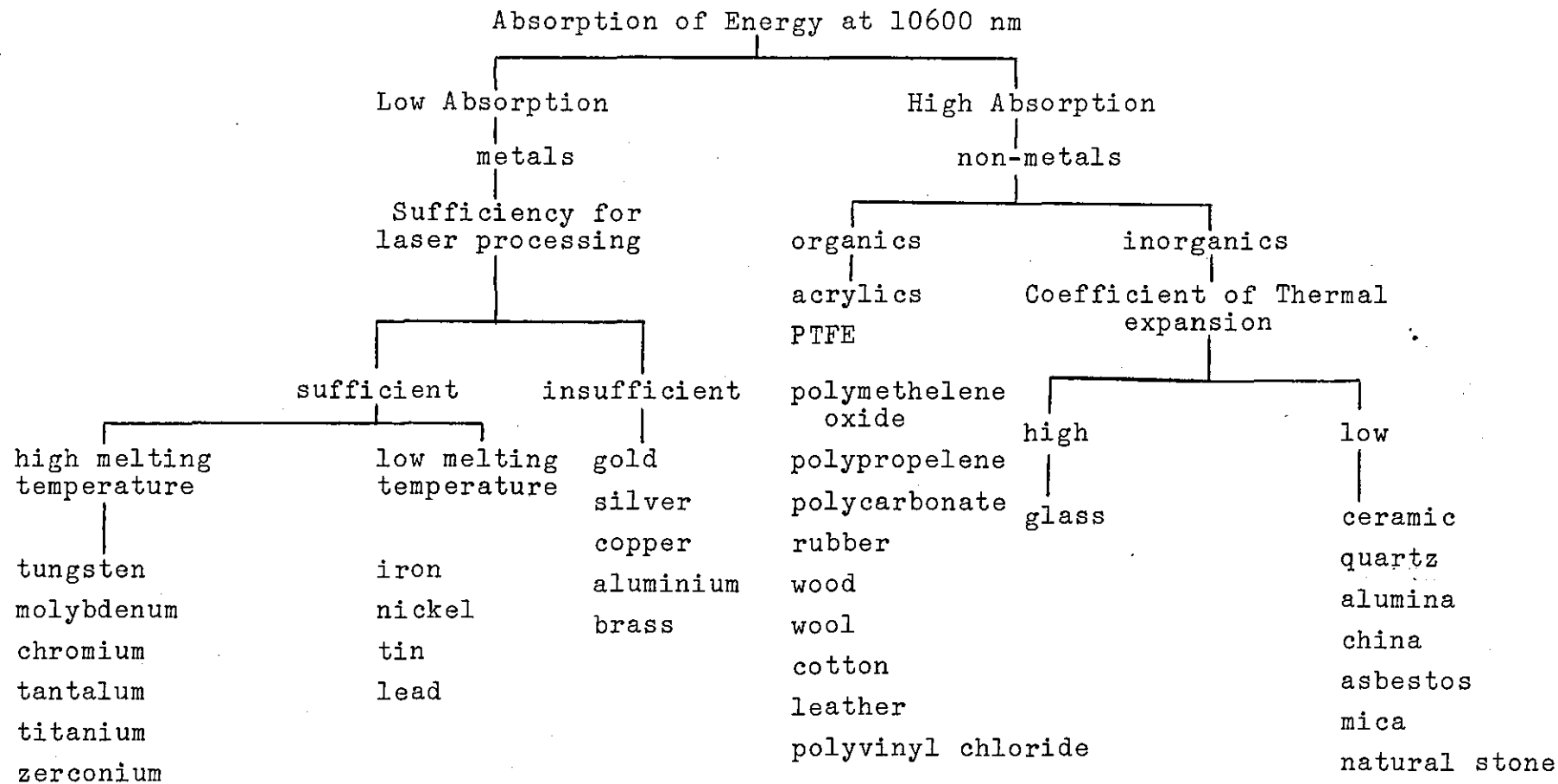


Fig. 2.1: Reaction of metals and non-metals to CO₂ laser energy (after Allan 1979).

The CO₂ laser is a suitable tool in cutting a wide range of non-metallic materials, some of these materials are shown in Table 2.2. Ceramics and glass materials can be cut by scribing (vaporisation of thin layer at the surface) followed by mechanical fracture. Only a small amount of material is removed from the top surface of the material during the scribing process. A gas jet is not essential and a pulsed output can be used. Lower power densities than those for cutting are needed and the heat affected zone is small.

Although most of the metals are normally reflective at the 10600 nm wavelength of the CO₂ laser, the cutting effectiveness of the CO₂ laser is high for metals. The second technique described above has been used with multikilowatt power for metals which do not oxidise easily, such as nickel alloys, and especially when it requires a cut edge that is square and clear of oxide formation (Locke et al, 1974). The reactive gas jet technique is useful for metals that are easy to oxidise, such as carbon steels, and titanium. Conventional techniques, such as oxyacetylene cutting, are also effective with these metals. However the advantage of CO₂ laser cutting is the accuracy and high cutting speed. Table 2.3 shows some cutting rates for different metals.

The CO₂ laser has also been used for surface heat treatment up to power level of 18 Kw in the automobile industry. The laser irradiates the surface and causes very rapid heating of a thin layer of material near the surface. When the laser beam is moved to a different area on the surface, the heat deposited in the thin layer will be quickly conducted away and the heated area will cool rapidly. The advantage of using CO₂ laser over alternative processes such as induction heating, furnaces, and salt baths, are the high degree of flexibility enabling selec-

Material	Thickness mm	Power (W)	Gas Used	Cutting rate mm/min	Reference
Asbestos compressed	6.4	180	Air	762	Harry et al 1972
Cement	6.4	335	Air	25	Harry et al 1972
Glass					
Soda lime	2	350	Air	750	Harry et al 1972
quartz	2	250	none	95	Harry et al 1972
Paper (gloss)	0.33	60	Air	40000	Harry et al 1972
Plastic (PVC)	3.2	300	Air	3600	Harry et al 1972
Acrylic	3.1	300	Air	1830	Harry et al 1972
Perspex	10	90	Air	330	Lunan et al 1969
Perspex	30	180	Air	110	Lunan et al 1969
Nylon	-	180	Air	3600	Harry et al 1972
Vinyl (36 stack)	-	330	Air	25	Harry et al 1972
Wood					
Oak	16	300	Air	279	Harry et al 1972
deal	50	200	Air	125	Harry et al 1972
plywood	4.8	350	Air	5300	Harry et al 1972
plywood	15.5	225	Air	300	Harry et al 1972
plywood	19	225	Air	280	Harry et al 1972
plywood	25.4	8000	Air	1524	Locke et al 1972
Glass	9.5	20000	Air	1524	Locke et al 1972
Concrete	50.8	8000	Air	50	Locke et al 1972
Fibreglass epoxy	12.7	20000	Air	4572	Locke et al 1972

Table 2.2: Cutting rates for non metals using CO₂ laser with gas jet assistance (after Saleh, 1981).

Material	Thickness mm	Speed mm/min	Power (W)	Gas	Reference
Mild steel	0.76	508	150	air	Stovell et al 1970
Mild steel	1.8	635	200	O ₂	Stovell et al 1970
Mild steel	2.84	889	350	O ₂	Stovell et al 1970
Stainless steel	0.3	4320	350	O ₂	Harry et al 1972
Stainless steel	3.25	299	350	O ₂	Harry et al 1972
Stainless steel	5	780	850	O ₂	Adams 1970
	12.5	225	3800	CO ₂	Banas et al 1971
Aluminium (2219) alloy	6	30	3800	CO ₂	Banas et al 1971
Titanium (pure)	0.51	1540	135	O ₂	Stovell et al 1970
Titanium	0.17	6100	240	O ₂	Harry et al 1972
Titanium alloy	5	3300	850	O ₂	Adams 1970
Titanium	25.4	5080	10000	O ₂	Locke et al 1974
Nimonic (75)	0.79	406	225	O ₂	Harry et al 1972
Steel	5	600	1200	O ₂	Ruffer et al 1972
Inconel	12.5	1270	11000	He	Locke et al 1974
Aluminium	12.5	2286	15000	None	Locke et al 1972
Carbon steel	6	2286	15000	None	Locke et al 1972

Table 2.3: Cutting rate for metal sheets using CO₂ laser with gas get assistance. (after Saleh, 1981).

tive treatment of regions which are difficult to reach by alternative methods.

The above are the most important applications of CO₂ in industry, although there are other applications such as holography, communications, information processing, etc. (Harry, 1974).

2.3 Vibrational Energy Levels of Carbon Dioxide Molecule

Carbon dioxide is a linear, symmetric, triatomic molecule. The three atoms lie in a straight line with the carbon atom in the middle O - C - O. Since it consists of three atoms, it can execute three basic internal vibrations, the so-called normal modes of vibration. These vibrations are shown schematically in Fig. 2.2, and they are as follows:

- a) The molecule is in an equilibrium position
- b) The carbon atom remains stationary and the oxygen atoms oscillate in opposite direction along the line of symmetry as illustrated by the arrows. This mode is denoted by the frequency $\frac{\nu_1}{c} = 1337 \text{ cm}^{-1}$
- c) All the atoms move in a plane perpendicular to the line of symmetry so as to produce bending with respect to the centre. This mode is denoted by the frequency $\frac{\nu_2}{c} = 667 \text{ cm}^{-1}$. This bending mode of vibration of CO₂ molecule can occur in two orthogonal planes, it is doubly degenerate (two states have the same energy).
- d) The atoms vibrate asymmetrically along the internuclear axis. This mode is referred to as the asymmetric stretching mode, and is denoted by $\frac{\nu_3}{c} = 2350 \text{ cm}^{-1}$.

The motion in each mode is a simple harmonic motion with all the atoms moving in a plane and oscillating about their equilibrium positions. The vibrational levels are designated by

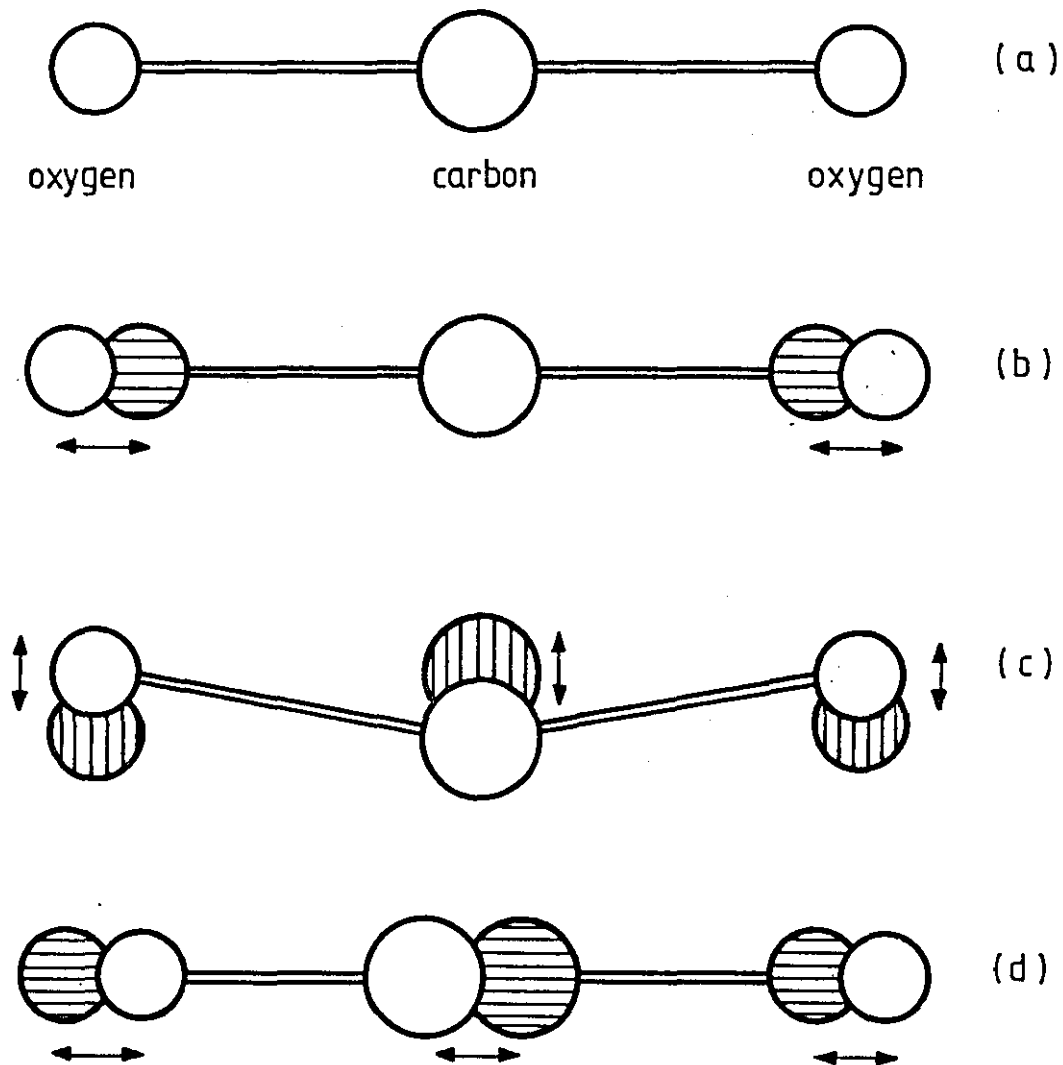


Fig. 2.2: Vibrational modes of carbon dioxide molecule.

- (a) equilibrium position
- (b) symmetric stretch mode
- (c) bending mode
- (d) asymmetric stretch mode

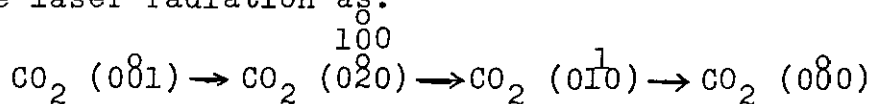
three numbers representing the number of vibrational quanta of each mode associated with the level and they are (ν_1, ν_2, ν_3) . The superscript on the bending quantum number arises because the degeneracy of the bending mode. Thus the state $(1\overset{0}{0}0)$ represents a state with one quantum of symmetric vibrational energy and no quanta in either of the other two modes. The energy associated with those vibrational modes according to quantum mechanism is quantized. Therefore the total energy of the CO_2 molecule is:

$$E(\nu_1, \nu_2, \nu_3) = h\nu_1(\nu_1 + \frac{1}{2}) + h\nu_2(\nu_2 + \frac{1}{2}) + h\nu_3(\nu_3 + \frac{1}{2}) \quad (2.1)$$

where ν_1, ν_2 , and ν_3 are the frequencies of the symmetric, bending and asymmetric modes respectively.

The CO_2 energy levels which are important for laser action are situated 2350 cm^{-1} , 1388 cm^{-1} , 1286 cm^{-1} , and 667 cm^{-1} above the ground state as shown in Fig. 2.3. These levels are designated $(0\overset{0}{0}1)$, $(1\overset{0}{0}0)$, $(0\overset{0}{2}0)$, and $(0\overset{1}{1}0)$ respectively. The transitions between $0\overset{0}{0}1$ to $0\overset{0}{0}0$, and $0\overset{1}{1}0$ to $0\overset{0}{0}1$, contain two strong bands at 4300 nm, (Hocker 1966) 15400 nm (Hartmann 1966) respectively.

The transitions between the $0\overset{0}{0}1$ to $1\overset{0}{0}0$ levels, and between $0\overset{0}{0}1$ to $0\overset{0}{2}0$ are responsible for the laser action at 10600 nm, and 9600 nm respectively. The molecule in the $0\overset{0}{0}1$ level decays to the ground state via the level $0\overset{1}{1}0$ after emitting the laser radiation as:



which behaves like the four level scheme.

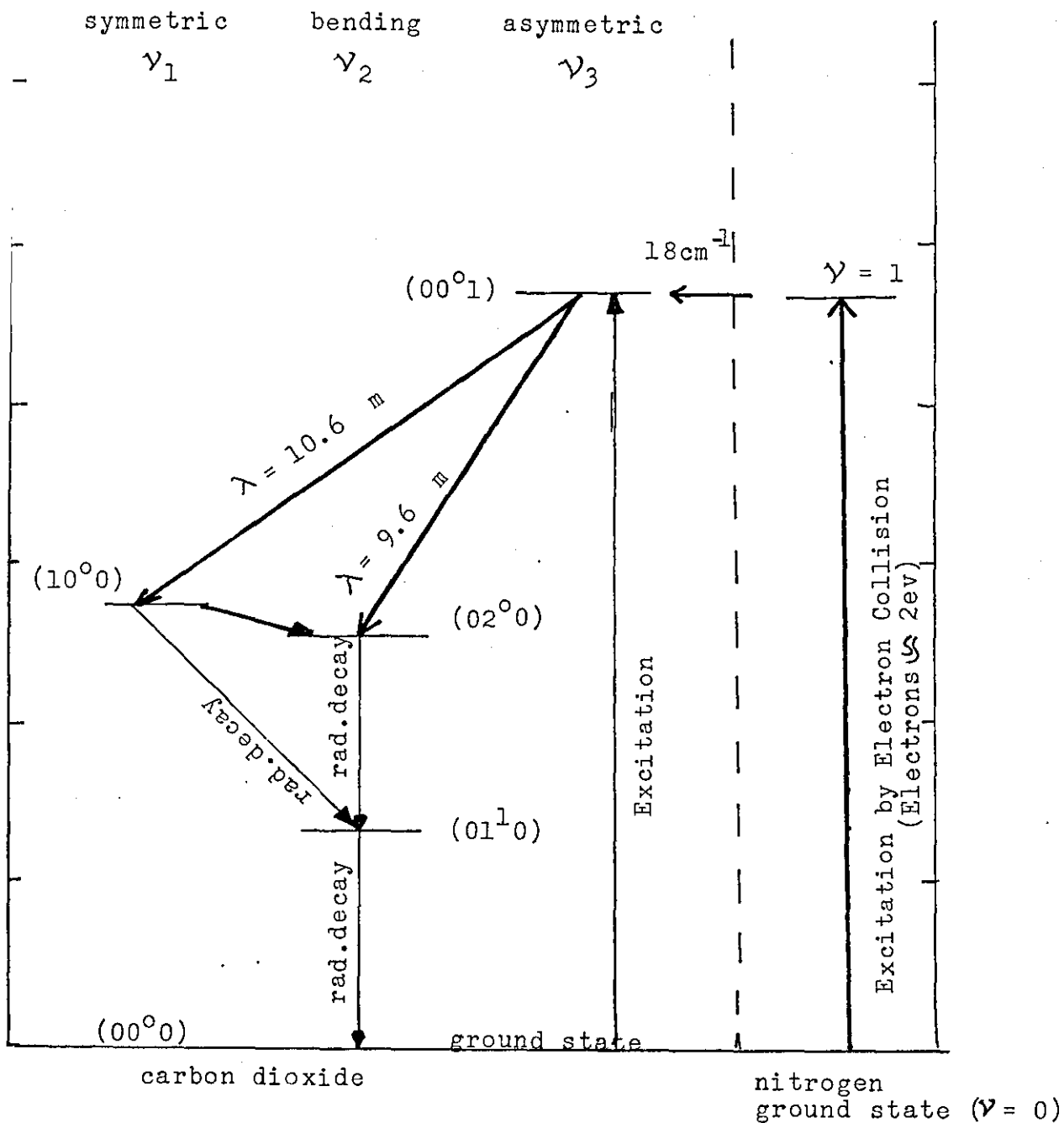


Fig. 2.3: Vibrational energy levels of the CO_2 , N_2 molecules and laser transitions.

2.3.1 Rotational energy levels of CO₂ molecule

CO₂ laser system involves transitions between states characterized not only by the vibrational quantum number ν , but by the molecular rotational quantum number J . Thus an eigenstate of the molecule has to be specified by ν_1, ν_2, ν_3 , and J , where ν_1, ν_2, ν_3 are the vibrational quantum numbers corresponding to the three degrees of freedom referred to earlier in Fig. 2.2. The rotational energies of a given vibrational level i (specified by ν_1, ν_2, ν_3) relative to the number $J = 0$ level is (Herzberg 1966):

$$E_{ij} = B_i hcJ(J+1) - DJ^2(J+1)^2 \quad (2.2)$$

where $D \ll B_i$ is a spectroscopic constant of the molecule, and B_i is the rotational constant of the i^{th} vibrational state and is equal to $\frac{h}{8\pi^2 I c}$, where h is Planck's constant, c is the light velocity and I is the moment of inertia of the molecule.

Transitions may occur between any components for which the change ΔJ in rotational quantum number J is $\Delta J = \pm 1$ corresponding to a R branch ($\Delta J = +1$), and a P branch ($\Delta J = -1$). Thus a transition $J(001) = 19$ to $J(100) = 20$ gives P(20) line of 10600 nm, and $J(001) = 19$ to $J(100) = 18$ gives R(18) line of the same transition. Fig. 2.4 shows the detail of the rotational structure.

The gain distribution for the lines in the 10600 nm transition as a function of the rotational quantum number J of the lower state is shown in Fig. 2.5. The separation of the P and R branches and the multiline nature of the emission are illustrated.

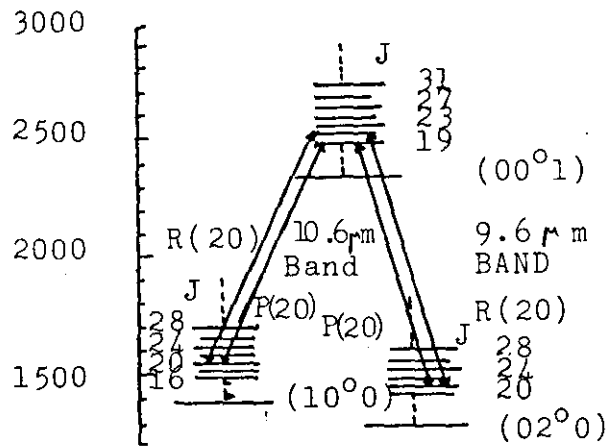


Fig. 2.4: Details of rotational substructure of CO_2 vibrational levels. (after Ready 1978).²

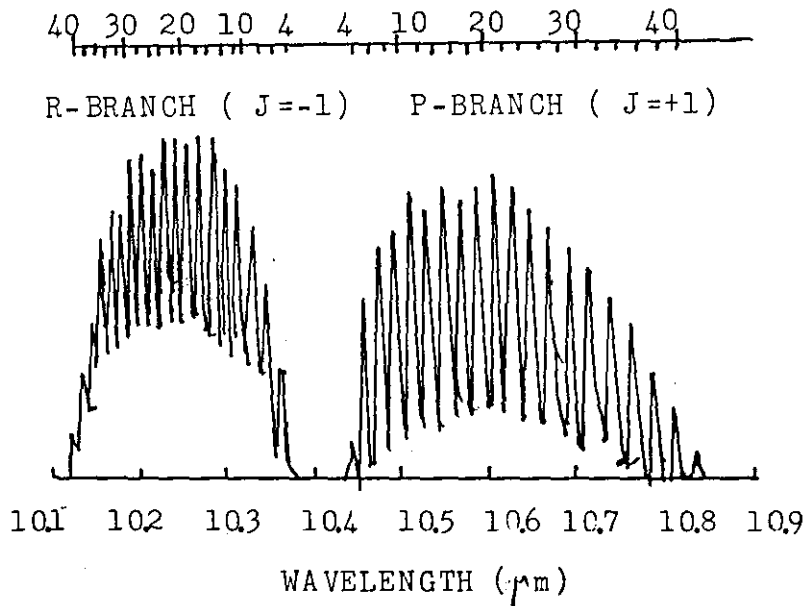


Fig. 2.5: Gain distribution in CO_2 as a function of wavelength and the quantum number J of the lower rotational level. (from Oppenheim 1968).

2.3.2 Vibrational energy levels of N₂

The nitrogen molecule has only one vibrational mode. The vibrational level of the unexcited ground state is given as $\nu = 0$. The first vibrationally excited level lies 2330 cm^{-1} above the ground state and is designated, $\nu = 1$. The second vibrational level lies at 4630 cm^{-1} with $\nu = 2$. Higher vibrational levels are denoted $\nu = 3, 4, \dots, n$. All those vibrational levels are approximately equally spaced. Since N₂ is a homonuclear molecule, it possesses zero dipole moment in the ground state. This means that the radiation rotation-vibration transitions are forbidden. The vibrational levels of N₂ molecule can be excited under gas discharge conditions by collision with electrons, and the molecule then decays to the vibrational level $\nu = 1$ which is a metastable level and can be very long lived having a lifetime of many milliseconds. Also this vibrational energy level can be turned into a translational energy by collision with other molecules, and can be transferred to other molecules having an energy level very close to the $\nu = 1$ level. Since the CO₂ molecule has the 001 level at 2350 cm^{-1} and is only 18 cm^{-1} above the level $\nu = 1$, then the N₂ molecule will transfer energy directly to the upper laser level of CO₂, which leads to an efficient laser action of the CO₂ laser, see Fig. 2.3.

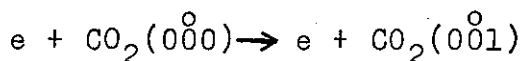
2.4 Excitation mechanisms of the CO₂ Laser

The processes which populate the 00⁰1 upper laser level are discussed in this section. The two principal pumping mechanisms are:

1. Direct Electron Impact
2. Resonant Transfer of Energy between N₂($\nu=1$) and CO₂(00⁰0).

2.4.1 Direct Electron Impact Excitation

When an electric current is passed through a gas mixture, free electrons are produced. These electrons are accelerated by the electric field and gain an additional kinetic energy which enables them to excite neutral atoms or molecules by elastic and inelastic collisions. The energy of the colliding electron in the elastic collision remains almost unaltered, and only its direction of motion will change. This means, the energy exchange rate between the electrons and the molecules is smaller in comparison with that resulting from the inelastic collisions where a large fraction of energy can be exchanged. Electrons with ≈ 5 eV energy can excite the CO₂, N₂ molecules by elastic collisions and raise them from the ground state to the excited vibrational states. The fast electrons with energy of 2 - 4 eV excite the nitrogen molecule to the level $\nu=1$, while the slower electrons (less energy ≈ 1 eV) excite it to $\nu=2, 3, 4, \dots$ etc. The collision with the electron excites the CO₂ molecule to level (00⁰1) as:



which has a large cross section of $1.5 \times 10^{-14} \text{ mm}^2$ (Nighan 1970). The collisions with electrons will populate the upper laser level (00⁰1) and not the lower laser level (01⁰0) and

($0\overset{\circ}{2}0$), because the $0\overset{\circ}{0}0 \rightarrow 0\overset{\circ}{0}1$ is an allowed optical transition, while the $0\overset{\circ}{0}0 \rightarrow 1\overset{\circ}{0}0$ transition is not permitted.

An important parameter connected to the electron impact in an electric gas discharge of CO_2 , N_2 , He is E/N ; the ratio of the electric field E to the neutral particle density N . The energy transferred from the electrons in a $\text{CO}_2 : \text{N}_2 : \text{He}$ (0.1 : 0.1 : 0.8) discharge to N_2 and CO_2 as a function of E/N and the average electron energy is shown in Fig. 2.6. (Nigham 1970).

For an E/N value of 10^{-16} v. mm^2 , approximately 45% of the electron energy goes directly into the CO_2 upper laser level ($0\overset{\circ}{0}1$), and 40% to the $\nu = 1$, vibrational levels of N_2 molecules. Thus 90% of all the electron energy goes directly into vibrational excitation levels of CO_2 ($0\overset{\circ}{0}1$) and N_2 (Demaria 1973). As E/N increases from $2 \times 10^{-16} \text{ v. mm}^2$, the average electron energy increases, and reaches $\approx 4 \text{ eV}$ at $E/N \approx 6 \times 10^{-17} \text{ v. mm}^2$ in the above mixture. Therefore the E/N range $10^{-17} - 10^{-18} \text{ v. mm}^2$ is the region in which the electron energy transfer processes change from vibrational excitation to electronic and ionization, see Fig. 2.6. A typical value of E/N in a higher pressure CO_2 pulsed discharge is in the range of $2 - 8 \times 10^{-18} \text{ v. mm}^2$, corresponding to an average electron energy of 1 eV , while in an electron beam controlled laser E/N is in the range of $1 - 2 \times 10^{-16} \text{ v. mm}^2$, corresponding to an electron average energy of $0.6 - 0.8 \text{ eV}$ (Nigham 1970).

The use of any E/N control method in the electric discharge such as e-beam, U.V radiation, and easily ionized gas additives, will lead to E/N optimization and help the CO_2 laser operation to be efficient and powerful especially when

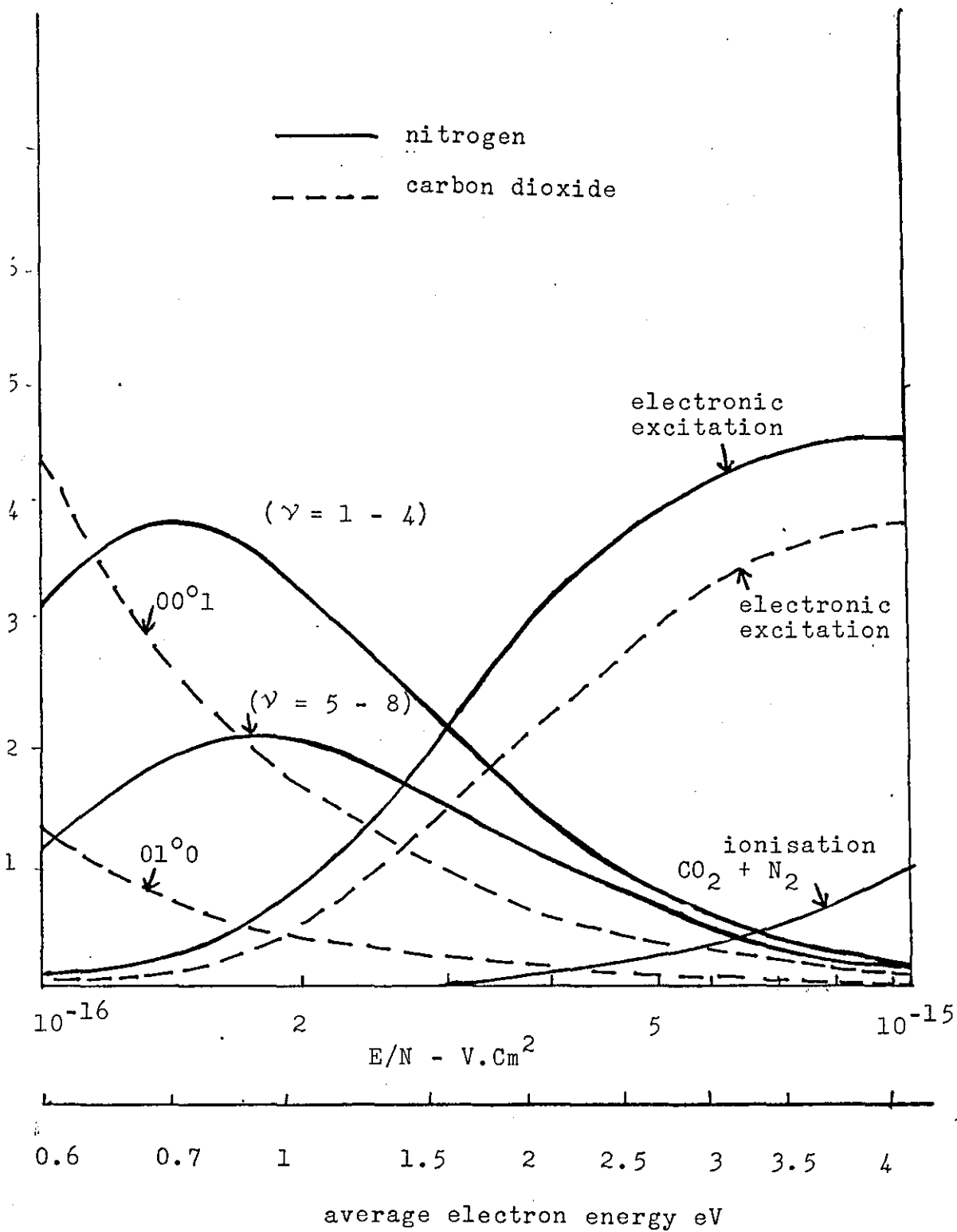
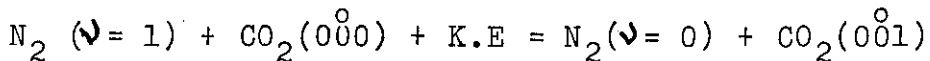


Fig. 2.6: Fractional electron power transfer to CO_2 and N_2 in a (1% CO_2 , 1% N_2 , 8% He) gas mixture, (after Nighan 1974).

it operates at higher pressures (Nighan 1970). However, U.v radiation has been used in the laser which was developed in our laboratory in order to preionize the gas before the main discharge.

2.4.2 Excitation by Resonant Energy Transfer

The transfer of energy from vibrationally excited nitrogen molecules to the ground state CO₂ molecule is the dominant excitation mechanism in the CO₂ laser. When the nitrogen molecules are excited by collision with electrons having $\approx 2\text{eV}$ of energy in the discharge, a very large fraction of them tend to collect in the level $\nu = 1$. Collision with ground state of CO₂ molecules result in transferring their excitation to the latter, thereby exciting them to the (00⁰1) level as shown in Fig. 2.3. The small discrepancy in energy ($18\text{cm}^{-1} \ll kT$) is made up by a decrease of the total kinetic energy of the molecules following the collision. This collision which can be represented by:



has a large cross section that at the pressures, and temperatures involved in the operation of the CO₂ laser, most of the N₂ molecules in the $\nu = 1$ lose their excitation energy by this process.

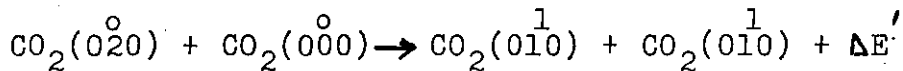
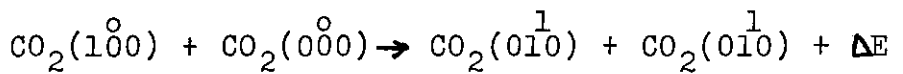
2.5 Relaxation Mechanisms of the CO₂ Laser

The relaxation mechanisms of the upper and lower laser levels are important in the laser action of the CO₂ molecule. The decay time of the upper and lower laser levels can be obtained from the gas mixture and the gas partial pressure

using the following formula:

$$\frac{1}{\tau_s} = \sum a_i P_i \quad (2.3)$$

where a_i are constants representing the gases characteristic in the discharge, and P_i are the partial pressures of the gases in the mixture. A gas mixture of 1.5 torr CO_2 , 1.5 for N_2 , 12 torr He, the lifetimes of the upper and lower laser levels are 0.4 m sec, and 20 μ s respectively (Demaria 1973). Thus the lifetime of the level $(010)^1$ is determined by the gas mixture and has a strong effect on the laser output. As mentioned before, all the transitions $100 \rightarrow 020$, and $020 \rightarrow 010^1$ are allowed, and can take place by a process involving collisions with the ground state of CO_2 molecule as:



since ΔE , and $\Delta E'$ are less than kT , therefore the levels (100) , (020) and $(010)^1$ reach thermal equilibrium in a very short time. The decay lifetime from $(010)^1$ to (000) level is important for the population inversion, and hence has a major effect on the laser efficiency. If the decay from $010^1 \rightarrow 000$ level is slow, an accumulation of CO_2 molecules can build up and hence bottlenecking is produced. This bottleneck effect will prevent the existence of population inversion between the upper and lower laser levels. Since the lifetime of the lower laser level depends on the gas mixture, therefore the use of helium gas in CO_2 , N_2 mixture is very important for the following reasons:

1. The helium gas has a large coefficient a_i (high thermal conductivity), which helps to shorten the lifetime of the (10^1) level. Therefore it helps the depopulation of CO_2 (01^0) level - (removing the bottleneck) by the reaction CO_2 $(01^0) + \text{He} \rightarrow \text{CO}_2$ $(00^0) + \text{He} + 667 \text{ cm}^{-1}$
2. The efficient relaxation of the lower laser level (10^0) by collision with helium, does not affect the population of the upper laser level (Cheo 1967, Moor et al 1961).
3. It cools the laser gases by transferring the heat to the walls.

To produce a high efficiency and high output power the radiative lifetime of the upper level of the CO_2 laser must be much greater than the lower level. Furthermore, the levels should be close to the ground level to achieve a high energy conversion efficiency. Relaxation of lower laser level molecules by collision are therefore vital to the creation of the population inversion.

2.6 CO_2 Laser Requirements

The population density of the lower state of the laser medium in a thermal equilibrium is higher than that of the upper state ($N_1 > N_2$), a Boltzmann distribution is obtained (Yariv 1963) as:

$$\frac{N_2}{N_1} = e^{-(E_2 - E_1)/kT} \quad (2.4)$$

where N_2 and N_1 are the population density (number of atoms/unit volume), of the upper and lower laser levels respectively, k is Boltzmann constant, T is the absolute temperature, and E_2 , E_1 are the energies of the states among which transition

takes place. When the laser gas medium is pumped by collisions with electrons in an electric discharge, an optical amplification, and hence an optical gain will build up at the laser transition frequency due to the net excess of stimulated emission rate together with spontaneous emission over the photons lost from the resonator.

The absorption coefficient (α) of a gas medium

$$\alpha = \frac{2\sqrt{\pi h^2}}{\Delta\nu_D} \frac{e^2}{mc} f_{21} \left(N_1 - \frac{g_1}{g_2} N_2 \right) \quad (2.5)$$

where f_{21} is the oscillator strength of transition from level 2 to level 1. g_2, g_1 are the statistical weights of levels 1 and 2 respectively. m, e are the mass, and charge of the electron. $\Delta\nu_D$ is Doppler width of the transition.

Since thermal equilibrium is not available in the gas discharge, where the laser medium provides a negative temperature, a population inversion between the upper and lower laser levels can occur, and hence a negative absorption occurs, thus for an optical gain the following condition must be satisfied:

$$\frac{g_1}{g_2} N_2 > N_1 \quad (2.6)$$

The equations which are expressed the pumping rates for the lower and upper levels in the absence of the laser action are given as follows (Lengyel 1971):

$$\begin{aligned} \dot{N}_1 &= W_{21} - N_1/\tau_1 \\ \dot{N}_2 &= W_{12} - N_2/\tau_2 \end{aligned} \quad (2.7)$$

where W_{12} , and W_{21} are the rate of the atoms pumping into the higher and lower levels respectively, and τ_2 , and τ_1 are the lifetimes of the upper and lower levels respectively.

Under steady states conditions, $\dot{N}_1 = \dot{N}_2 = 0$, therefore equations (2.7) give:

$$N_1 = W_{21} \tilde{\tau}_1$$

and

$$N_2 = W_{12} \tilde{\tau}_2 \quad (2.8)$$

Here $W_{21} = N_2 A_{21}$, where A_{21} is the spontaneous emission probability of the transition from level 2 to level 1. Thus the optical gain condition (equation 2.6) becomes:

$$W_{12} \tilde{\tau}_2 > \frac{g_2}{g_1} W_{21} \tilde{\tau}_1 \quad (2.9)$$

or

$$1 > \frac{g_2}{g_1} A_{21} \tilde{\tau}_1$$

when the lifetimes are determined by radiative transitions, we have

$$\tilde{\tau}_1 = \frac{1}{\sum_i A_{1i}} = \frac{1}{A_1} \quad (2.10)$$

and

$$\tilde{\tau}_2 = \frac{1}{\sum_j A_{2j}} = \frac{1}{A_2} \quad (2.11)$$

where the summations are extended over the states i lower than 1, and over the states j lower than 2 respectively. Therefore the condition for the optical gain becomes:

$$A_1 > \frac{g_2}{g_1} A_2 \quad (2.12)$$

which means that the spontaneous decay rate of the lower laser level should be greater than that of the upper laser level.

The above equation can be written in terms of the lifetimes as:

$$\tau_2 > \frac{g_2}{g_1} \tau_1 \quad (2.13)$$

For CO₂ laser, where $g_1 \cong g_2$ (two laser levels are almost equal, the upper laser level lifetime should be greater than that of the lower laser level to produce a laser action. The above condition explains the necessity of using helium gas in CO₂ laser.

For obtaining laser oscillation, the conditions, (2.9) and (2.13) are not sufficient. The electromagnetic wave bounces back and forth inside the cavity is damped due to the losses, such as diffraction, and reflection losses at the mirrors. The losses in the laser cavity can be expressed in term of the decay lifetime (photon lifetime) of the radiation in the cavity mode and is defined (Yariv, 1973) by:

$$\frac{dI}{dt} = - \frac{I}{t_{\text{photon}}} \quad (2.14)$$

where I is the intensity stored in the cavity mode. If the fractional loss per pass is L , and the length of the resonator is d , then the fractional loss per unit time is $\frac{cL}{d}$, therefore

$$\frac{dI}{dt} = - \frac{cL}{d} I \quad (2.15)$$

and from

$$t_{\text{photon}} = \frac{d}{cL} \quad (2.16)$$

For a large enough population inversion, the optical gain (γ) in a single pass through the medium should exceed the single pass loss, i.e.

$$\exp(-\alpha d) > \text{Loss} \quad (2.17)$$

where $\gamma = -\alpha$. By substituting α from (equation 2.5), the gain becomes related to the population inversion as follows:

$$= \frac{(2\pi \ln)^{\frac{1}{2}}}{mc \Delta\nu_D} e^{2f_{21}} (N_2 - N_1) \quad (2.18)$$

where (g_1, g_2 assumed to be equal). Thus the condition (2.17) becomes:

$$N_2 - N_1 = \frac{\text{loss}}{d} \frac{\Delta\nu_D mc}{2 \ln 2 (e^{2f_{21}})} \quad (2.19)$$

or

$$W_{12} \bar{c}_2 - W_{21} \bar{c}_1 > \frac{\text{loss}}{d} \frac{\Delta\nu_D mc}{2 \ln 2 (e^{2f_{21}})} \quad (2.20)$$

The equation (2.20) indicates the following aspects of the laser medium:

1. In addition to the requirements imposed by equations 2.13 and 2.20, the excitation rates should satisfy the the equation 2.20 too. This yields an important condition that regardless of how favourable the life-times of the laser levels may be, unless a means of selectively exciting the atoms to the upper level exists, a population inversion cannot be obtained and hence laser transition is not possible.
2. Since the threshold condition of the transition is proportional to the line width of the transition as indicated in equation (2.20) therefore for a low threshold, transitions with small line width are more suitable.
3. Optically allowed transitions are more favourable for laser action because the oscillation strength appears in the denominator.

Two important factors govern the obtaining of population in CO_2 laser medium. The first factor concerns the upper lifetime which must be larger than the lower level lifetime. The second factor involves the excitation processes to the upper laser should be selective. The fast transverse excitation method discharge was used in the CO_2 laser system operated in the work of this thesis.

2.7 CO₂ Laser Cavity

2.7.1 Modes Configurations

It is necessary to provide a strong electromagnetic field to achieve a high rate of stimulated emission from an optical gain medium. The frequency of the field must be close to the transition frequency of the gain medium. The laser provides its own field by generating a standing wave system. The S.W. system is made of two travelling waves which bounce back and forth between two mirrors, and are amplified by stimulated emission at each pass through the active medium. The output power from the laser is obtained by making one of the mirrors semi-transparent, so some of the radiation will pass out of the resonator. The spatial intensity distributions of the standing wave system are referred to as the modes of the cavity. Modes are normally described in terms of the transverse electric field distributions. The distribution of the power density in the mode may be obtained from the square of electric and magnetic fields amplitude distributions. There are many possible mode configurations in which the laser can oscillate and they are shown in Fig. 2.7. The simplest modes are the axial or longitudinal modes. These modes have the least diffraction loss, and therefore they usually oscillate at low power levels of excitation close to the oscillation threshold. At higher levels of excitation, where a sufficient gain can be achieved, other modes can oscillate too. These higher modes called transverse modes, unlike the longitudinal modes which lie along the axis, the transverse modes are inclined to the resonator axis. The axial mode which gives rise to the most important properties

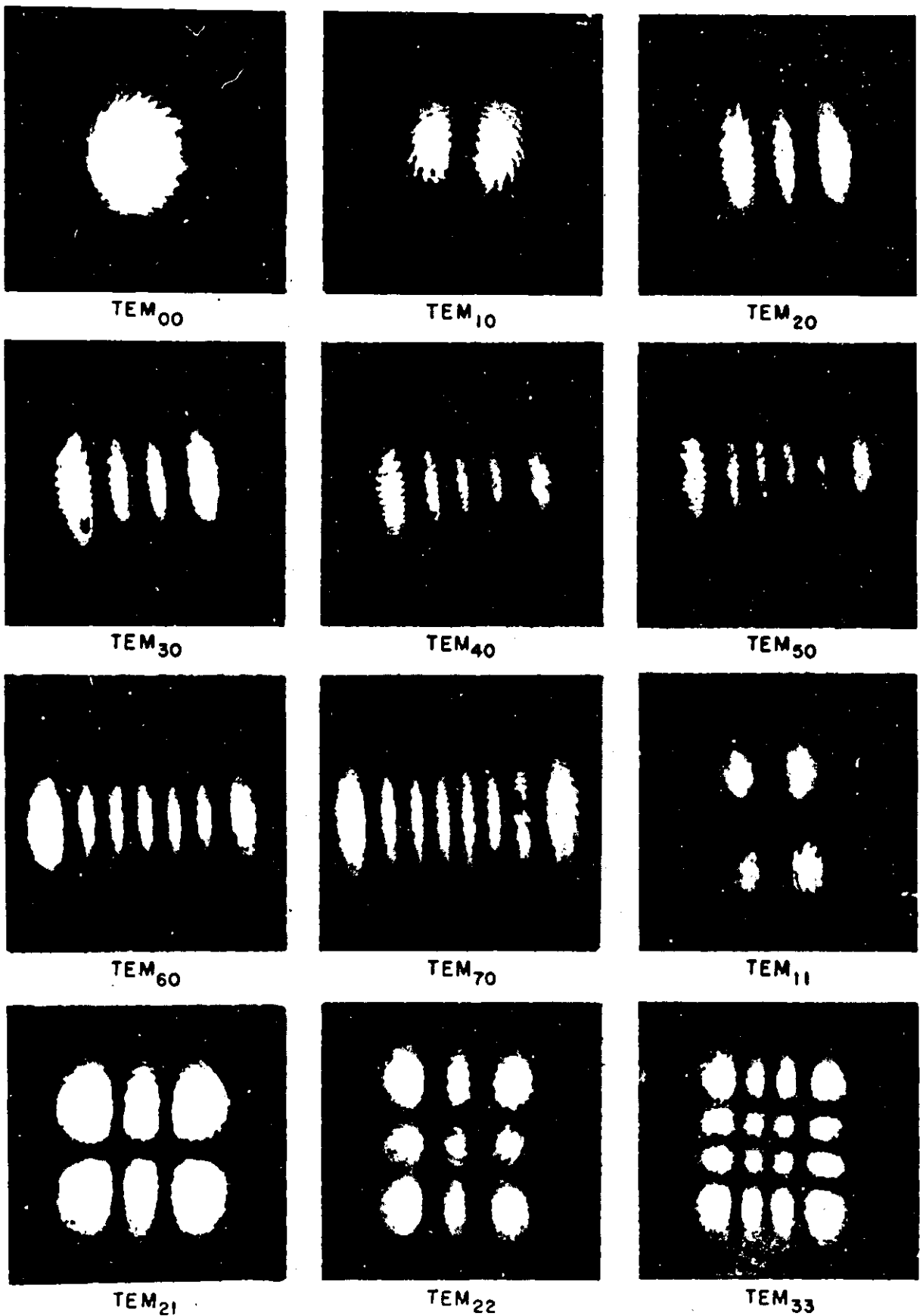


Fig. 2.7: Typical Mode Configurations of a Gas Laser Oscillator. (after Kogelnik and Li 1966)

of the laser light having the least possible divergence and the capability to be focused to a very small spot size is the TEM_{00} mode. The field and intensity distribution of the TEM_{00} mode is Gaussian (Kogelnik and Li 1966). The higher order modes have more complicated field distributions with greater divergence and are therefore less useful.

If λ is the wavelength at which the axial oscillation is required then the resonator mirror separation distance (d) must be equal to an integral number of half wavelengths (resonance condition for half round trip):

$$d = q (\lambda/2) \quad (2.21)$$

where q is an integer.

Since $f = c/\lambda$, where c is the velocity of light in the active medium, and f is the frequency of the q th mode.

The above equation can be expressed in terms of the frequency as:

$$f = q c/2d \quad (2.22)$$

Therefore different integers q will give rise to different frequencies, which constitute the axial modes of the cavity. If the q , and the $(q+1)$ axial modes are assumed, the frequency separation between successive axial modes is given by:

$$\Delta f = c/2d \quad (2.23)$$

If the gain of the laser medium is sufficiently high, then it is possible that the laser will oscillate in more than one axial mode. To select one single mode, the laser cavity can be made sufficiently short or by inserting any selective device in the resonator such as a Fabry-perot etalon.

Some lasers will oscillate at several frequencies corresponding to different transitions of the atoms or molecules of the

gain medium of the laser. If the transitions have a common level then the oscillations at different frequencies will compete with each other. By suitably tuning the resonator e.g. with a diffraction grating, the laser can usually be made to oscillate at the desired frequency.

2.7.2 Optical Resonance and the Resonant Stability

Resonators of flat and curved mirrors have been studied by (Fox, 1963, Kogelnik, 1964), because of their importance in laser applications. Various geometrical considerations such as the diameter of the mirrors, radii of the curvatures and the separation between the mirrors, determine whether the laser action can occur. Several different combinations of mirror geometries are shown in Fig. 2.8. The choice of mirror configuration depends on the stability and filling of the laser medium by the radiation. Stability means that the radiation will be re-entrant. Thus the following condition is obeyed:

$$0 \leq \left(1 - \frac{d}{R_1}\right) \left(1 - \frac{d}{R_2}\right) \leq 1 \quad (2.24)$$

where R_1 , R_2 are the radii of the mirrors, and d is their separation. Good filling of the active medium means that the spatial profile defined by the rays fills all the volume of the laser medium between the mirrors which leads to a high efficiency of the laser. The plane-parallel resonator is very susceptible to high losses due to the misalignment of the mirrors. The two mirrors must be as near to parallel as possible to decrease the diffraction losses at the mirrors edges. The plane-parallel cavity is commonly used in pulsed lasers where stability requirements are often less and where

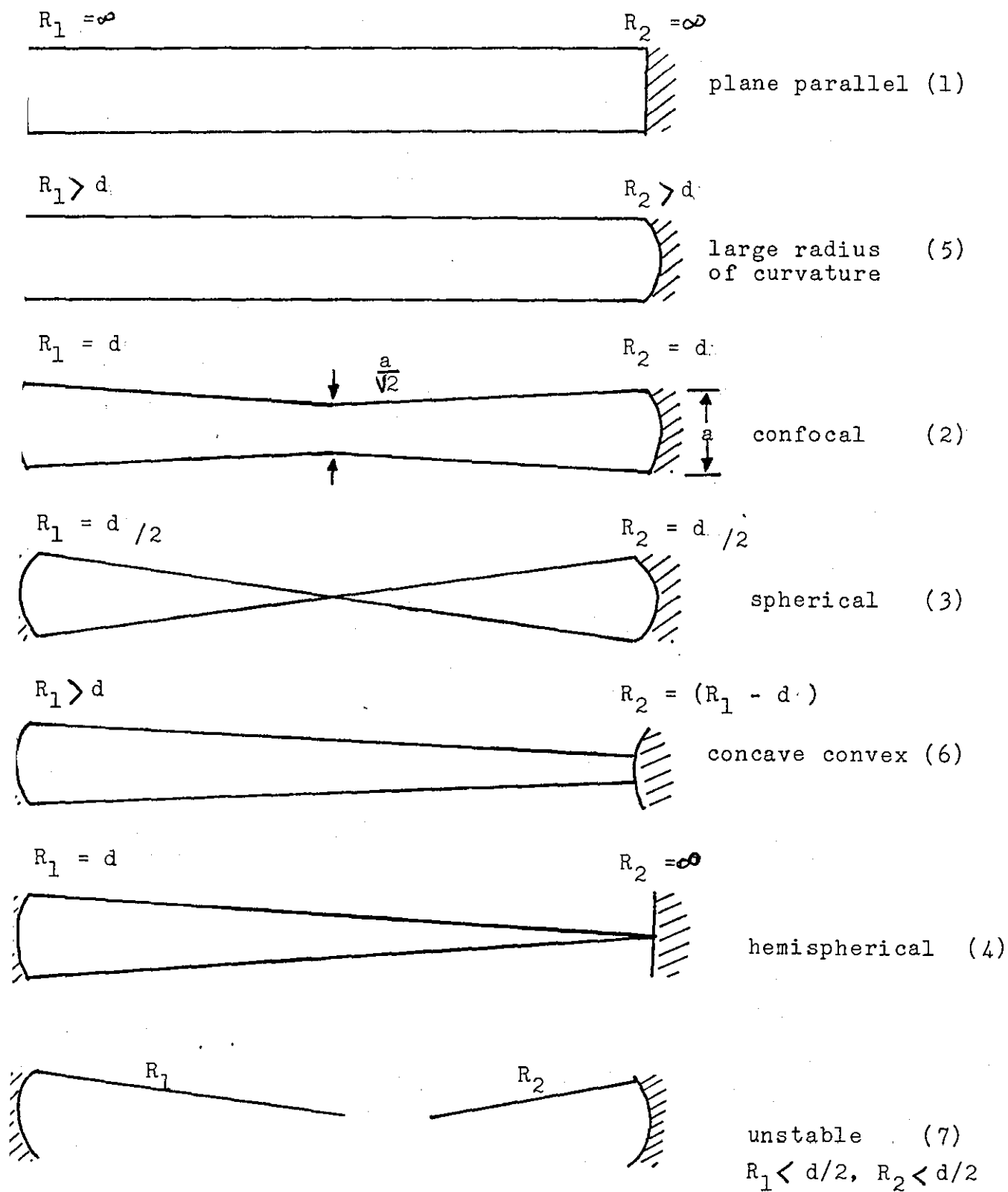


Fig. 2.8: Some laser resonator geometries (after Ready 1978).

a minimum divergence of the output is required (Ready 1978). The combination of spherical mirrors with a considerable stability and a large filling volume are efficiently used in the laser cavity, see Fig. 2.9. If the radii of both mirrors are equal to the mirrors separation ($R_1 = R_2 = d$), the resonator is said to be confocal. The confocal resonator enables a higher level of stability to be achieved at the expense of reducing the active volume in the cavity (poor filling). The hemispherical configuration ($R_1 = d, R_2 = \infty$) offers good stability, but do not fill the active medium. Lower order modes can be achieved using the hemispherical configuration where a large gain rate is not needed (Harry 1974). Spherical mirrors ($R_1 = R_2 = d/2$) have poor stability and poor filling which make it useful in the solid state lasers. The long radii geometry in which $R_1 \gg d$, and $R_2 \gg d$, has good stability and good filling, and is most often used on modern commercial lasers. Unstable resonators are used for high gain lasers, and they are useful for lasers with a Fresnel number much larger than unity. The Fresnel number is given by:

$$F_N = a^2/d \cdot \lambda \quad (2.25)$$

where a is the radius of the laser medium. If $F_N \cong 1$, the cavity is stable and a large radii geometry can be used, but if F_N is larger compared to unity, and the beam divergence is large, the unstable resonators are used. The unstable resonators (positive, negative branches) have been used where a collimated output beams is needed in CO_2 laser (Dyer 1978), and in excimer lasers KrF, XeF (Barber 1977, McKee 1977).

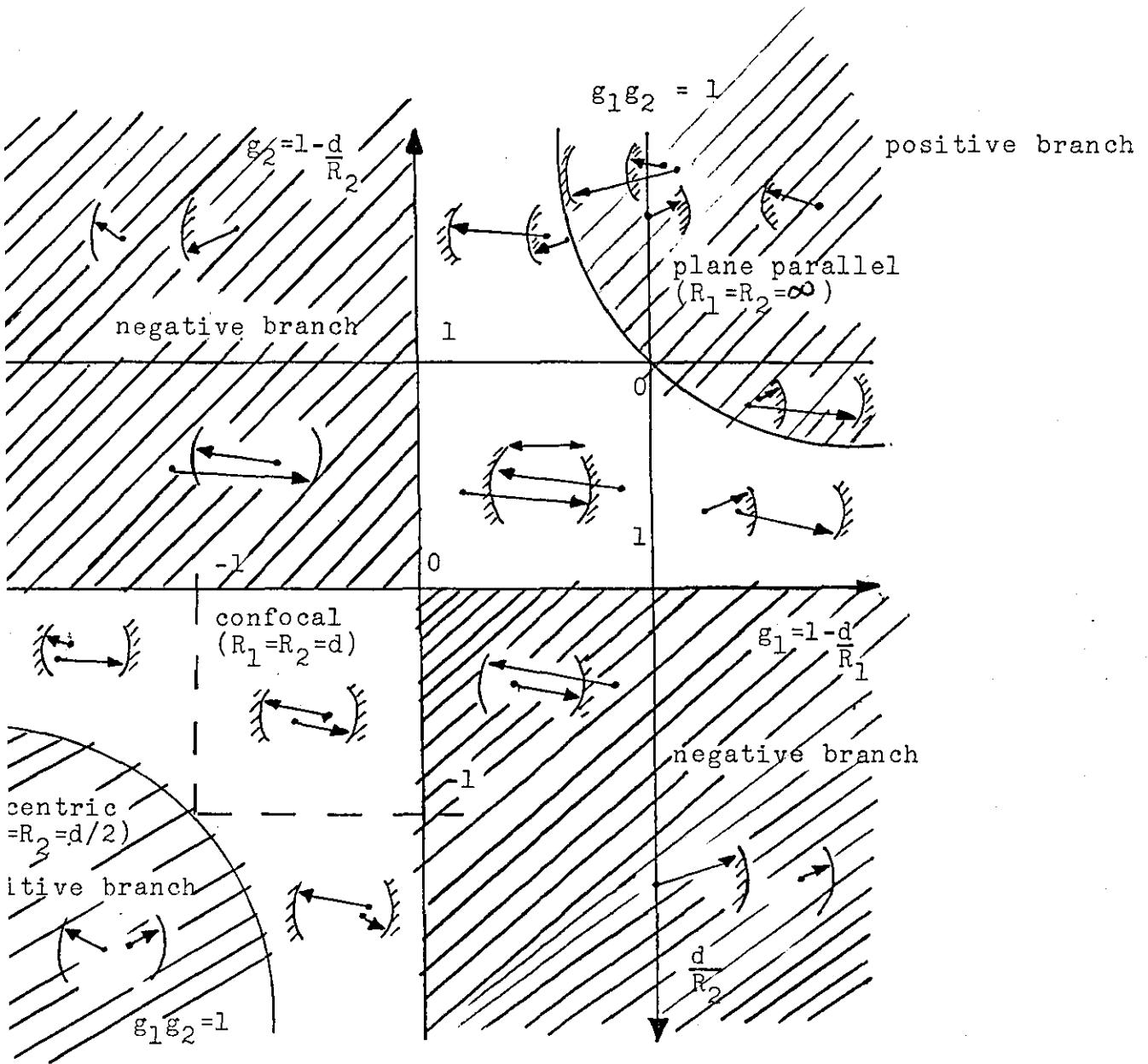


Fig. 2.9: Stability diagram. Unstable resonators lie in shaded region. (Kogelnik et al 1966).

2.8 Review of the Published Work on TEA CO₂ Laser

2.8.1 Introduction and Original

It was well established that CO₂ lasers operated best with an electric field to pressure ratio (E/P) of 10 - 50 V/cm Torr. Thus for a 1-m discharge at 800 Torr, voltages of 8×10^5 to 4×10^6 volts are required for proper operation of CO₂ laser. Since steady state discharges at such high pressures are difficult to operate without having the discharge degenerate into an arc, CO₂ lasers operating at such high pressures have only been pulsed. In addition, voltages around the megawatt region are easier to achieve under pulsed conditions with pulse transformers, Marx bank generators, etc. The first demonstration of the pulse CO₂ laser at high pressure was given by Hill (1968) using a longitudinal discharge excited by a high voltage pulse transformer. A peak power of about 1 Mw (10J/pulse) has been achieved from a 2.4m optical cavity at a total pressure of up to about 13kpa. The device operated at repetition rates up to 100 pulse/sec, and 210 watts of average power with efficiency of 6% have been achieved.

The use of pulsed (axial) discharges at high pressures is not practical due to the very high voltage required, and operation at atmospheric pressure has been confined to short discharges transverse to the laser axis. Dumanchin (1969) reported a 3mJ/cm^3 and a total energy of 240mJ/pulse in a transverse excited laser operating at 67kpa using a mixture of CO₂, N₂, He, with a capacitor discharge transverse to the laser axis. Trigger electrodes were used to preionize the gas, and a large volume of uniformly distributed discharge was initiated in the high pressure gas without localised arcs

forming.

The first atmospheric pressure CO_2 laser was developed by Beaulieu (1970), describing a transversely excited atmospheric pressure (T.E.A.) CO_2 laser Fig. 2.10, utilized a line of ballast resistivity stabilised pins to a solid anode electrode transverse to the laser axis to obtain distributed discharge in the gas. Energies of 150mJ and a peak power 0.5 Mw were obtained from this device. The individual pins were separately stabilized with series of resistors. He also obtained 2J/pulse at 17% efficiency in an improved 1-m long laser. To obtain higher energies in high pressure lasers reduction the electrodes separation is recognised as an obvious method. As the pressure is increased, a plasma glow-to-arc transition becomes more probable at a lower value of E/p ratio. Such a transition is marked by a sudden increase in plasma current, bright arcs in the discharge, and a decrease in the voltage drop across the gap. When an arc discharge occurs, it will terminate laser action by a combination of two factors:

1. Dropping the electron temperature
2. Heating the gas

The development of the TEA lasers has demonstrated that since a finite time is required for the arc to develop, the glow-to-arc transition may be avoided by the use of short excitation times. To achieve increased pulse energies with TEA lasers, the discharge currents may be increased by increasing the voltage drop across the gap or by increasing the discharge area in which a large volume of gas is excited. Various electrode configurations have been used for exciting without arcing in the gas mixture in the CO_2 laser cavity.

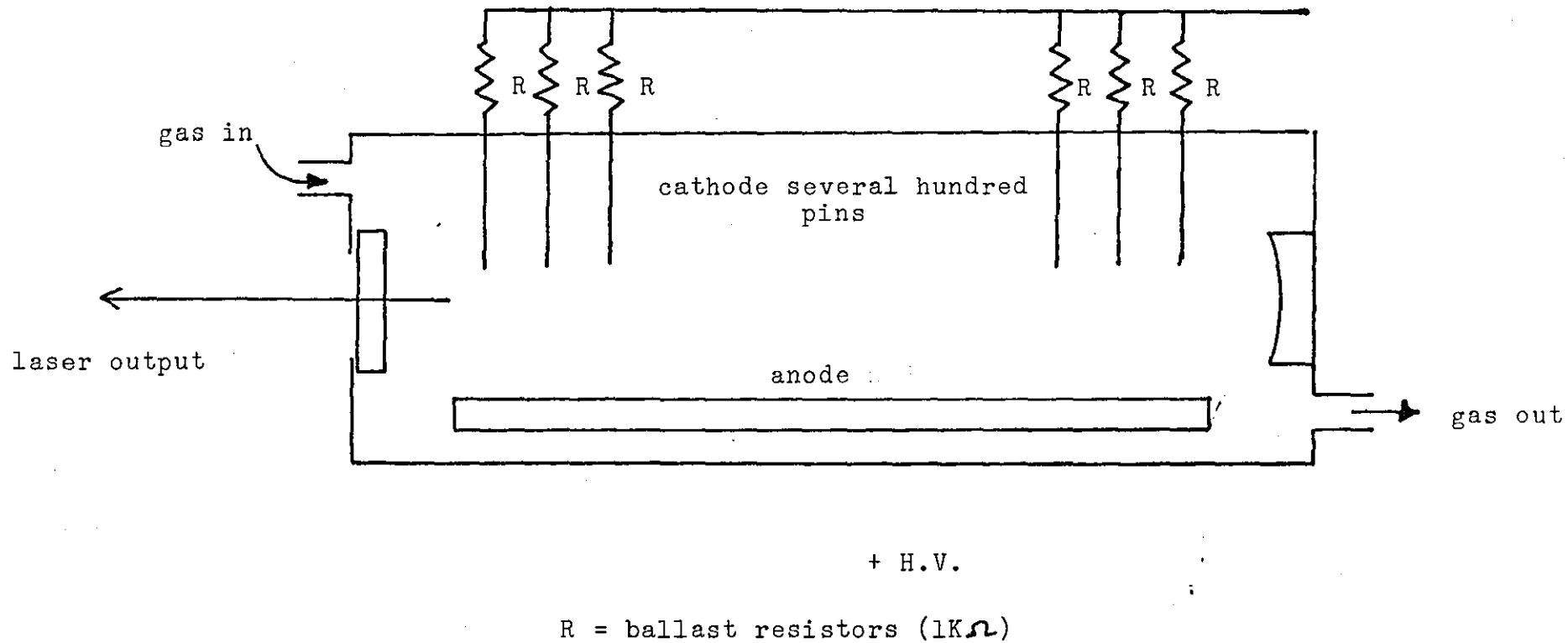


Fig. 2.10: Original TEA CO_2 laser configuration (after Beaulieu 1970).

2.8.2 TEA Laser Electrode Configuration

Numerous techniques have been developed and used to obtain a uniform transverse discharge distribution over the length of the laser cavity. The simplest electrodes system consists of a long tubular anode, and a large number of ballast carbon resistors in parallel using their leads as a cathode, and distributed along the optical cavity. Peak powers of the order of 10^4 w/mm² at atmospheric pressure from an optical cavity of 3750 mm with a 3%-5% efficiency were reported by Fortin (1971). Pulsed lasers using this type of electrode configuration as shown in Fig. 2.10 and Fig. 2.11(a) have been operated at atmospheric pressure with an efficiency of 5%. The use of ballast resistances is to stabilise the discharge by preventing large currents from being drawn through any pin of the cathode. The efficiency in the resistively stabilised electrodes structure is lowered due to the energy dissipation in the resistors (I^2R losses), and the energy input is also limited. Thus the loaded pin electrode lasers are only convenient to excite a small volume of gas. The loaded pin rod structure shown in Fig. 2.10 has the discharges successfully used in the inductance of the pin leads to stabilise without series resistors, Lawrine (1971). A pulse energy of 0.2J and a peak power of 0.2Mw at an efficiency of 4.4% with a pulse duration of 200-3000 ns, have been obtained using shower discharges upto a voltage of 60kv. The use of a small discharge capacitor for each of the cathode pins was studied by Johnson (1971). Fig. 2.11(b) shows this method where a ballasted resistance is no longer used. This technique ensures that the energy per discharge is the same for all the discharge pins and the possibility of excessive

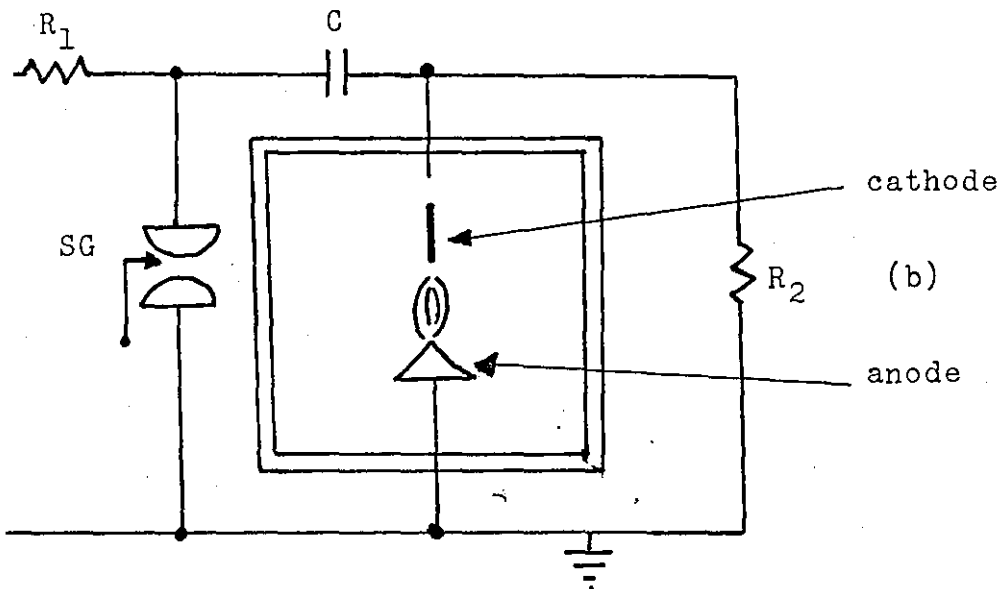
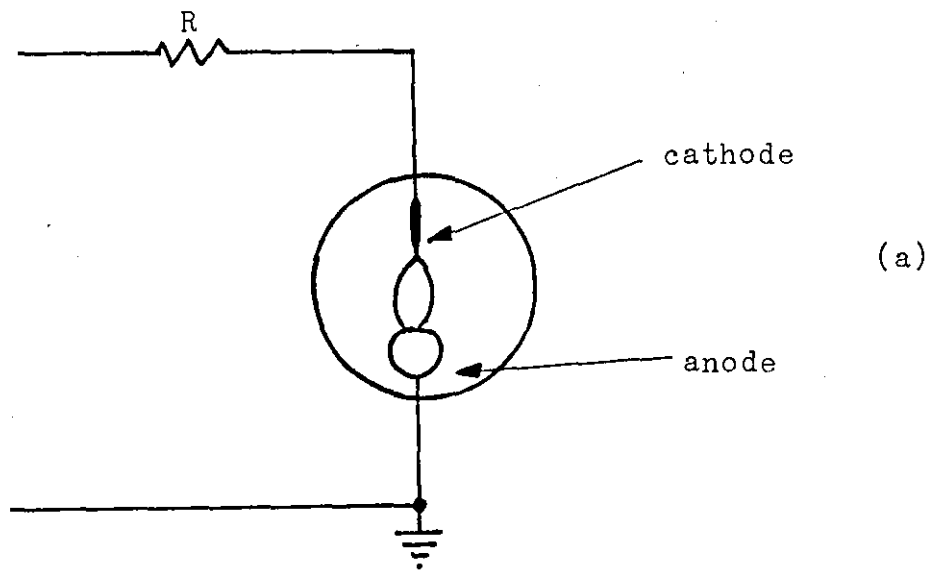
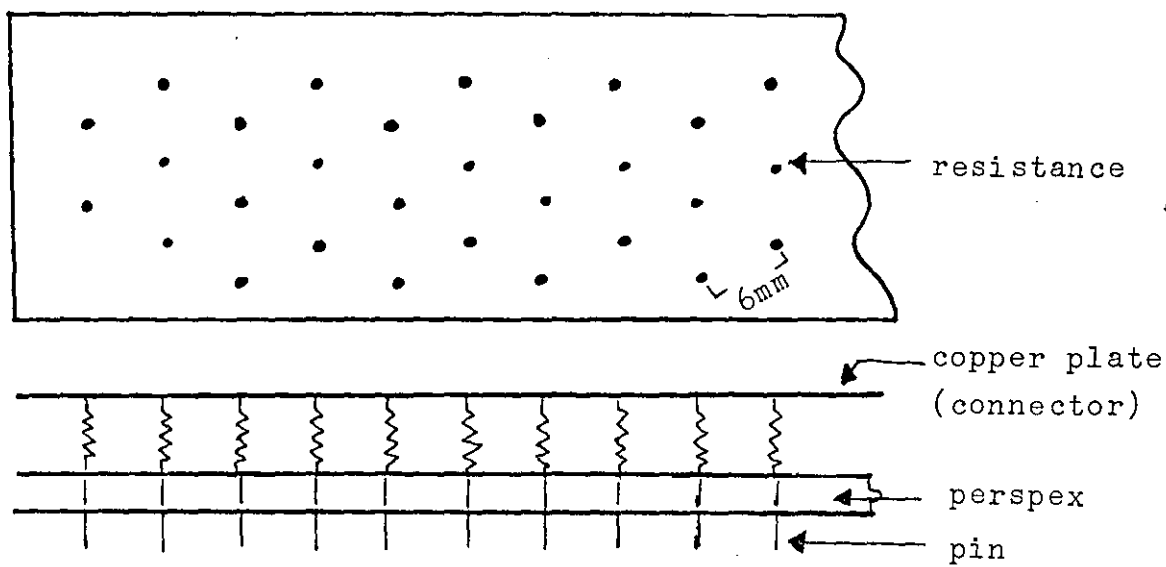


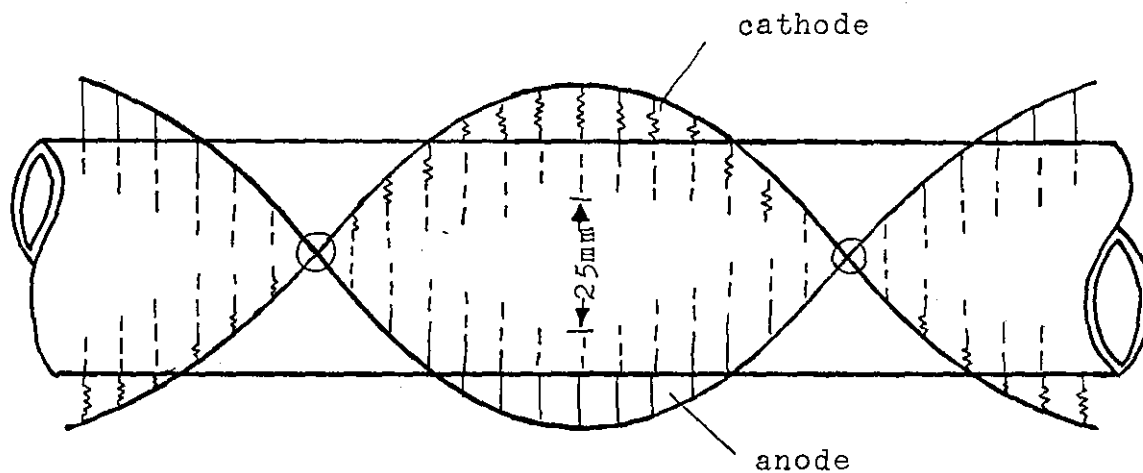
Fig. 2.11: (a) Resistively stabilised pin rod electrodes (Fortin 1971).
 (b) Capacitively stabilised pin rod electrodes (after Johnson 1971).

discharge concentration into a single pin is eliminated with resistive losses. An output energy of 1.2J with a peak power of 0.2Mw was obtained.

The discharge of the laser cavity in all of the pin-rod structure consists of a series of a conical shaped region located along the optical axis of the laser system. Thus the excited volume is much less than that of the whole volume between the anode and the cathode. The active volume can be increased by using multiple staggered rows of pins, Robinson (1971) as shown in Fig. 2.11.(c). A helical pin to pin electrode distribution which is shown in Fig. 2.11.(d) mainly generating TEM_{00} mode was constructed by Fortin (1971). The discharge was stabilised by ballast resistors connected to one side and the system generated 1J/pulse with a peak power of 1Mw at atmospheric pressure. Preionization techniques have been used in TEA lasers for obtaining large volumes of gas discharge and thus more pulse energy. The first double discharge system was developed by Laflamme (1970), and Dumanchin et al (1969), Fig. 2.12.(a), 2.12.(b). An insulated trigger electrode is mounted close to the cathode such as the insulated wires interlaced with the cathode blades in Fig. 2.12.(a) or the bar next to the wire grid in Fig. 2.12.(b) and which is electrically connected through a small capacitor to the anode. When the spark gap breaks down in both systems, the voltage of the main storage capacitor appears on the cathode. As the voltage on the cathode rises, the field gradient between the cathode and the triggered electrode grows more rapidly than between the cathode and the anode. This produces a corona discharge between the cathode and the insulated electrodes. The small capacitor charges, reducing the field between the



(c)



(d)

Fig. 2.11: (c) Multiple pin two dimensional cathode (after Robinson 1971).

(d) Helical pin to pin electrodes (after Fortin et al 1971).

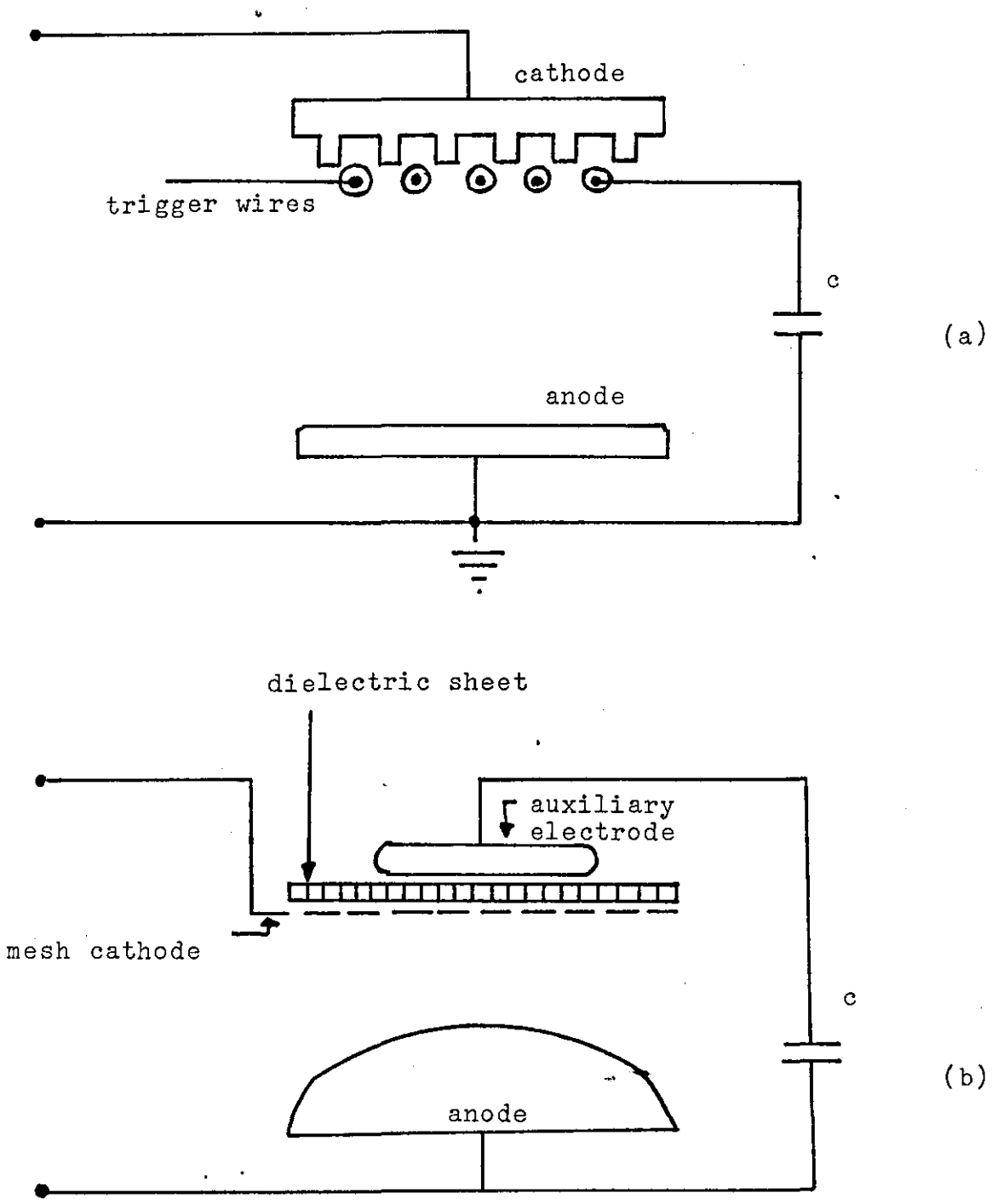
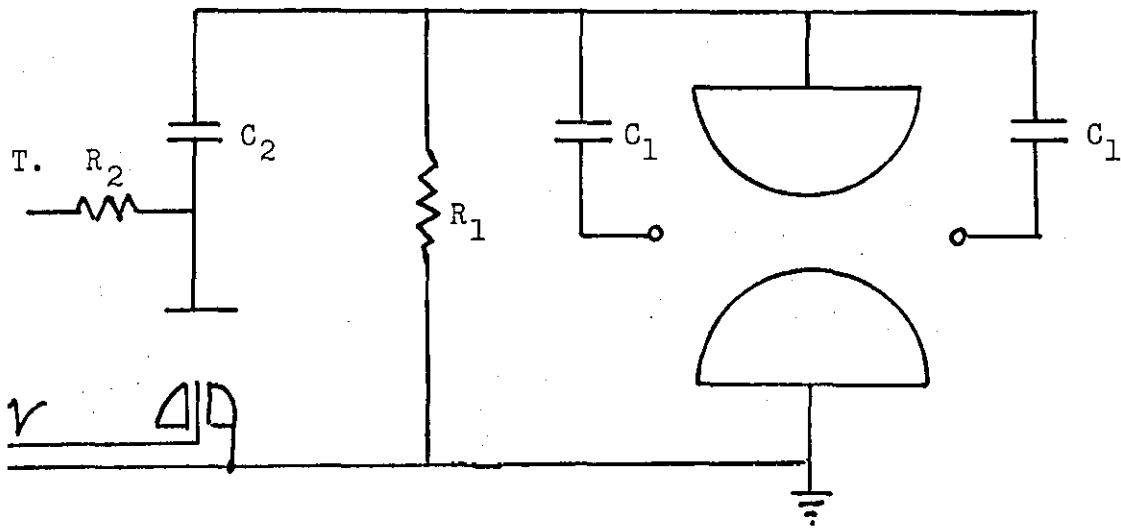


Fig. 2.12: (a) Double discharge electrode configuration with parallel blade cathode (Dumanchin et al 1969).
(b) Double discharge electrode configuration with mesh cathode (Laflamme 1970).

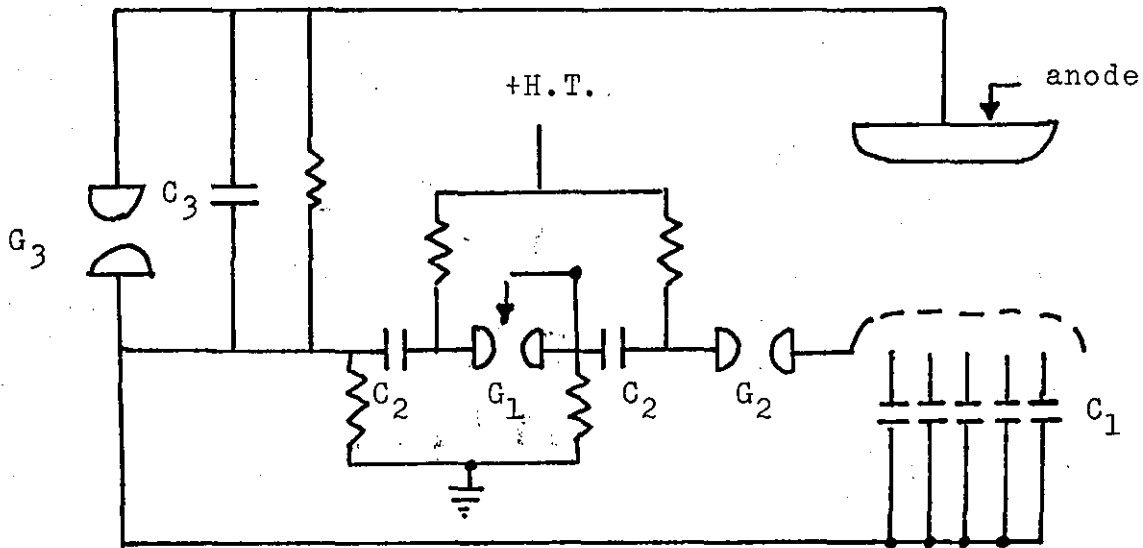
cathode and the triggered electrode, and trapping the electrons in the area of the cathode. These electrons are released into the main gap of the discharge lowering the gas impedance and initiating the main discharge. When the main current pulse is shaped to preclude arc formation, the preionization electron pulse will permit the formation of a uniform glow discharge between anode and cathode.

An output of energy density of $5 \times 10^{-6} \text{ J/mm}^3$, with an output energy of 9J/pulse, probe power 12mW, and efficiencies varying from 5%-10% have been reported by Laflamme (1970) from 4m CO₂ laser cavity. Dumanchin et al (1969) have obtained 140J/pulse from 3m long and with cross section 5000 mm³ discharge. Other preionization techniques (double discharges) have been also described by Lamberton and Pearson (1971), Pearson and Lamberton (1971), as shown in Fig. 2.12(c). The discharge occurs between an identical pair of solid electrodes shaped to a Rogowski profile. Two fine Tungsten wires are placed parallel to the main electrodes but offset from the centre line and each wire is connected to the cathode by a small coupling capacitor. When the voltage is applied to the main electrodes, field emission from the wires induces a discharge between the wires and the anode. This discharge then initiates a very uniform and repeatable discharge between the main electrodes along their whole length. 4.3% efficiency has been achieved with output energy 2J at 60Kv applied voltage.

Figure 2.12(d) shows the electrode structure and the circuit of the improved double discharge laser obtained by Richardson et al (1973). The system was capable of generating 300J/pulse with a peak power exceeding 3Gw at an efficiency of



(c)



(d)

Fig. 2.12: (c) Double discharge electrode configuration with Rogowski profile electrodes (after Pearson et al 1972).

(d) UV preionised double discharge electrode configuration with pin mesh cathode (after Richardson et al 1973).

10%. It has shown as well that volumetric preionization with UV radiation may be extended to large aperture high pressure laser systems by optimising the configuration of the UV source, and laser electrodes. Using an array of spark discharges generated from a series of closely spaced electrodes on an insulating substrate, it was found possible to initiate discharges distributed over a large volume with cross sectional areas of $\approx 6 \times 10^4 \text{ mm}^2$ in a system with 30 mm separation between anode and cathode.

2.9 Conclusion to the Chapter

A brief summary of the spectroscopy of the CO_2 and the N_2 molecules has been made together with the principle optical theory relevant to the excitation of the CO_2 laser.

The fundamental principle of the operation of the CO_2 laser has also been shown.

At higher values of E/N (the ratio of the electric field to the total neutral particle density) a significant percentage of the electrical energy will excite the CO_2 and N_2 electronically. This is near zero for $E/N = 1 \times 10^{-14} \text{ v. mm}^2$, Fig. 2.5 but increases rapidly to 80% near 10^{-5} v. mm^2 . For the CO_2 laser which operates at E/N values below $2.5 \times 10^{-14} \text{ v. mm}^2$, it is clear from Fig. 2.5 that electronic excitation can be neglected.

The relevant work published on the excitation of TEA pulsed CO_2 laser has been reviewed. Electrode configurations for TEA CO_2 lasers have also been included.

Chapter 3

NITROGEN LASER

3.1 Introduction

Since its discovery in 1963, the N_2 laser has found increasing importance due to the emission in the UV, the short pulse width, the high repetition rate and the reliability. Today it is the most widely used pulsed UV laser.

The laser emission at 337.1 nm is based on an electronic transition in the triplet system of molecular nitrogen. Excitation must be by a very fast high voltage discharge as the lifetime of the upper laser level is only 40 ns. As the laser transition involves a long lived metastable level, this laser can only operate pulsed with pulse half widths of less than 15 ns. The high gain of the excited nitrogen of up to 340 dB/m allows the N_2 laser to be operated in the super-radiant mode and in general does not require a resonator. However a rear mirror increases the output power and also improves the beam quality. The efficiency of the N_2 laser and the maximum power at a given cavity length is dependent on the speed of the electric discharge.

The high peak power (Kw) in the UV, the short Gaussian pulse and the high repetition rate (100-500 Hz) are only some of the characteristics of the N_2 laser which permit new applications. Examples are photo-chemical research, pollution control, lifetime measurements in the subnanosecond range, Raman spectroscopy and medical and biological research.

The peak power in the ultraviolet, the short risetime, the small beam divergence, and the pulse-to-pulse amplitude stability, make the N_2 laser an ideal pump light source for the excitation of high repetition rate dye lasers. The combination offers continuous tunable short pulsed laser radiation from 217 to 950 nm.

3.2 Nitrogen Molecule Spectra

Extensive studies of the nitrogen molecular spectra have been published, and more than 48 band systems have been observed involving 32 singlet and 7 triplet states (Tyts et al, 1966). The energy levels of the N_2 molecule are shown in Fig. 3.1; the full horizontal lines represent the electronic states, while the short thin bars indicate the vibrational levels in the electronic states. The atomic states of the dissociation products of some of N_2 molecular states are also shown in the right side of this diagram, and they are $4S$, $2D$, and $2P$, correspond to the three lowest energy states of the nitrogen atom. The downward arrows in the diagram represent the transitions observed in emissions (stimulated and spontaneous), and the upwards arrows those observed in absorption. When both emission and absorption occur together up and down, transitions are indicated. The potential energy diagram for some of the N_2 states is shown in Fig. 3.2.

3.2.1 Band Systems of Nitrogen

There are many band systems of nitrogen. The first and second positive systems are the most readily developed in the emission processes. Other band systems which appear are the fourth positive, Vegard-Kaplan, Herman-Kaplan, Lyman-Birge, fifth positive bands. The most important band systems are as follows:

3.2.1.1 The First Positive System ($B \ ^3\Pi_g - A \ ^3\Sigma_u^+$)

The first positive system of nitrogen extends from 472 to 4000 nm (Nicholls 1964), and is a $^3\Pi_g - ^3\Sigma_u^+$ transition, see Fig. 3.1. This system occurs most strongly in the positive column of a discharge tube containing nitrogen. The $A \ ^3\Sigma_u^+$, and

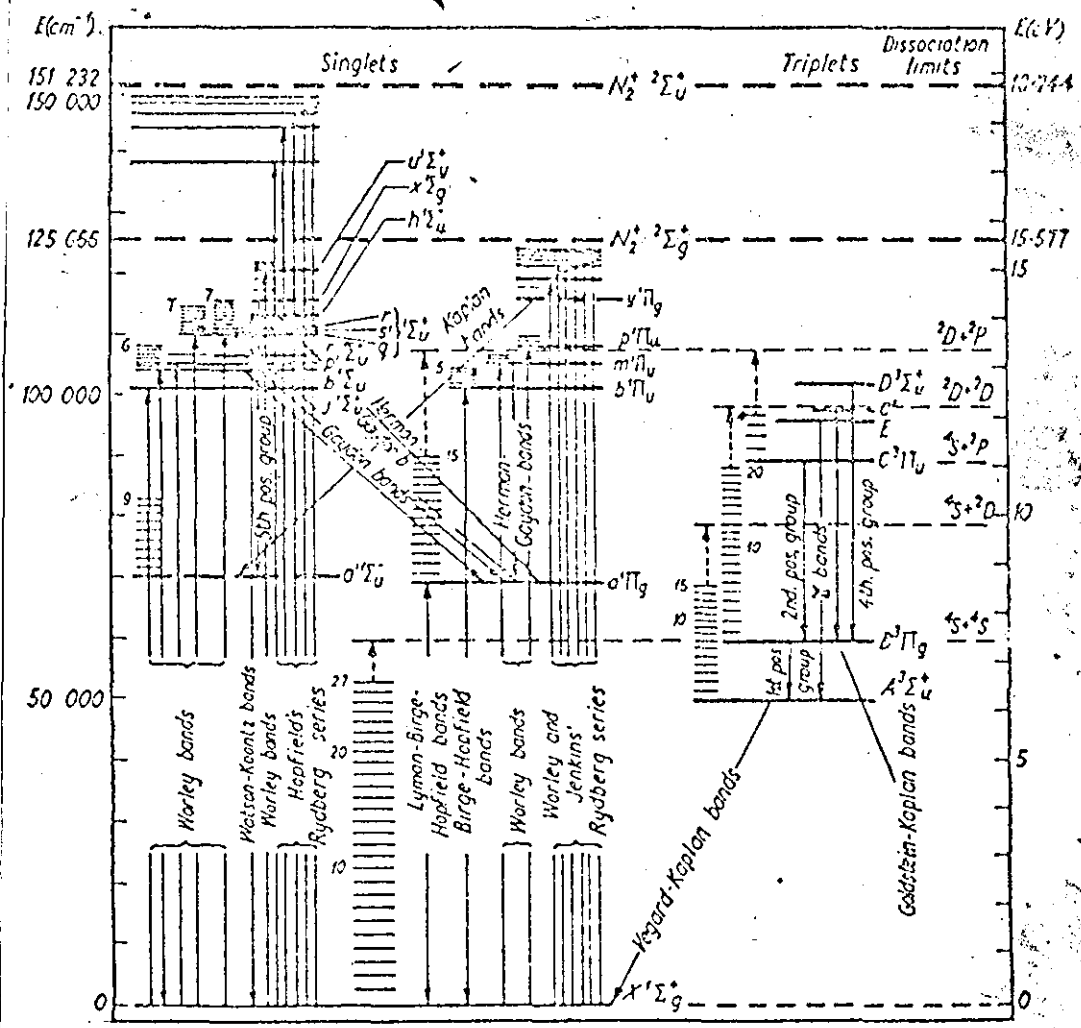


Fig. 3.1: Energy level diagram and electronic transition of N_2 molecule

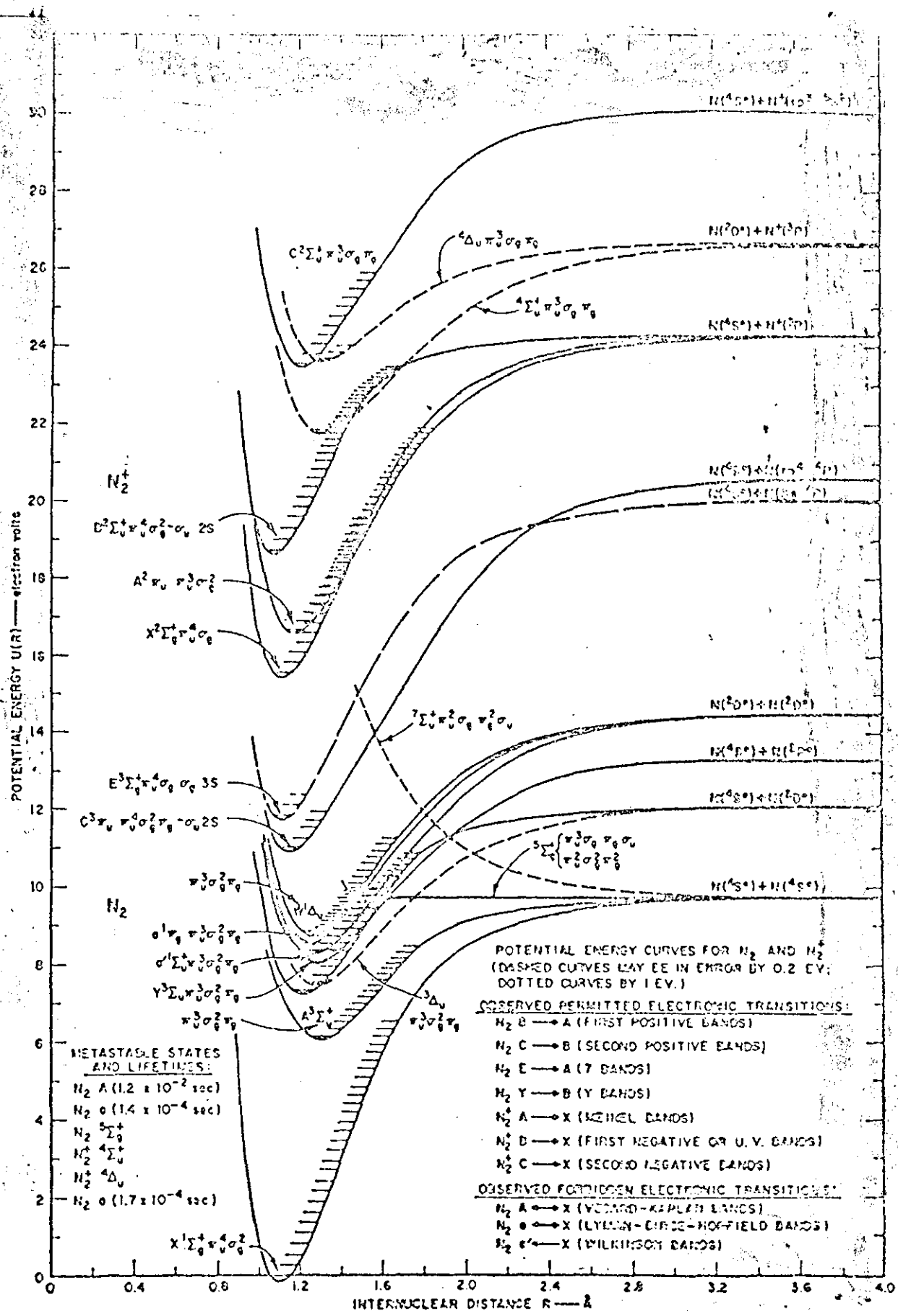


Fig. 3.2: Potential energy diagram of N_2 molecule (after Young 1964).

$B \ ^3\Pi_g$ are the lower and upper states of first positive system. Various bands, wavelengths, band strength, and transitions probability for the first positive system have been studied by Nicholls, and are reproduced in Table 3.1. Bands with $V > 12$ (V is the vibrational quantum number) are not observed because of the predissociation of the $B \ ^3\Pi_g$ state by the $4S \ 4S$ dissociation limit (Tyts 1966). The lifetime of the level $V' = 1$ of the $B \ ^3\Pi_g$ state has been quoted as 10000 ns by (Gerry 1965).

3.2.1.2 The Second Positive System ($C \ ^3\Pi_g - B \ ^3\Pi_g$)

This system extends from 270 - 550 nm, and is the most intense emission feature of the N_2 spectrum in this wavelength region. The upper state C is the highest excited state of the neutral in mildly condensed discharges (Pearse 1964). All the bands of this system are blue degraded, having definite heads and forming four well defined sequences. The most important bands of these sequences are as below:

<u>Band (Vibrational Level)</u>	<u>Wavelength (nm)</u>	<u>Relative Intensity</u>
02	380	3
01	356	7
00	337	10
10	315	7

Since the nature of the transition in the system is triplet, see Fig. 3.1, all the bands exhibit heads. More than 50 bands of the system have been observed within range of vibrational quantum numbers $V' \leq 4$, $V'' \leq 11$. Various bands, wavelengths, are given in Table 3.2 (Nicholls 1964). The lifetime measurements of the $V = 0$ level of $C \ ^3\Pi_4$ state has been calculated to be 40 ns (Bennett 1959).

Table 3.1

Absolute Transition Probabilities for Bands
Of the N₂ First Positive System (*)
 (after Nicholls 1964)

Band	Wave-length (Å)	Transition Probability $A_{v'v''}$ (sec ⁻¹)	Oscilla- tor Strength $f_{v'v''}$	Band Strength $S_{v'v''}$ (a ₀ ² e ²)
0,0	10,387	8.65 + 4	1.4 - 3	2.82 - 1
0,1	12,211	6.17 + 4	1.38 - 3	3.27 - 1
0,2	14,735	2.46 + 4	8.01 - 4	2.29 - 1
1,0	8851	1.29 + 5	1.521 - 3	2.62 - 1
1,1	10,200	5.18 + 2	8.08 - 6	1.6 - 3
1,2	11,800	2.10 + 4	4.39 - 4	1.00 - 1
1,3	14,043	2.54 + 4	7.51 - 4	1.95 - 1
1,4	17,192	1.36 + 4	6.03 - 4	2.01 - 1
2,0	7694	7.21 + 4	6.407 - 4	9.57 - 2
2,1	8673	6.90 + 4	7.78 - 4	1.31 - 1
2,2	9850	3.13 + 4	4.55 - 4	8.70 - 2
2,3	11,436	4.30 + 2	8.43 - 6	1.87 - 3
2,4	13,420	1.17 + 4	3.17 - 4	8.26 - 2
2,5	16,163	1.34 + 4	5.24 - 4	1.64 - 1
3,0	6824	1.38 + 4	1.28 - 4	1.70 - 1
3,1	7569	1.09 + 5	9.41 - 4	1.38 - 1
3,2	8504	1.29 + 4	1.4 - 4	2.31 - 2
3,3	9594	4.61 + 4	6.36 - 4	1.18 - 1
3,4	11,116	6.95 + 3	1.29 - 4	2.78 - 2
3,5	12,844	1.56 + 4	3.87 - 5	9.65 - 3
3,9	15,370	8.16 + 3	2.89 - 4	8.62 - 2
4,0	6300	1.88 + 3	1.12 - 5	1.37 - 3
4,1	6741	4.90 + 4	3.34 - 4	4.37 - 2
4,2	7451	9.98 + 4	8.31 - 4	1.20 - 1
4,3	8315	3.39 + 2	3.52 - 6	5.68 - 2
4,4	9368	3.35 + 4	4.41 - 4	8.02 - 2
5,1	6098	8.95 + 3	4.99 - 5	5.90 - 3
5,2	6661	7.60 + 4	5.06 - 4	6.54 - 2
5,3	7338	6.75 + 4	5.45 - 4	8.78 - 2
5,4	8200	1.57 + 4	1.58 - 4	2.52 - 2
5,5	9147	1.35 + 4	1.69 - 4	3.01 - 2
6,1	5571	7.85 + 2	3.66 - 6	3.96 - 4
6,2	6039	1.91 + 4	1.05 - 4	1.23 - 2
6,3	6583	9.31 + 4	6.04 - 4	7.73 - 2
6,4	7229	3.05 + 4	2.39 - 4	3.36 - 2
6,5	7981	3.76 + 4	3.59 - 4	5.56 - 2
7,2	5533	2.03 + 3	9.33 - 6	1.00 - 3
7,3	5985	3.28 + 4	1.77 - 4	2.06 - 2
7,4	6505	9.54 + 4	6.06 - 4	7.65 - 2
7,5	7121	7.31 + 3	5.56 - 5	7.69 - 2
7,6	7831	4.46 + 4	4.10 - 4	6.24 - 2

Table 3.1 (continued)

Band	Wave-length (Å)	Transition Probability $A_{v'v''}$ (sec ⁻¹)	Oscilla- tor $f_{v'v''}$	Band Strength $S_{v'v''}$ ($a_0^2 e^2$)
8,3	5496	4.44 + 3	2.91 - 5	2.15 - 3
8,4	5931	5.04 + 4	2.66 - 4	3.06 - 2
8,5	6432	8.45 + 4	5.25 - 4	6.56 - 2
9,4	5459	8.41 + 3	3.76 - 5	3.99 - 3
9,5	5879	6.16 + 4	3.19 - 4	3.64 - 2
9,6	6360	6.58 + 4	4.00 - 4	4.91 - 2
10,5	5424	1.26 + 4	5.55 - 5	5.85 - 3
10,6	5829	6.85 + 4	3.49 - 4	3.95 - 2
10,7	6291	4.48 + 4	2.66 - 4	3.25 - 2
11,6	5390	1.95 + 4	8.50 - 5	8.89 - 3
11,7	5779	7.85 + 4	3.93 - 4	4.40 - 2
11,8	6221	1.79 + 4	1.18 - 4	1.43 - 1
12,7	5352	9.63 + 4	4.02 - 4	4.18 - 2
12,8	5730	1.24 + 4	6.12 - 5	6.81 - 2

(*) The positive or negative number in an entry indicates the power of ten by which the entry is multiplied.

Table 3.2

Absolute Transition Probabilities for Bands
Of the N₂ Second Positive System (*)

(after Nicholls 1964)

Band	Wave-length (Å)	Transition Probability $A_{v'v''}$ (sec ⁻¹)	Oscilla- tor Strength $f_{v'v''}$	Band Strength $S_{v'v''}$ (a ₀ ² e ²)
0,0	3371.3	1.11 + 7	1.90 - 2	1.24 + 0
0,1	3576.9	7.27 + 6	1.40 - 2	9.65 - 1
0,2	3804.9	2.83 + 6	6.15 - 3	4.52 - 1
0,3	4059.4	9.33 + 5	2.31 - 3	1.82 - 1
0,4	4343.6	2.54 + 5	7.18 - 4	6.03 - 2
0,5	4667.3	5.11 + 4	1.67 - 4	1.05 - 2
1,0	3159.3	1.02 + 7	1.53 - 2	9.35 - 1
1,1	3339	5.59 + 5	9.34 - 4	6.03 - 2
1,2	3536.7	4.70 + 6	8.82 - 3	6.03 - 1
1,3	3755.4	3.93 + 6	8.31 - 3	6.03 - 1
1,4	3998.4	1.95 + 6	4.68 - 3	3.62 - 1
1,5	4269.7	6.68 + 5	1.83 - 3	1.55 - 1
1,6	4574.3	2.17 + 5	6.82 - 4	6.03 - 2
1,7	4916.8	8.75 + 4	3.17 - 4	3.02 - 2
2,0	2976.8	3.55 + 6	4.72 - 3	2.72 - 1
2,1	3136.0	8.43 + 6	1.24 - 2	7.53 - 1
2,2	3309	8.61 + 5	1.41 - 3	9.05 - 2
2,3	3500.5	1.45 + 6	2.67 - 3	1.83 - 1
2,4	3710.5	3.26 + 6	6.73 - 3	4.82 - 1
2,5	3943.0	2.54 + 6	5.93 - 3	4.52 - 1
2,6	4200.5	1.26 + 6	3.35 - 3	2.72 - 1
2,7	4490.2	4.60 + 5	1.39 - 3	1.21 - 1
2,8	4814.8	1.86 + 5	6.48 - 4	6.03 - 2
3,0	2819.8	4.64 + 5	5.53 - 4	3.02 - 2
3,1	2962.0	6.40 + 3	8.43 - 3	4.82 - 1
3,2	3116.7	4.47 + 6	6.51 - 3	3.92 - 2
3,3	3285.3	2.93 + 6	4.75 - 3	3.02 - 1
3,5	3671.9	1.89 + 6	3.82 - 3	2.72 - 1
3,6	3894.6	2.64 + 6	6.01 - 3	4.52 - 1
3,7	4141.8	1.61 + 6	4.14 - 3	3.32 - 1
3,8	4416.7	7.24 + 5	2.12 - 3	1.82 - 1
3,9	4723.5	2.96 + 5	9.91 - 4	9.05 - 2
4,1	2814.3	1.40 + 6	1.66 - 3	9.03 - 2
4,2	2953.2	7.27 + 6	9.51 - 3	5.43 - 1
4,3	3104.0	1.39 + 6	2.01 - 3	1.21 - 1
4,4	3268.1	3.87 + 6	6.21 - 3	3.92 - 1
4,5	3446	5.08 + 5	9.05 - 4	6.03 - 2
4,6	3641.7	6.46 + 5	1.29 - 3	9.05 - 2
4,7	3857.9	1.81 + 6	4.04 - 3	3.02 - 1
4,8	4094.8	1.82 + 6	4.57 - 3	3.63 - 1
4,9	4355.0	1.00 + 7	2.87 - 2	2.42 - 1

(*) The positive or negative numbers in an entry indicate the power of ten by which the entry is multiplied.

3.2.1.3 The Fourth Positive System (D $\frac{3}{\Sigma_u^+}$ - B $\frac{3}{\Pi_g}$)

This is a system of seven bands between 225 - 290 nm, and it occurs in a mildly condensed discharge through nitrogen. (Pearse 1964). The lifetime of the D $\frac{3}{\Sigma_n^+}$ state was found to be 14 ns (Kurzweg 1973).

3.2.1.4 Vigard-Kaplan Bands (X $\frac{1}{\Sigma_g^+}$ - A $\frac{3}{\Sigma_u^+}$)

This is a relatively weak system and is observed only under special conditions of excitation used in after glow studies. The system was first discovered by Vegard and Kaplan. Later Wilkinson (1959) has observed this system in absorption also, using path lengths of 9-13 bar meter. The wavelength range is from 170 - 500 nm (Nicholls 1964).

3.2.1.5 The Fifth Positive (Van der Ziel) System

$$(X \frac{1}{\Sigma_g^-} - a \frac{1}{\Sigma_u^-})$$

This system is obtained in mildly condensed discharged or high current discharges in N_2 . They are single headed bands lying between 230 - 280 nm (Pearse 1956).

3.2.1.6 Herman Kaplan System (E $\frac{3}{\Sigma_g^+}$ - A $\frac{3}{\Sigma_u^+}$)

Twelve weak bands lying between 210 - 275 nm have been observed by Herman using a very long discharge tube.

The above is a very brief description of the most important bands of the nitrogen molecule. The N_2 laser operated in this thesis works on the positive system.

3.3 Population Inversion Requirements in the N₂ Laser

If the C $\frac{3}{\pi}_4$ level of N₂ molecules can be populated within a time which is short enough with respect to the excited state, a population inversion achievement is possible between the C $\frac{3}{\pi}_u$ (see Fig. 3.1), and B $\frac{3}{\pi}_g$ levels of the second positive system of N₂ to obtain stimulated emission.

The requirements to obtain the population inversions in the N₂ laser at 337 nm is explained in this section by treating it as a three level laser system, Fig. 3.3 shows the three level laser system.

Let N₁, N₂, and N₃ be the population densities of X¹ Σ_g^{-1} (ground level 1), B $\frac{3}{\pi}_g$ (lower level 2), and C $\frac{3}{\pi}_g$ (higher level 3) respectively. Let X_{ij} denote the rate of collisional excitation by electron impacts from level i to level j where i < j; Y_{ji} is the rate of collisional de-excitation from level j to level i. This "quenching" process, leads to reduction of light emission with an increase in gas density and can be characterised by the quenching density N_q. The ratio of emission acts to excitation acts has been expressed as (Legler 1963):

$$\frac{\delta}{\delta_0} = \frac{1}{1 + \frac{N}{N_q}} \quad (3.1)$$

For the excited state, assume τ_{ji} is the natural lifetime for photon emission, and τ_{jq} is the mean time for quenching; therefore the resultant mean lifetime of the excited state can be written as:

$$\frac{1}{\tau_{ji}^m} = \frac{1}{\tau_{jq}} + \frac{1}{\tau_{ji}} \quad (3.2)$$

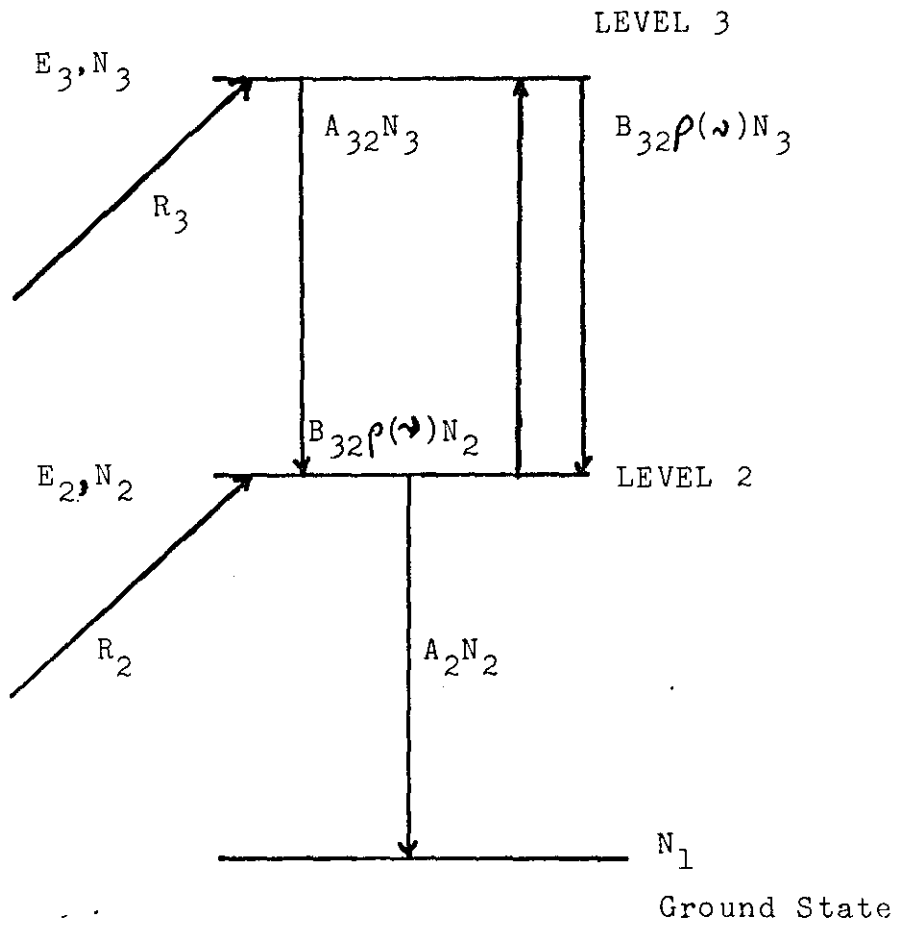


Fig. 3.3: Simple energy level to explain spontaneous and stimulated transitions.

Finally, let R_{ij}^i denote the rate of stimulated emission which includes the line width, Einstein's B sufficient, and the energy density. The rate equation governing the population densities of these levels can be written as (Ali et al 1967):

$$dN_3/dt = X_{13}N_1 + X_{23}N_2 - (Y_{31} + Y_{32} + \tau_{32}^{-1} + \tau_{31}^{-1}) N_3 - R_{32}^i (N_3 - \frac{g_3}{g_2} N_2) \quad (3.3)$$

$$dN_2/dt = X_{12}N_1 + (\tau_{32}^{-1} + Y_{32})N_3 - (\tau_{21}^{-1} + Y_{21} + X_{23}) N_2 + R_{32}^i (N_3 - \frac{g_3}{g_2} N_2) \quad (3.4)$$

$$dN_1/dt = -(X_{12} + X_{13})N_1 + (\tau_{21}^{-1} + Y_{21})N_2 + (\tau_{31}^{-1} + Y_{31})N_3 \quad (3.5)$$

where g_3 and g_2 are the statistical weights of the high and lower laser levels respectively.

Since $\tau_{31} \gg \tau_{32}$ (Ali 1967), $\tau_{21} > \tau_{32} \approx 40$ ns (Gerry 1959) and $\tau_{21} = 10$ ps (Gerry 1959), the rate equation governing the population densities of the upper and lower laser levels are simplified and can be written as:

$$dN_3/dt = X_{13}N_1 + X_{23}N_2 - (\tau_{32}^{-1} + Y_{32}) N_3 - R_{32}^i (N_3 - N_2) \quad (3.6)$$

$$dN_2/dt = X_{13}N_1 + (\tau_{32}^{-1} + Y_{32})N_3 - (\tau_{21}^{-1} + X_{23}) N_2 + R_{32}^i (N_3 - N_2) \dots \quad (3.7)$$

The above two equations can be solved to become (see Appendix 1):

$$N_3 = N_1 X_{13} t - \frac{1}{2} N_1 (Y_{32} + \tau_{32}^{-1}) t^2 \quad (3.8)$$

$$N_2 = \frac{1}{2} N_1 X_{13} (Y_{32} + \tau_{32}^{-1}) t^2 \quad (3.9)$$

Thus to obtain a population inversion, i.e. $N_3 > N_2$, the condition $\zeta < (1/Y_{32} + \frac{-1}{32})^{-1}$ must be satisfied which implies that inversion must take place in a small time compared to $(Y_{32} + \frac{-1}{32})^{-1}$. Using equation (3.1) the value of $(Y_{32} + \frac{-1}{32})^{-1}$ can be calculated. They are 7.5 ns for τ_q equal 12 ns corresponding to 100 torr, and 5.9 ns for $\tau_q = 8.7$ ns corresponding to a nitrogen pressure of 140 torr (Legler 1963); thus the excitation should preferably take place in periods shorter than these times.

The de-excitation by electron collision which give an additional contribution to Y_{32} , has times that are comparable with the natural lifetime of the excited states $C \frac{3}{\pi u}$ at electron densities of more than $6 \cdot 10^{+14} \text{ cm}^{-3}$ (Ali 1963). Therefore such a process would further reduce the inversion duration and hence emphasise the need for fast excitation.

Two important factors can be drawn out from the N_2 population inversion requirement:

- a. The excitation must be by a very fast high voltage discharge as the lifetime of the upper laser level is only 40 ns.
- b. As the laser-transition involves a long lived metastable level $\approx 10 \mu\text{s}$, this laser can only operate pulsed with pulse half widths of less than 15 ns.

As a result of these two points, the laser which was constructed in our laboratory operated with N_2 gas too.

3.4 Excitation Criterion Circuits

There are two basic types of circuit design which are most commonly used in N_2 excitation. In the first, known as the "capacitor discharge" design, the high voltage source charges capacitor C_1 but not C_2 , see Fig. 3.4.a. When the switch (thyatron or spark gap) is closed, the charge on C_1 is transferred rapidly to C_2 producing a voltage across the discharge channel. At breakdown across the channel electrodes, the energy stored in C_2 plus some of that left in C_1 is delivered to the gas. Thus, the "capacitor discharge" design can be described as a "series charge, parallel discharge" circuit. The more rapidly C_2 is charged, the higher the voltage achieved before the gas breaks down, hence the higher the energy delivered to the gas. If either circuit loop contains too much inductance, the output energy is reduced. Typical pulse durations with this circuit are 8-10 ns.

The second common design is known as the "Blumlein" circuit. In this design both C_1 and C_2 are charged in parallel to a high voltage, see Fig. 3.4.b. When the switch is closed, C_1 discharges through the switch, increasing the voltage across the channel. At gas breakdown C_2 discharges into the channel. Thus, the Blumlein can be described as a "parallel charge, series discharge" circuit. The design is usually of higher speed, has higher peak power currents than the "capacitor discharge" design and produces pulses with 3-5 ns duration. The term "stripline design" is usually applied to the Blumlein circuit but may actually apply to both types. "Stripline" refers to the design of the capacitors, either C_1 or C_2 or both, in which the capacitance is formed by two parallel plates separated by a film or sheet of dielectric material.

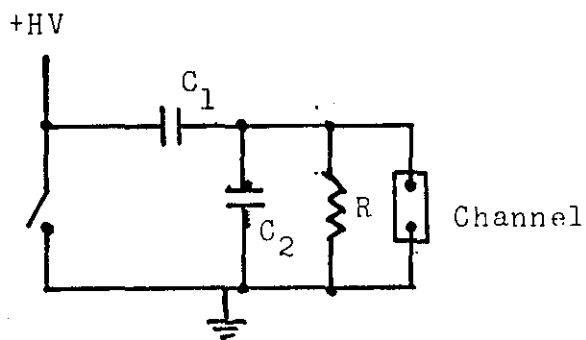


Fig. 3.4.a: Capacitor Discharge Type

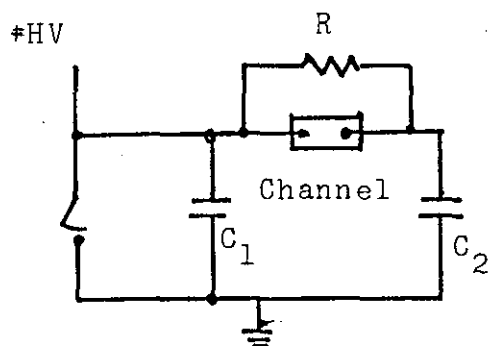


Fig. 3.4.b: Blumlein Circuit Discharge Type

Since the efficiency of a nitrogen laser is not determined by the choice of circuit design or type of capacitor, but is determined by other design factors, the most important of which is energy density in the discharge. Efficiencies in the range of 0.08 - 0.11% at optimum energy densities have been achieved (Bergman, 1976).

The laser described in this thesis uses the first type of circuit, see Chapter (5,6).

3.5 Practical Electrodes Configurations

In addition to the two types of circuit designs, there are also two types of channel design. The first, known as the "channelized discharge" and used in early lasers, consists of two electrodes separated by glass plates. These plates are close together, 2-3 mm, as a result the discharge occurs along the surface of the glass and produces a beam with two prominent lines, see Fig. 3.5.a.

The advantage of this design is that it is well-suited for high repetition rate operation because unwanted metastable N_2 molecules can relax to their ground state via collision at the wall in the immediate vicinity of the discharge. The disadvantage of this design is that breakdown along the walls occurs at a relatively low voltage, limiting the output energy.

Most N_2 lasers today use the unchannelized or open discharge (Fig. 3.5.b) design which will operate at higher voltages producing higher output energies. The output beam is also very uniform, ideally suited for dye laser pumping. The disadvantage of this design is that metastable molecules must be swept out of the discharge region after each pulse to maintain high pulse energy. As a result, high gas flow rates are required at high



Fig. 3.5.a: Channelized Discharge

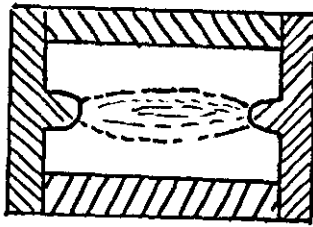


Fig. 3.5.b: Unchannelized Open Discharge

repetition rates.

3.6 Review of Published Work on Nitrogen Lasers

3.6.1 Nitrogen Low Pressure Triplet System

This section is a review of published work referring to the nitrogen molecular laser. To aid the discussion, an energy level diagram of the principal levels involved is given in Fig. 3.6 with the laser transitions drawn in. The main features of the various papers referring to the molecular triplet system are given in Table 3.1.

Mathias et al (1963) observed stimulated emission in the first positive system of nitrogen $B \ ^3\Pi_g - A \ ^3\Sigma_u^+$. 28 separate oscillations in the range 860 - 1240 nm, in the four bands (2,1), (1,0), (0,0) and (0,1) have been observed using excitation by 20 kv, 35 A pulses and a discharge tube having end windows mounted at the Brewster angle. The tube was 7 mm bore and 400 mm discharge length. The mirrors used were silver coated and they report that the laser pulse "started within a microsecond of the excitation pulse". Stimulated emission was observed from two other band systems (2,10) and (3,1), using excitation by 40 kv, 90 A pulses and dielectric mirrors.

Stimulated emission in nitrogen in the second positive system $C \ ^3\Pi_u - B \ ^3\Pi_g$ has been observed by (Heard 1963), with wavelengths lying between 300 - 400 nm. The strongest line was at 337 nm in the (0,0) band head. The excitation was provided by a "100 - 150 kv submicrosecond pulse generator". A new type of excitation was formulated by (Leonard 1965) to populate the $C \ ^3\Pi_u$ level in order to obtain a fair intensity of the 337 nm record positive transition in nitrogen. The device, shown in Fig. 3.7.a, was capable of very high pulse power output (200 kw),

Ref.	Pressure Torr.	Current pulse length μ s	Current rise time μ s	Pulse current A	Pulse voltage kV	Mirrors	Tube details diam. x length mm	Output peak power	Observed transitions
6	4	1.0	-	35	20	silvered	7x400	0.5W	First positive system (0,1)
54	2	1.0	-	90	40	dielectric	10x1860 capillary	100W	(0,0), (1,0) & (2,1)
51	-	-	-	-	100-150	silvered	-x1220	10W	2nd positive system 337.1nm line strongest.
78	1-3	0-5	0.2	30	50	dielectric	4,15x1080	-	1st positive system (2,0).
11	20	0.18	0.09	675/cm ²	15-25	single silvered mirror	3x25x2000 Transverse	200kW	2nd positive 337.1 superradiance.
9	2 for (0,0) 1 for (0,0)	1.5	-	-	40	dielectric	3x900	-	2nd positive system (0,0) and (0,1) superradiance at 337.1nm
0	6	0.1	0.04	3500/cm ²	30	only one mirror (unspecified)	-x680 capillary	20kW	2nd positive system Superradiance 337.1nm. Coaxial laser.
8	30	0.03	0.004	400,000	equiv- alent voltage 150	no mirror	-x17x1800 Transverse	-	2nd positive system 337.1nm superradiance. Blumlein pulse generator.
0	30	0.03	0.004	500,000	75	no mirror	3x100x1830	2.5mW	2nd positive system 337.1nm superradiance. Blumlein pulse generator

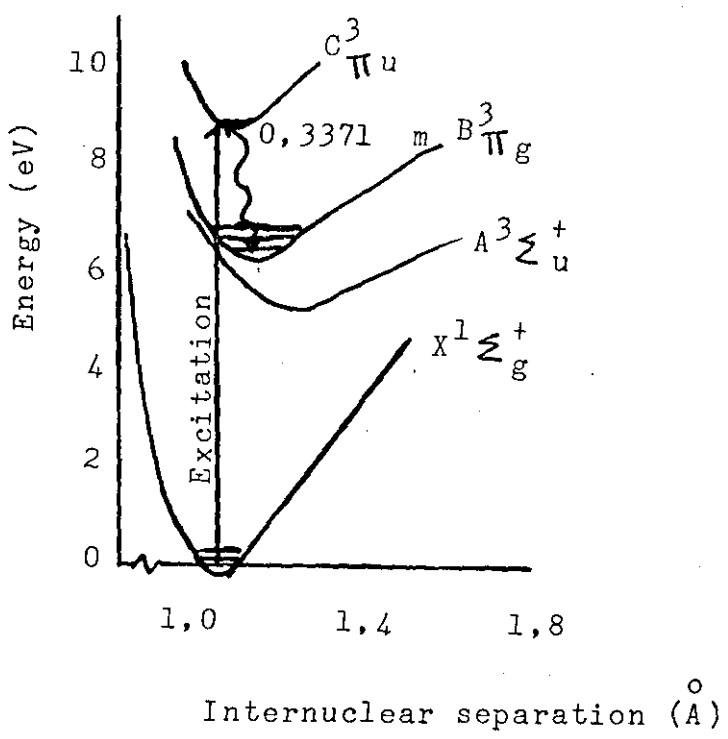


Fig. 3.6: Nitrogen energy levels diagram with the laser transitions

and operated with only a single mirror, in the superradiant mode. In this device the electric field is applied perpendicular to the direction of stimulated emission as opposed to the conventional longitudinal discharge, which is found in many He-N₂ lasers and was also the configuration leading to the first superradiance in N₂ at 337 nm.

To achieve high rates of rise of current a coaxial transmission line laser with a minimum of circuit inductance was constructed (Geller 1960) as shown in Fig. 3.7.b. The energy storage element was a 5 Ω line made up of 10 parallel lengths of 50 Ω coax cable. The length of the line was such as to give a 50 ns pulse. A coaxial spark gap switch was designed to have an impedance of 5 Ω. The gas discharge tube was divided into two independent sections, each being powered by one half of the cables. The plasma tube is glass with three copper ring electrodes. The outer electrodes were the high voltage electrodes and the centre electrode was the ground return.

The silver braid surrounded the plasma tube and served as the outer conductor, the discharge plasma as the centre conductor. The laser tube thus constituted a continuation of the coaxial transmission line. The inner and the outer diameters of the tube were chosen to match the impedance of the cable, and very fast rising large amplitude current pulses were produced. Superradiance was observed at 337 nm using one mirror.

To increase the rate of rise of current further, a special Blumlein pulse generator was employed in a transverse excitation arrangement (Shipman 1966), and the 337 nm superradiance studied. A 6ft by 12ft flat plate Blumlein transmission line storing 320J was used and the discharge channel

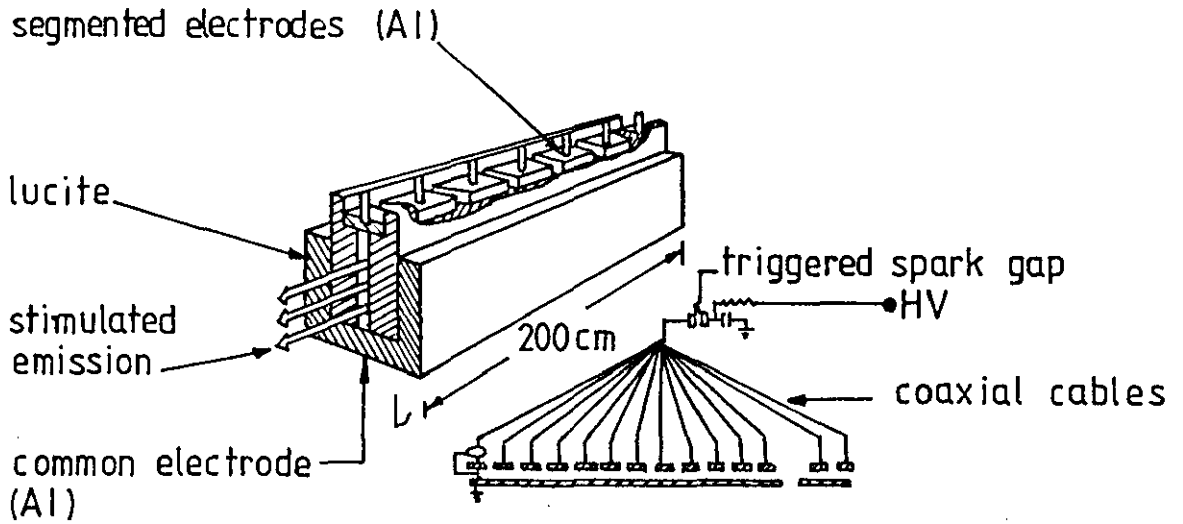


Fig. 3.7.a: Schematic of apparatus in which the electric field is perpendicular to the stimulated emission. (after Léonard 1965).

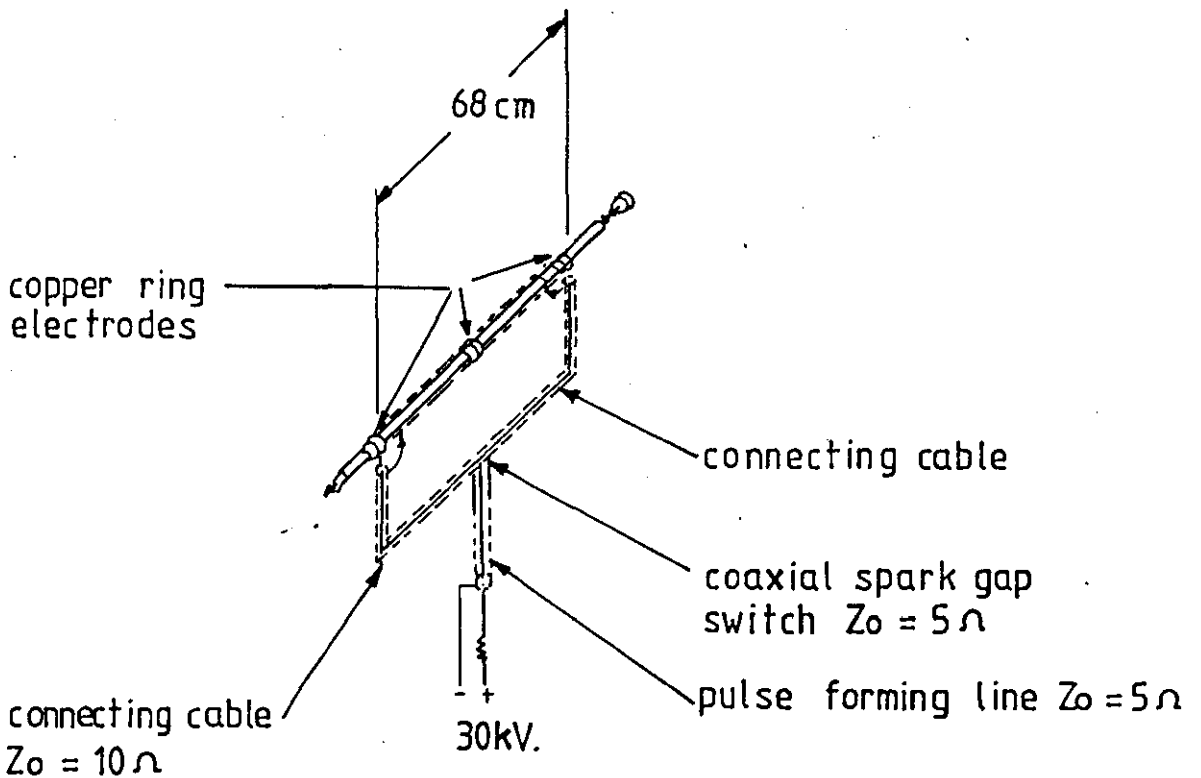


Fig. 3.7.b: Coaxial transmission line nitrogen laser (after Geller 1960).

was between the two segments of the top plate. The triggered switches were located at one end of the plate and after they closed a discharge occurred across the gap in the top plate. The pulse duration was about 30 ns and the pulse amplitude was 150 kv. The line impedance was 0.3Ω and the current had risen to 400 kA in 4 ns.

Shipman (1967) extended this technique to achieve travelling wave excitation of the laser, Fig. 3.7.c. In this method the switches in the Blumlein pulses were closed sequentially and a wave of excitation current started from one end of the discharge gap and progressed towards the other or output end. The time sequence of the switches was so adjusted that the velocity of the travelling wave of excitation current equalled the velocity of light. A plasma element at the starting end would emit spontaneous radiation, but subsequent elements would be preferentially stimulated to emit toward the output end by the amplified emission of the first element, before having time to emit very much spontaneous radiation in other directions. The power output in the direction of the wave of excitation was at least 10 times that in the other direction and was 2.5 Mw in magnitude.

Small and Ashasi (1972), have modified the Blumlein discharge circuit by using a modified electrode configuration (Fig. 3.7.d), which allows uniform excitation over a large cross-section. An interesting feature of this design is that the discharge can be confined, at suitable operating pressure, to a region between the electrodes and completely away from the walls: for instance for N_2 at 30 torr, there was no interaction with the walls. At that pressure and for an applied voltage of 20 kv, a discharge length of only 15 cm produced 20 kW of peak power output.

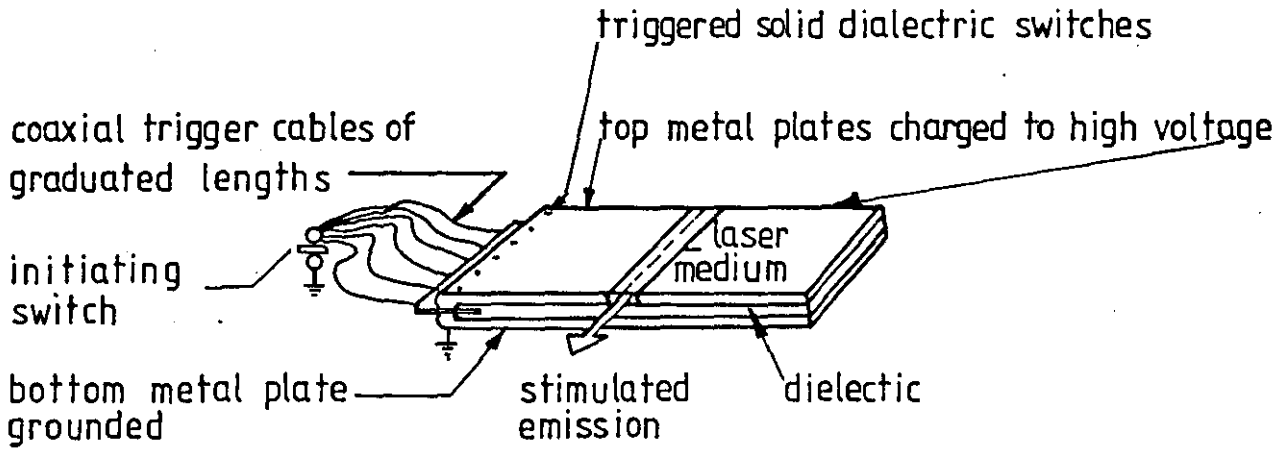


Fig. 3.7.c: Schematic of the Blumlein generator with flat plate transmission line. (after Shipman 1967)

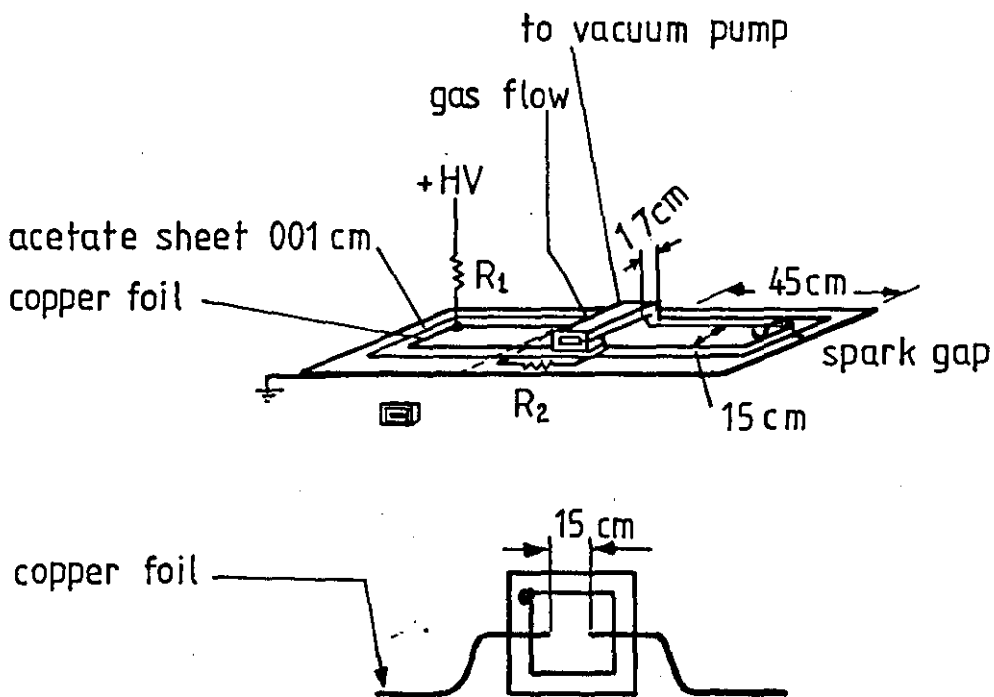


Fig. 3.7.d: The modified Blumlein excitation method in which the discharge is pressure confined and does not touch the vacuum enclosure. (after Small et al 1972).

A double parallel-plate transmission line, Fig. 3.7.e, giving half the impedance of the simple line was used by (Basting et al 1972). It had an additional advantage that the outer conductors are at ground potential, thus reducing electromagnetic interference caused by the high voltage transient on the inner conductor and in the plasma. A peak power of 1.2 MW in an active length of 30 cm was obtained.

3.6.2 Nitrogen High Pressure Laser (TEA)

Since the first transverse excited N_2 low pressure laser by (Leonard 1965), a transverse excited N_2 laser operated at 1 atm in order to achieve high peak power suitable for dye lasers pumping has been constructed.

The first transverse excitation N_2 laser at 1 atm was developed by (Salzmann 1974) using a Blumlein circuit. The energy storage capacitors consisted of 60 parallel strips each 6 mm wide, spaced by 2 mm. Using 0.6 mm thick mylar foil as insulator this resulted in an impedance of $\approx 25 \Omega$ of a single strip line. The strip lines were interconnected by inductance coils, thus permitting simultaneous slow charging but preventing coupling when the Blumlein circuit is switched. The electrodes of the discharge consisted of two parallel rows of copper cylinders. A peak power of 1 MW from this laser with 400 ps pulse duration was achieved.

Bergmann (1976), used a Blumlein type discharge in a TEA N_2 double discharge laser (fig. 3.8). Preionization was achieved by permitting the end of the upper electrode on the spark gap to extend slightly into the laser cavity as indicated in Fig. 3.8. An output energy of 355 J/pulse at 21 kv with an efficiency of 0.039%, and with repetition rates of 5-25 p.p.s. at 337 nm were obtained.

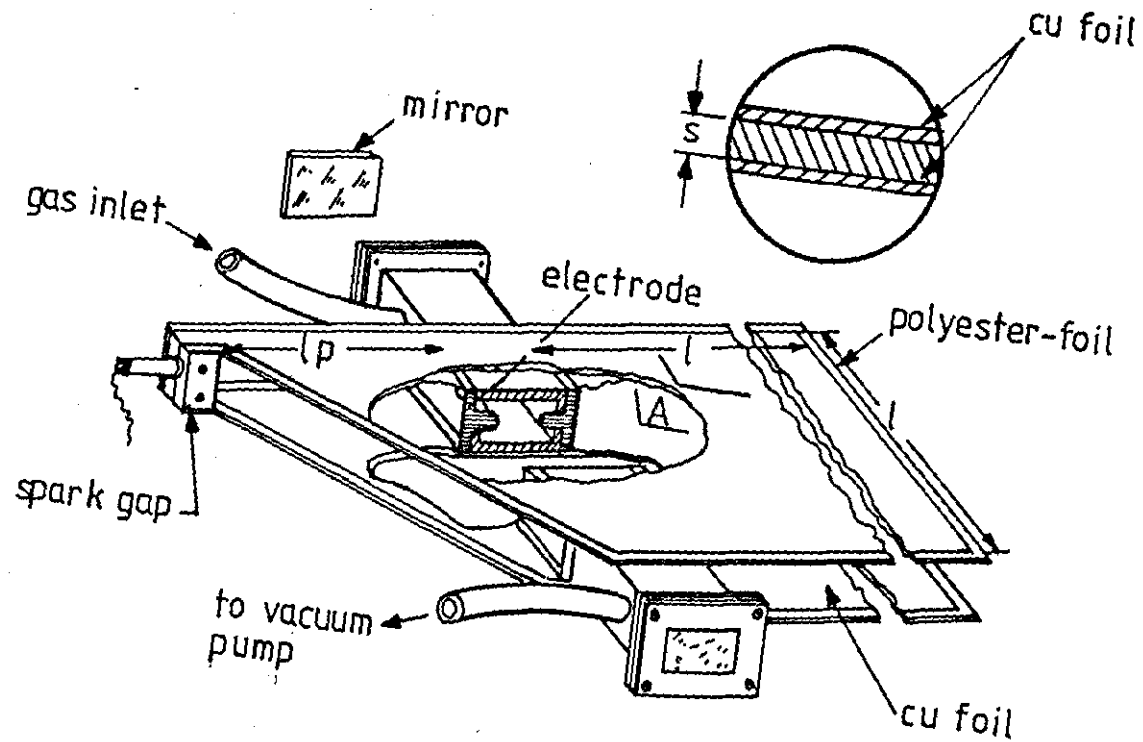


Fig. 3.7.e: Perspective view and partial cross section of the laser. (after Basting et al 1972).

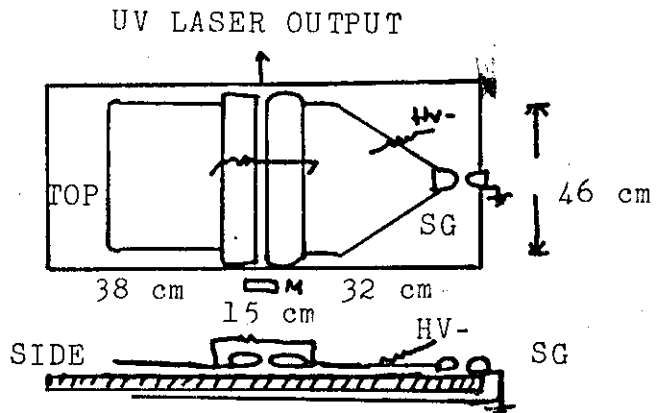


Fig. 3.8: Blumlein type discharge TEA N_2 laser. (after Bergmann 1976).

3.7 Summary

A brief summary of the spectroscopy of the N_2 molecules has been made together with the various band systems. The second positive bands system is the most important band system in which most of the N_2 lasers are operated.

The theory of obtaining a population inversion in the nitrogen molecule has been made together with the various excitation circuit and electrode configuration. It is clear that a fast excitation circuit is needed for N_2 laser since the lifetime of the upper laser level is short.

Finally the relevant work published on the excitation of TEA nitrogen triplet laser systems and TEA N_2 lasers has been reviewed.

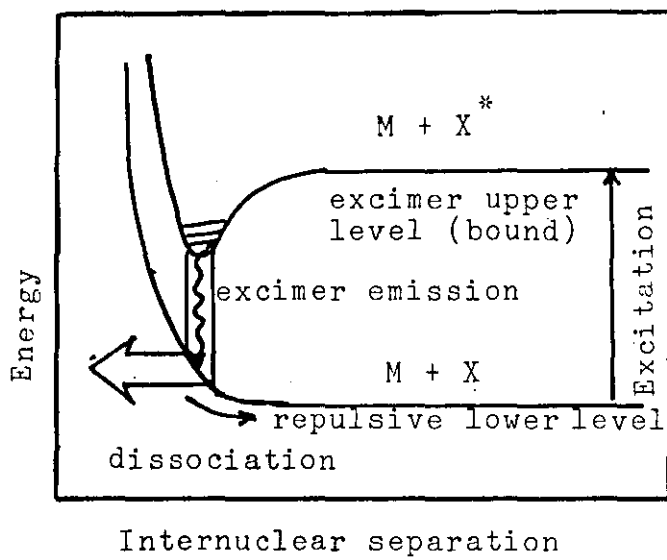
Chapter 4

RARE GAS HALIDE EXCIMER LASERS

4.1 Introduction and Background

Before 1975 the only efficient high power lasers were the infrared gas lasers: CO_2 , CO , and HF . In the ultra-violet region this changed with the introduction of the excimer lasers. The term "excimer" is a condensed term for "excited dimer", and refers to a two atomic molecule that exists only in the excited state. In principle this word is correct only if it concerns two identical atoms, or molecules, but in practice it is used also for "exciplexes", excited complexes, consisting of different atoms. The distinguishing feature of the molecules used in these lasers is that the excited molecule exists in a stable configuration (bound) but the ground state molecule does not (unbound). The basic molecular structure is shown in Fig. 4.1. The transition from the bound upper level to the unbound (free) ground state is followed very rapidly (10^{-13} s) by dissociation which implies an automatic population inversion. There are some implications of such a system (bound-free), as follows:

- (a) Since the transition is a bound-free, laser action should be tunable over a wide range.
- (b) Because of the broad line width (tunability) the gain on the laser transition is low, allowing a substantial amount of energy to be stored in the upper state (high power).
- (c) Since the transition occurs from a low excited state to a state near ground, the efficiency (laser output energy over excitation energy) is very high.



Vib. 4.1 Basic molecular structure for a bound-free excimer

The idea to use such a bound-free electronic transition to provide gain was first expressed by (Houtermans 1960), the same year as the first demonstration of a laser by (Maiman 1960). Later (Basov 1971) observed laser action in a Xe_2 excimer at (170 nm), using an e-beam to pump liquid xenon. Kohler et al (1972) have demonstrated laser action in high pressure gas Xe, pumped by an e-beam. The output power from these lasers and other lasers; Ar_2^* , Kr_2^* demonstrated by (Hughes 1974, Hoff 1973), was not reproducible due to their sensitivity to impurities and mirror damage. Velazco and Setzer (1975), discovered a new class of excimer laser when they observed the emission spectra of halogens in a low pressure xenon mixture. But the first of this class that could be made to lase was XeBr^* at 282 nm, (Searles and Hart 1975), using an e-beam pumping technique, followed by XeF^* , XeCl^* and KrF^* (Brau and Ewing 1976). Table 4.1 gives a survey of all possible combinations of rare gas halide excimer lasers and their wavelengths. Due to the higher efficiency and pulse energy of the rare gas halide compared with other excimer lasers such as mercury halides (Parks 1978) they became the most attractive lasers. Of these, the KrF laser (351 nm) which has the highest intrinsic efficiency $\approx 12\%$, and the highest single pulse output energy 350 J (Hunter 1978). The KrF laser has recently become a promising candidate for laser fusion having a more appropriate wavelength and possibly a higher total efficiency than CO_2 laser (Krupke et al 1979).

Stimulated Raman scattering has been used to shift the wavelengths of XeF, KrF and ArF lasers (Djeu 1977, Loree 1977). The wavelength capability of these lasers has been used in a number of techniques including optical pumping of other laser

Table 4.1: Rare gas halide laser wavelengths. Central wavelengths in nanometers. Laser action has been observed in the combinations above the dashed line.

	Ne	Ar	Kr	Xe
dimer		126	146	172
F	107	193	249	351 (483)
Cl		170	222	308
Br		166	206	282
I			185	252

media. Optically pumped dyes are attractive because they are continuously tunable over a broad range. XeF (351 nm) laser radiation is useful for pumping a variety of visible dyes with greater overall efficiency than N_2 (337 nm) lasers and less dye degradation than flashlamps. Since the photon energy is in the range of many chemical bands, then lasers are usable in a wide new field of photochemistry, such as photochemical separation, micromachining and lithography processes.

4.2 Rare-Gas Halide Spectroscopy

The general structure of the rare gas halide excimer molecule is shown in Fig. 4.2, in which M and X represent the rare gas and halogen atoms respectively. The deeply bound upper laser level (MX^*) is ionic in nature and is represented by M^+X^- . The excited state consists of a positive charge rare gas ion M^+ , and a negative halogen ion X^- , held together by Coulombic forces. An electron from the complete P shell of the rare gas atom is transferred to the partially occupied P shell of the halogen atom, resulting in a term configuration of $2P$, and $1S$ of the rare gas ion M^+ , and halogen ion X^- respectively. Therefore the upper ionic species M^+X^- which form the upper laser level has $1S$ (halogen ion) and $2P$ (rare gas atom) characters. It is apparent from Fig. 4.2, that the upper laser level (MX^*) is bound with respect to dissociation into an inert gas atom M and an excited halogen atom X^* . It is also bound with respect to an excited inert gas atom M^* and a halogen atom X. Forecasts of various properties of the rare gas halide excited state (MX^*) are similar to the ionic ground states of the alkali halide molecules. This is obtained from the fact that a rare gas halide ionic excited state differs by only one electron

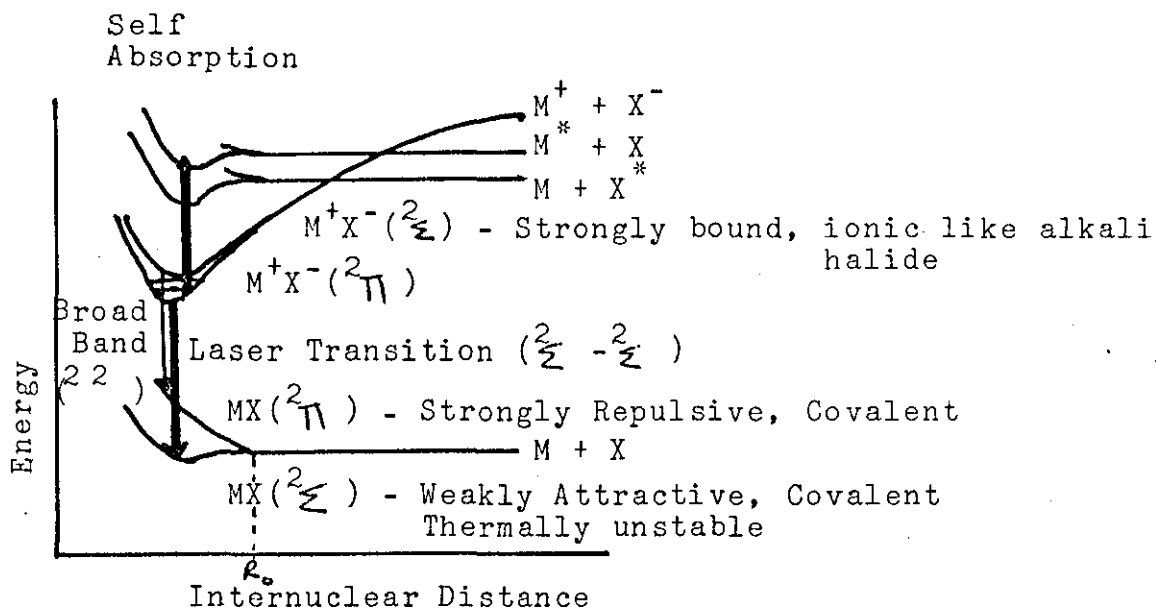


Fig. 4.2: Potential energy diagram of rare gas halide molecule showing laser and self-absorption transitions. (after Brau 1978).

from an alkali halide. Therefore many properties of, for example KrF^* can be derived directly from the ground state of the RbF molecule. Furthermore, the rare gas excited states atom such as Kr^* have low ionization potential $\approx 4 \text{ eV}$ resulting in similar chemical properties of Rb .

At close internuclear separation R_0 , the upper laser level splits into a ${}^2\Sigma$ and a ${}^2\Pi$ states due to the two possible orientations of the incompleting P shell of the rare gas ion. The ${}^2\Sigma$ state is the lowest and it is referred to as the B state, while the ${}^2\Pi$ state is referred to as the C state. The lower laser level is the covalent ground state that results from the interaction between the rare gas atom and halogen atom in their ground state (1S, 2P respectively). Once more in the region of the equilibrium internuclear separation R_0 , the ground state splits into a ${}^2\Pi$ state and a ${}^2\Sigma$ state. This split in the ground state is similar to that in the upper level except this time it is the halogen atom which has the incompleting P shell. The ${}^2\Sigma$ is the lowest state and since it forms the ground state of the dominant laser action, it is referred to as the X state. It has a fairly flat potential energy at R_0 and is most weakly bound; 255 cm^{-1} for XeCl (Tellinghusion 1976). Since it is fairly flat, the emission width, terminating at the ${}^2\Sigma$ state, near wavelength λ_1 , is narrow (Ewing 1976). On the other hand, the ${}^2\Pi$ state is strongly repulsive at the equilibrium internuclear separation R_0 of MX^* , because more electrons are between the halogen and rare gas nuclei. This state is referred to as the A state. Since it is strongly repulsive, the emission terminating on the ${}^2\Pi$ state, near λ_2 is characterized by a broad continuum band width. Therefore the gain ($\approx \lambda^2/\Delta W$) for this transition is smaller than that for

the B - X transition which gives rise to the dominant laser action. These laser transitions are strongly allowed with lifetimes of the order of 10 ns, and gain cross section of the order of 10^{-10} cm² (Brau 1977) with stimulated cross section of the order of 10^{-6} cm² (Searles 1977).

Since the Coulomb potential is a slow function in the equilibrium internuclear region R_0 , therefore the excitation energy E^* of the excimer (B state) may be approximated by the formula (Brau 1978):

$$E^* \approx IP \text{ (rare gas atom)} - EA \text{ (halogen atom)}$$

where IP is the ionization potential, and EA is the electron affinity. The smaller the halogen ion, the smaller the length of the ionic M - X band will be and so the greater the ionic dissociation energy.

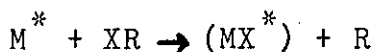
Since the halogen atoms have similar EA (≈ 3 ev), the smallest ions, the fluorides, will have the lowest B states. Therefore the B - X emission wavelengths of the halides of a given rare gas decreases monotonically with increasing atomic number of the halogen, see Table 4.2. Also, since the IP of the rare gases increase with decreasing atomic number, therefore the B - X emission wavelengths of a given halide of different rare-gases decreases monotonically with decreasing atomic number (see Table 4.2).

Table 4.2: Showing the different wavelengths of each noble gas halogen lasers with respect to different halogens.

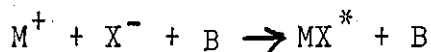
<u>Excimer molecule</u>	<u>Lasing Wavelength/nm</u>
KrF	248
KrCl	222
XcF	352
XeCl	308
XeBr	283
ArF	193
ArCl	175

4.3 Rare Gas Halide Kinetic Reactions

The basic reason for the higher power and efficiency of the rare gas halide lasers lies in very favourable kinetics for the formation of the upper laser level. Since the gas mixtures used in rare gas halide lasers contain approximately 90% buffer gas (He, Ar), less than 10% of the noble gas (Kr, Xe) and less than 0.5% of the halogen donor such as F₂, Cl₂, NF₃, HCl, etc. Therefore the result of electrical excitation or electron beam excitation of rare gas halide mixtures is to produce excited rare gas atoms, ions, and electrons. They form rare gas halides through two major types of reactions. The first reaction is the so called "harpooning" reaction involving an excited rare gas atom M^{*} and the halogen donor XR:



where R is a radical attached to the halogen X. In all cases, rates are large $\approx 5 \times 10^{-10} \text{ cm}^3 \text{ s}^{-1}$, and where XR is the X₂ halogen molecule the reaction rate is largest and the selectivity of the process approach unity (Green 1978). The term "harpooning" is derived from considering the electron that hops from M^{*} over to the halogen molecule XR at a point where the potential is large. Then the Coulomb force pulls apart the covalent bond of the halogen molecule and the harpoon electron is returned to the noble gas ion and a stable excimer is the result. The second reaction is three body ion-ion recombination:

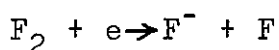


where B is a third body, often a buffer gas.

Both these reactions are very fast, occurring in times typically of the order of 10 ns (Brau 1978).

The dominant reaction for populating the upper laser level depends on the excitation conditions, the partial pressures of the constituents, the constituents themselves, and the overall pressure. Therefore the harpooning reactions are the dominant mechanism in the electric discharge excitation while the ion-ion recombinations are dominant in the electron-beam excitation (Hutchinson 1979).

In the monofluorides, ion-ion recombination reaction is dominant due to the rapid production of F^- ions (10 ns) by dissociative attachment with the electrons as:



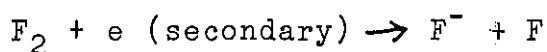
The formation of KrF^* excimer, particularly by electron-beam excitation methods has been studied by many groups (Rakni et al 1977). By way of example and due to their high efficiency, consider the formation of KrF^* excimer molecule with argon as a buffer gas and fluorine as the halogen donors.

(a) Ion-Channel Processes

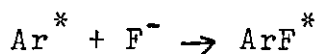
Since the mixture contains only Ar, the largest part of the deposited energy results in argon ion-electron pairs:



The dominant loss of secondary electrons is through the dissociative attachment to F_2 with a very fast rate of $5 \times 10^{-9} \text{ m}^3 \text{ s}^{-1}$:



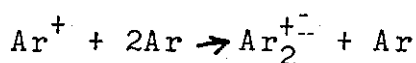
The Ar^+ ion can recombine with the fluorine ion to form ArF^* as:



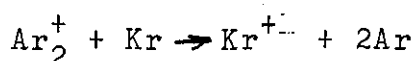
This excimer can emit radiation at 193 nm, and has a lifetime of about 4 ns, but it is likely that the Ar is replaced by Kr:



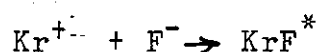
The above ion channel processes for the formation of KrF^* occurred at low pressure ($1 < \text{atom}$). Therefore at higher pressures, the most important route is through the argon dimer ion which is formed in the three body reaction:



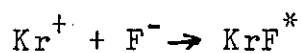
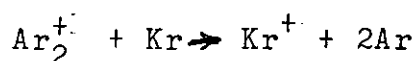
then the Ar_2^+ ion undergoes charge transfer to the less energetic Kr^+ ion:



After which recombination with fluorine ion occurs:

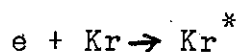
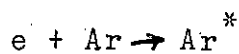


Other kinetic reactions can occur:

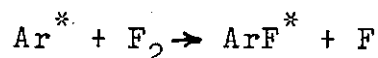


(b) Harpoon Reactions

The direct electron impact with the rare gas atoms produces metastable excited state more efficient than ions:

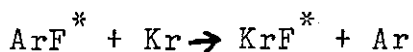


The harpoon reaction for Ar is

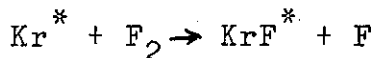


and then the ArF^* excimer can again react with Kr in a

displacement reaction to give KrF^* excimer:



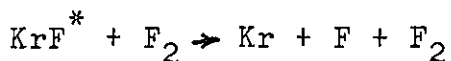
The Kr^* also undergoes harpoon reaction:



4.4 Excimers Quenching Processes

The formation of the upper excimer laser level MX^* with very large efficiency does not necessarily lead to a high laser energy output. Quenching of the laser upper level may compete with stimulated emission and so terminate the laser action. The most effective loss processes of the upper laser level is the collisional quenching and photo-absorption.

The major problem is the quenching by collision with the halogen such as:

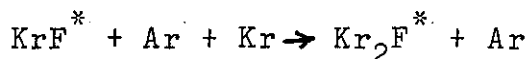


The fluorine F_2 quenching of the upper laser level and the radiative decay (for KrF^* in 8 ns) are equal at a fluorine pressure of ≈ 6 Torr (Green 1978). Therefore this reaction determines the upper limit of the F_2 concentration to a low level usually less than 0.5%.

Other significant collisional loss processes is the quenching by the rare gases:

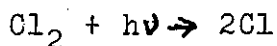
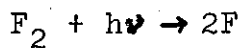


and

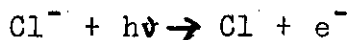


These reactions are extra harmful, because their products are strong absorbers for the radiation.

Photo-absorption by the halogen is most important in XeCl (308 nm) and KrF (248 nm) excimer lasers (Brau 1978). Reactions such as photo-dissociation of the halogen



and photo-detachment of negative ions found in the plasma



The problem can be avoided in XeCl laser by using HCl or CH_2Cl_2 , BCl_3 , in place of Cl_2 (Burnham 1978), and in KrF by using NF_3 , SF_6 , N_2F_2 , in place of F_2 (Bhannick 1976, Andrew 1978).

Finally there is a possibility of absorption by the excited rare gas halide molecules themselves. The transitions responsible for self absorptions from the upper laser level are indicated schematically in Fig. 4.2.

4.5 Excitation Schemes

The excitation methods for pumped rare gas halide excimer lasers are discussed in this section. All excimer lasers can be excited by means of pulsed electron beams, and by discharge pumping which includes electron beam stabilized and fast electrical discharges.

4.5.1 Electron-Beam-Excitation

An excimer laser pumped by a high intensity, relativistic electron beam is shown schematically in Fig. 4.3.a. Most e-beam pumped systems contain a Marx generator to attain the high voltage needed to accelerate the electrons. The Marx bank consists

of an array of capacitors charged in parallel at low voltage and discharge in series through the load by means of spark gaps, and so an output voltage pulse of order of 0.2 - 2 Mv can be generated. For long pulse e-beam systems, the Marx bank is coupled directly to the cathode of a vacuum diode. But when pulses shorter than 100 ns are required, this arrangement cannot be used because of the non-zero inductance of the discharge circuit. Therefore a pulse forming network (PFN) such as a water-dielectric transmission line (known as a Blumlein), is frequently used and slowly charges with a Marx bank. When the voltage has risen to a high enough value, a low inductance spark gap spontaneously closes, transmitting the charge to the load (diode) to give a clean pulse with a pulse length determined only by the length of the PFN line. The electron beam current density is typically of the order of 5 - 500 A cm⁻² over the area of the cathode with total currents of the order of 5 - 50 kA. The pulse duration is typically of the order of 50 ns to 1 μ s. To obtain such high current density over a large area, cold cathodes are used rather than thermionic emitters (Brau 1978). Even with the cold cathode, the diode impedance must be matched by the line impedance to achieve an optimum coupling of energy. Therefore the maximum current density in the diode is limited according to the Child-Langmuir Law: (Langmuir 1913):

$$J = 2.3 \times 10^3 \quad V^3/d^2$$

where J is the current density in A/cm², V is the diode voltage in Mv and d is the cathode-anode gap of the diode in cm.

Electrons emitted from the cathode are then transmitted by a screen anode, passing through a thin metal foil, and enter the laser cell. The metal foil is required to isolate the

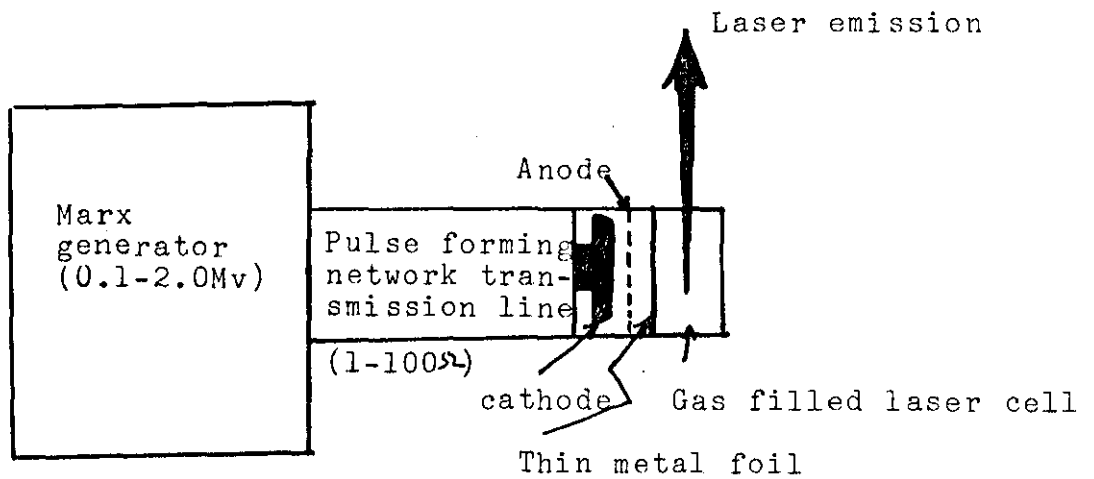


Fig. 4.3.a: Electron-beam pumping excitation method. (After Burnham 1979).

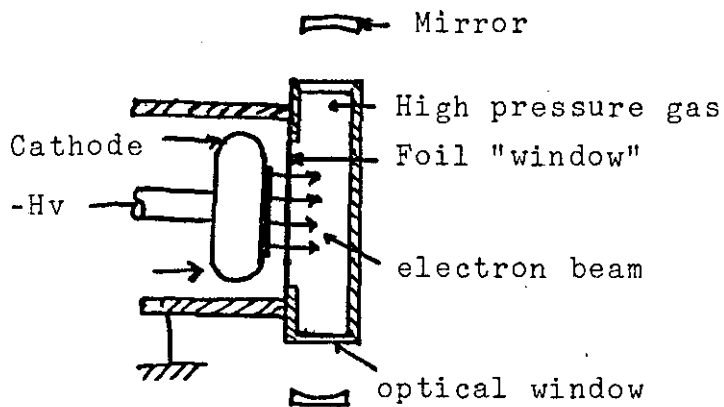


Fig. 4.3.b: Schematic diagram of a transverse electron beam pumping geometry. (After Brau 1978).

cell (usually filled with several atmospheres of a gas mixture) from the diode region. This requires a vacuum of about 10^{-4} torr for the generation of the electron beam (Burnham 1979).

The most simple and commonly used geometry is the transverse pumping geometry shown in Fig. 4.3.b, but coaxial geometries (Ault 1975) in which the electron beam is accelerated radially inward, entering the laser cell through a cylindrical foil, and axial geometries in which the e-beam is injected near one end of the laser and guided along the axis by a magnetic field (Hoffman 1976) have also been used. Since the transverse geometry is simplest, the target gas in the laser cavity is usually thin, therefore most of the electrons pass through the laser cell and deposit their energy in the far wall. Typically, of the order of 5 - 50% of the e-beam energy entering the cell is deposited in the gas in the laser cavity.

As the electrons pass through the laser gas, they produce excited rare gas atoms and ions, with an average energy $\bar{W} \approx 20$ ev deposited in the gas for each ion and excited state produced (Lorents 1976). Thus in a KrF laser with a photon energy $h\nu$ (5 ev), the maximum possible efficiency is $\eta(\text{max}) = h\nu (\text{KrF}) / \bar{W}(\text{Argon}) = 25\%$. Intrinsic efficiencies (laser energy/deposited in gas) as high as 15% have been achieved from KrF (Brau et al 1976), but overall ("wall plug") efficiencies have been much lower (Bhaumik 1976). Using a large area electron beam, pulses are as large as 350 J with an intrinsic efficiency 10% have been obtained from KrF (Hunter 1977). This was achieved in a 600 ns pulse using a large area (2 m by 20 cm), relatively low current density (10 A cm^{-2}) electron beam to pump a 60l volume in a transverse

geometry. The highest intrinsic efficiency reported is 15% obtained from KrF (Bhaumik 1976). This was achieved in a 1.5 J, 125 ns pulse from a coaxial electron beam. However, large pulses are possible, but ultimately the pulse energy becomes limited to something of the order of the kilojoule/meter of laser length by problems of closure of the diode (the collapse of the diode impedance as the cathode plasma expands across the vacuum gap) (Bugave 1969), and by self pinching of the electron beam by its own magnetic field (Livingston 1962).

The length of the laser also is limited by photo-absorption processes (Section 4.4), and by the onset of parasitic oscillations under high gain conditions. The gain may be reduced to suppress parasitic oscillations by pumping at reduced current densities for longer periods, but must remain large compared with the absorption for efficient laser energy extraction. Overall laser lengths of a few meters appear to be possible, corresponding to pulse energies as large as several kilojoules (Brau 1979). The pulse repetition frequency and therefore, the average power is limited by the rate at which the foil can be cooled, and by the clean laser medium.

In conclusion, the e-beam pumped rare gas halide excimer lasers to large pulse energy at higher average power is quite difficult, because the mentioned problem described above. Hence other techniques (discharge excitations) seem to be more efficient.

4.5.2 Discharge pumped rare gas halide excimer lasers

Compared with e-beam, discharges offer the potential for higher pumping efficiency and higher average power. The reason for the higher pumping efficiency is that it is possible, using a carefully controlled discharge, to pump the metastable levels of the rare gases directly by electron impact with very high efficiency. The high average power is achieved by avoiding or (in e-beam stabilized discharges) reducing the problems of foil heating and beam pinching mentioned before.

4.5.2.1 Electron-beam sustained/stabilized discharger lasers

In both e-beam-produced and discharge plasmas, the kinetic reactions favour the production of ions over metastable species. But in the e-beam sustained discharge method, it allows the applied electric field to be reduced in order to optimize the net production rate of metastable atoms rather than of ions and electrons. This can be achieved by a simultaneously applied e-beam which provides the auxiliary ionization rate in the plasma necessary to sustain the discharge, see Fig. 4.4a.

Since it takes less energy in the discharges to form an excited rare gas atom with a thermal electron than it takes to form an ion with a relativistic electron, therefore the electronic excitation reactions involving metastable atoms rather than ions can be used to populate the upper laser level which leads to a high laser efficiency (Green 1978). Pumping by electron beam sustained discharges offers several potential advantages over pure electron beam pumping. Since the main precursors of the excimer are metastable atoms rather than ions, the quantum efficiency is given by the ratio of the

photon energy $h\nu$ to the rare gas atom excitation energy E^* . This in KrF excimer laser, $\eta(\text{Max}) = h\nu (5 \text{ eV})/E^*(\text{Kr}) = 5/10 = 50\%$, which is twice that of an e-beam pump system. In a sustained discharge, the plasma impedance maintains low ($< 1\Omega$) which is resistant to arc formation when an auxiliary electric field is applied (Green 1978) and electrical coupling from the discharge circuit to the plasma should be relatively efficient. Since most of the pumping power is supplied to the gas from the discharge circuit rather than from the more complex e-beam system, the e-beam sustained discharge system has higher efficiencies. Longer pulses ($\sim 1 \mu\text{s}$) can be achieved by using e-beam ionization of the gas to stabilise the discharge (Braun 1979). Pulses as large as 50 J (KrF) and as long as 300 ns have been achieved by this way (Hunter 1978). The electric field strength was $2 - 2.5 \text{ kv cm}^{-1} \text{ atm}^{-1}$, and the discharge current density was of the order of 15 A cm^{-1} , corresponding to an electron density of the order of 10^{14} cm^{-3} . The maximum efficiency was 3%.

4.5.2.2 Avalanche Discharge

For many applications short pulses, lower efficiency, and high repetition rates are acceptable in the interest of simplicity. For these purposes it is possible to use unstable, fast transverse discharge as shown in Fig. 4.4.b. Discharges of this type have been used for pulsed N_2 (337 nm) and CO_2 (10600 nm) lasers. Although simple fast transverse unsustained discharges have been used very successfully to pump rare gas halide excimer of limited output energy (0.1 - 1 J) and pulse duration (10 - 40 ns) (Burnham 1978, Sze 1979). At atmospheric pressures and high electric fields, and as soon as the gas breaks down, the electrons multiply very

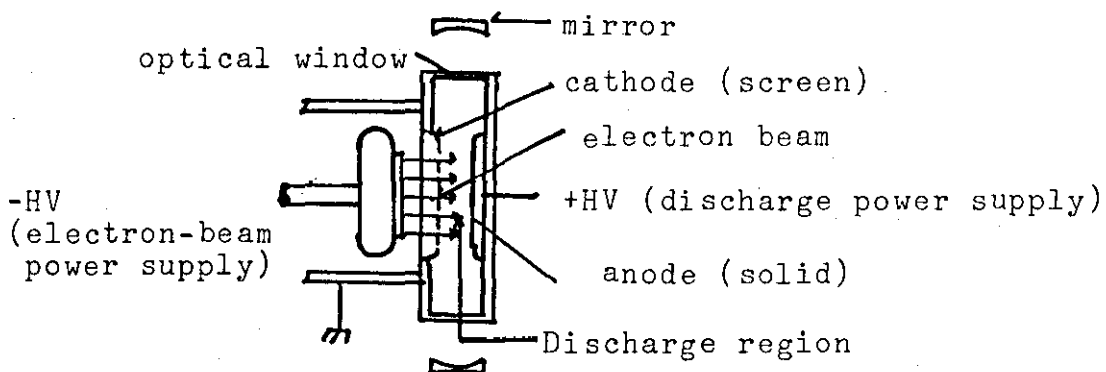


Fig. 4.4.a: Schematic diagram of a laser pumped by an electron beam stabilized discharge

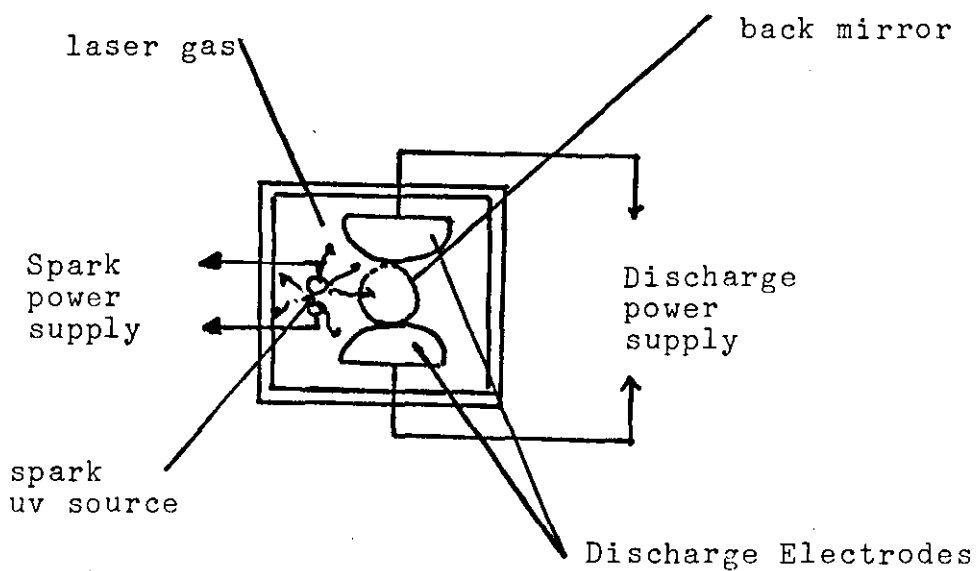


Fig. 4.4.b: Schematic diagram of a laser pumped by a transverse discharge using uv radiation from a spark source to preionize the gas.

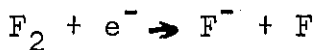
rapidly, and the plasma impedance collapses. The plasma current is then inductance limited, reducing the voltage across the discharge (Green 1978). Spatial nonuniformities in the discharge grow to form arcs in times which, at pressures of several atmospheres, can be short as a few tens of nanoseconds.

For these reasons it is therefore desirable to use, fast transverse discharges (Burnham 1976), to supply sufficient pumping energy in the short time during which the plasma impedance is high and the discharge uniform. It is also essential to minimize the inductance in the discharge and keep the current pulse short.

Various circuit designs have been used. These include Blumlein circuits with strip transmission lines (Hasson et al 1977), charged coaxial cables (Sze et al 1977), and low inductance capacitor-dumping (Andrews et al 1977), (Burnham et al 1976, McKee et al 1979). The power supply may be switched into the discharge with a low inductance spark gap (Sarjent 1977), or the series inductance of the switch may be eliminated by impulse charging the power supply (Andrews 1977), or allowing it to ring up to voltage (in a Blumlein or L-c inversion circuit) (Burnham 1976, Sze 1978), and then allowing the laser gas to break down when the voltage is high enough. Fig. 4.5 shows some of these charging circuit.

The growth of arcs in the discharge will limit the stability of the discharge to about 30 ns at low pressure (≤ 0.5 atm) (Burnham 1976), and less at higher pressures (Wange 1976). To suppress the nonuniformities in the discharge at higher pressures, two solutions have been employed. The first is to use a fast Blumlein pulse forming circuit with voltage rise times less than 10 ns. (Ewing 1975). With

this method arc formation does not have time to occur. The second method is to preionize the gas before the main discharge. This can be done by means of short preionizing corona discharge pulse (Sutton 1976), but better results have been achieved by weakly preionizing the gas with u.v radiation from a series of sparks distributed along the length of the laser (Andrews 1977, Sze 1978). The u.v radiation from the spark gaps ionizes impurities with the laser gas and produces electrons (Babcock 1976). Most of these electrons rapidly undergo dissociation attachment with the halogen donor to form a negative ion as:



These negative ions and the unattached electrons act as a secondary source which releases electrons when the discharge voltage is applied (Hsia 1977). A large and more uniform electron density will be obtained as a result of this than would be the case otherwise. The rate of the electron dissociation attachment is very fast $\approx 10^{-9} \text{ cm}^3/\text{s}$, and all the initial electrons should be attached within 10 ns (Green 1978).

Preionization using a series of spark gaps mounted along the side of the discharge channel can result in nonuniform preionization and the discharge may be constricted to the region close to the spark gaps, thereby impairing the laser beam quality.

An alternative arrangement which overcomes this problem is the mounting of the spark gaps behind a screen which forms one of the electrodes of the main discharge (McKee 1979) or by mounting a flash-board on both sides of the main discharge. This tends to produce two gain regions, which can be overcome by properly profiling the electrodes (Tallman 1980). Fig. 4.6

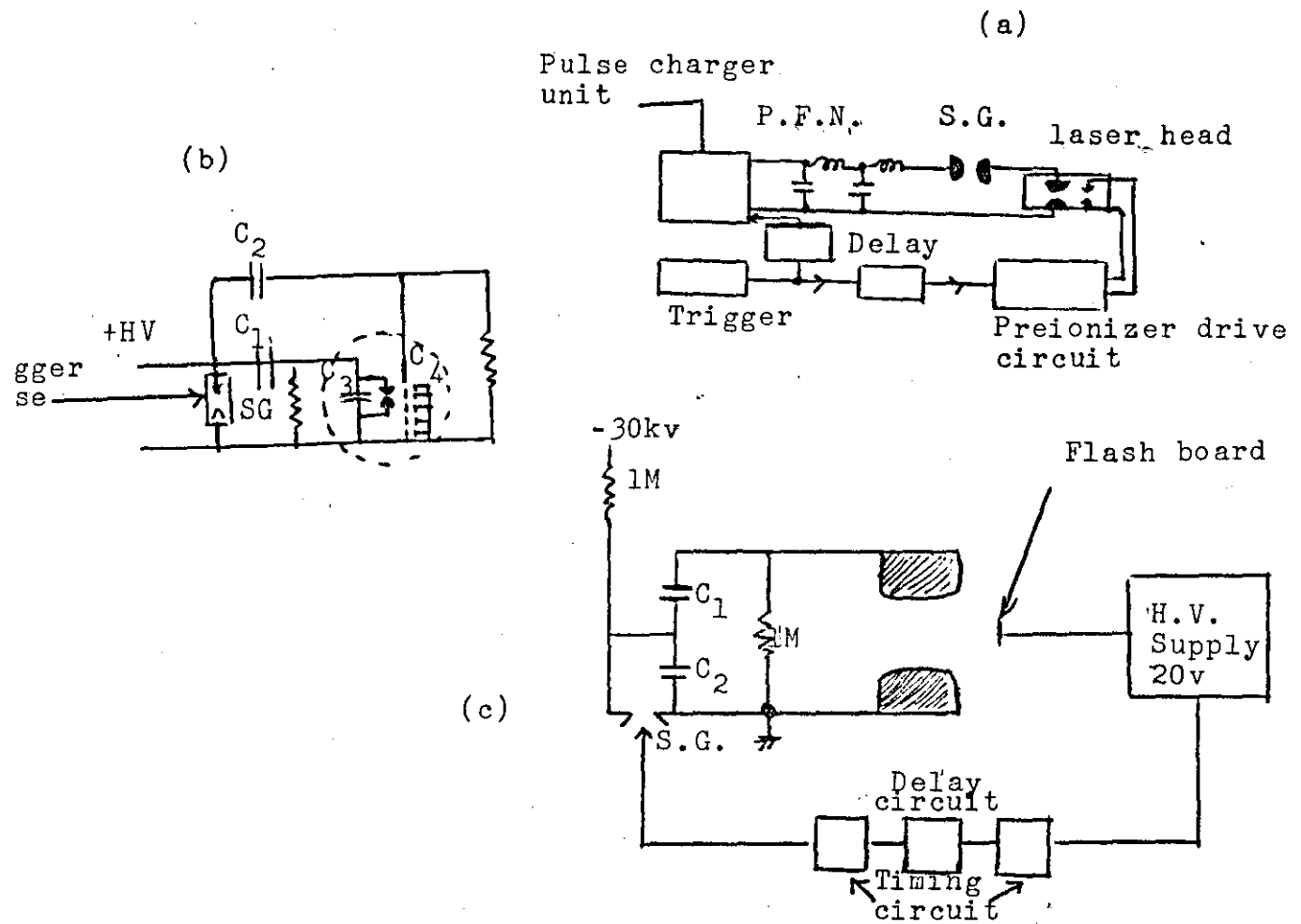


Fig. 4.5: Some electrical circuits have been used for exciting excimer lasers.

- (a) Low inductance capacitor, dumping
(After Andrews et al 1972)
- (b) Pulse forming network (PFN)
(After Sarjent et al 1978)
- (c) L-c inversion circuit
(After Burnham 1970).

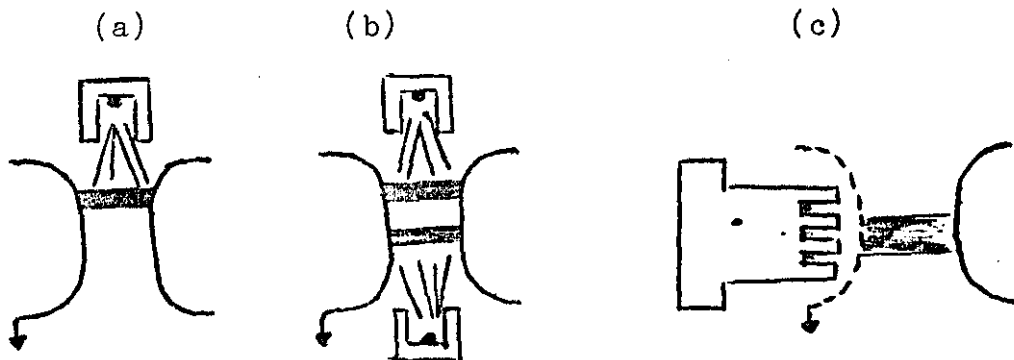


Fig. 4.6: The Different Types of Preionization (after Tallman 1980)
(a) One side; (b) Two sides; (c) Behind mesh screen

shows the different types of preionization.

The amount of the preionization produced is determined by the breakdown voltage between the electrodes and the preionizer. Therefore the level of the preionization produced is limited. The preionizer also is pulsed on just prior to the start of the main discharge, so the discharge starts at the peak of the preionization (Burnham 1979). Since the delay between the two discharges are important and could affect the laser output energy, therefore, the preionizer circuit is separated from the main discharge circuit and hence a delay unit to control the delay is required (Szeo 1979). But in most discharge circuits, an automatic delay is provided (McKee 1979).

The largest pulse energy which has been reported with an avalanche discharge is 880 J from KrF (Taylor 1978), with rather poor efficiency $< 0.1\%$. A short lumped-element, 0.15Ω pulse forming network was impulse charged to more than 100 v and switched into the discharge through an overvolted surface rail gap. This provided a very fast voltage rise-time which, together with the high voltage, made it possible to operate at as much as 6 atm. The total volume was 180 cm^3 , gave an output energy density of $0.6 \text{ J l}^{-1} \text{ atm}^{-1}$. The gas mixture was preionized with u.v radiation from a series of sparks and yielded a 15 ns laser pulse duration with no evidence of arc formation. The peak power was 40 Mw. The same system produced 250 mJ XeF laser pulses from mixtures of He with Xe and NF_3 (Sarjent 1977). Much higher efficiencies have been achieved in smaller devices with lower pulse energies. 130 mJ pulse with 1.4% efficiency from KrF have been obtained (Burnham 1976).

Lumped-element L-c inversion doubling circuit with charging voltage of 25 kv was used in this device. The same device produced 65 mJ XeF laser pulses and 60 mJ ArF laser pulses from He: Xe: NF_3 and He: Ar: F_2 mixtures respectively. The largest output energy density achieved is $10 \text{ J l}^{-1} \text{ atm}^{-1}$, obtained in a 17 mJ pulse from XeF (Godard 1976). No pre-ionization was used in this laser device, and the pulse was very short (6 ns), the pressure was only 0.7 atm.

The most important advantage of the rare gas halide excimer lasers is the pulse repetition frequency rate. The highest pulse repetition rate has been 2KHz for an XeF laser, with an average power of 24 w have been obtained by using a fast-flow system (Wang 1979). Repetition rates of 1000 Hz and average powers of 10 w have been also achieved with simple gas circulation systems (Fahlen 1978, Lumonics Ltd 1978).

For KrF and XeF lasers, the output power decreases with increasing number of shots due to the generation of contaminants (Chow 1977). The typical lifetime for each refill of gas for XeF, and KrF lasers, is 1,000 - 2,000 shots (Hutchinson 1980). Lifetimes for XeCl are much greater and by using closed-cycle gas circulation and clean up systems, fill lifetimes of $\approx 2 \times 10^5$ shots may be achieved, (Burlamacchi 1978).

4.6 Summary

The spectroscopy of the rare gas halide excimer lasers with their kinetic energy reactions and quenching process have been shown.

The excitation method, including electron-beam, electron-beam stabilized discharge, and avalanche discharge, have been made.

Chapter 5

THE LASER CONSTRUCTION

5.1 Introduction

To achieve laser action in nitrogen, excimer and carbon-dioxide lasers, a fast pulsed electrical discharge is required. Since the double discharge technique has been discovered, it has been very successfully used in different gas mixtures. Several methods have been used in order to obtain a good and uniform preionization (Chapters 2,3,4). However, this chapter describes the design and construction of a fast transverse preionizer double discharge laser. A typical design was used previously (McKee et al 1979, Tallman 1980), in which the uv radiation was provided from sparks located behind a mesh screen to preionize the gas mixture, hence a large number of electrons are produced to initiate the main discharge.

5.2 The Operating Requirements

5.2.1 Spark gap design

As a switching device, a pressurized gap was chosen. A diagram of the spark gap is shown in Fig. 5.1.a, 5.1.b. The wall of the spark gap was made of nylon. Two circular, 6 mm thick aluminium plates were inserted into the nylon and a seal was formed by means of O-rings in the nylon. A tungsten-copper hemisphere electrode was threaded to the lower circular aluminium plate by its flat side. The other electrode, threaded to the upper circular plate, consisted of the external part of a spark plug (Champion type) Fig. 5.1.c. The central electrode of it was the trigger electrode. The distance between the electrodes was kept fixed at 8 mm, giving an electrode aspect ratio $(r/d) = 3:1$ (Fig. 5.1.d.). The voltage was altered by varying the nitrogen gas pressure applied through holes in the nylon wall, serving as an inlet/outlet. The outlet side was connected to a pressure compressor.

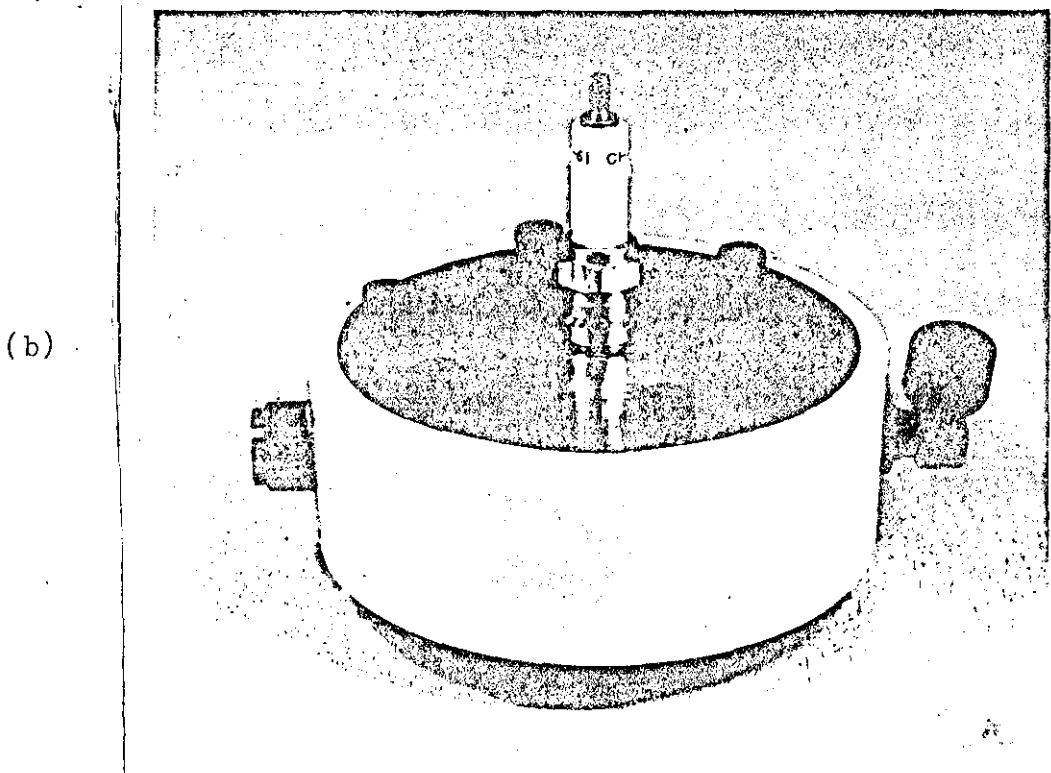
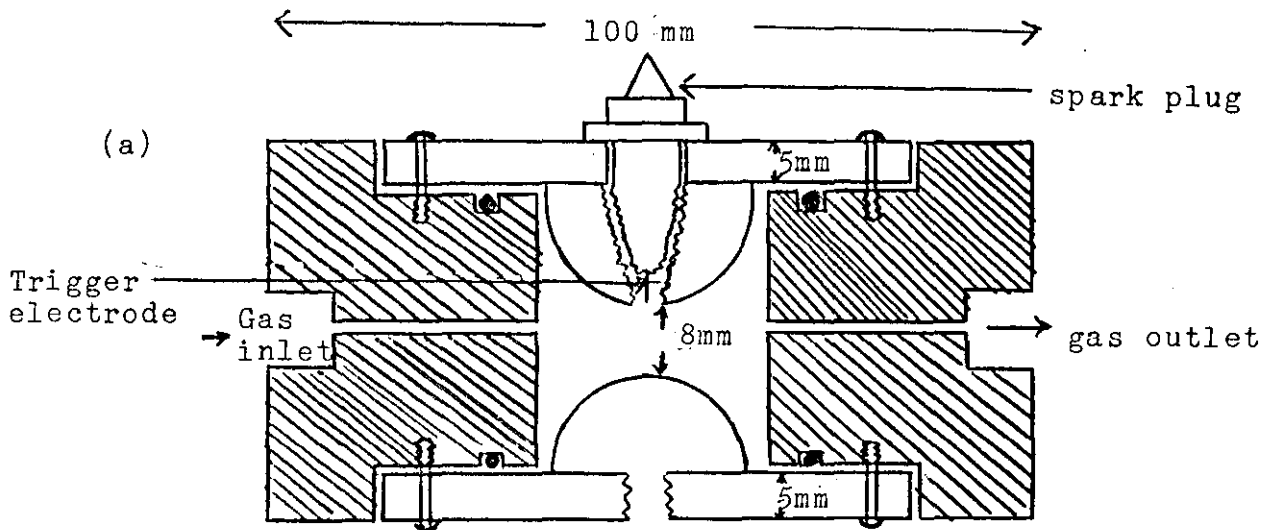


Fig. 5.1: The spark gap used with the laser:

(a) Cross section

(b) A photograph of the spark gap.

The voltage polarity configuration of the electrodes in the spark gap is shown in Fig. 5.1.d. This polarity minimises the jitter time of the main discharge (EG eG notes), and consequently requires a positive d.c. output voltage to charge the main storage capacitor.

5.2.2 Trigger Circuit Unit

The low voltage trigger box was built locally. It basically consists of a charged $1\mu\text{F}$ capacitor switched to ground by thyristor or thyration (2D21) to produce a 300v, $0.1\mu\text{s}$ rise time pulse, Fig. 5.2.a. This is applied to the primary of a car coil, which in turn is applied to the trigger electrode of the trigatron spark gap, Fig. 5.2.b.

5.2.3 The Operating Test of the Spark Gap

The output voltage from the trigger box (300v) was fed into the primary circuit of the car coil which gave a high voltage output (15kv). The photographs which were taken of the coil output voltage showed a slow rising time in the order of $7\mu\text{s}$, Fig. 5.3. This slow rising time in the coil output voltage was due to the high inductance of the coil. However, when this voltage rose to a high enough value, the trigger gap (3mm) broke down and an arc was produced which was accomplished with a sudden drop in the voltage, Fig. 5.4. Therefore, the N_2 molecules ionized due to the uv radiation from this arc - photo : emission process - which helped to breakdown the main gap of the spark gap and transferred the energy to the load (laser). Since the trigger gap was breaking down at a certain value of voltage, the gap showed a different value of voltage breakdown at different nitrogen pressure giving a jitter time $0.5\mu\text{s}$, see Table 5.1.

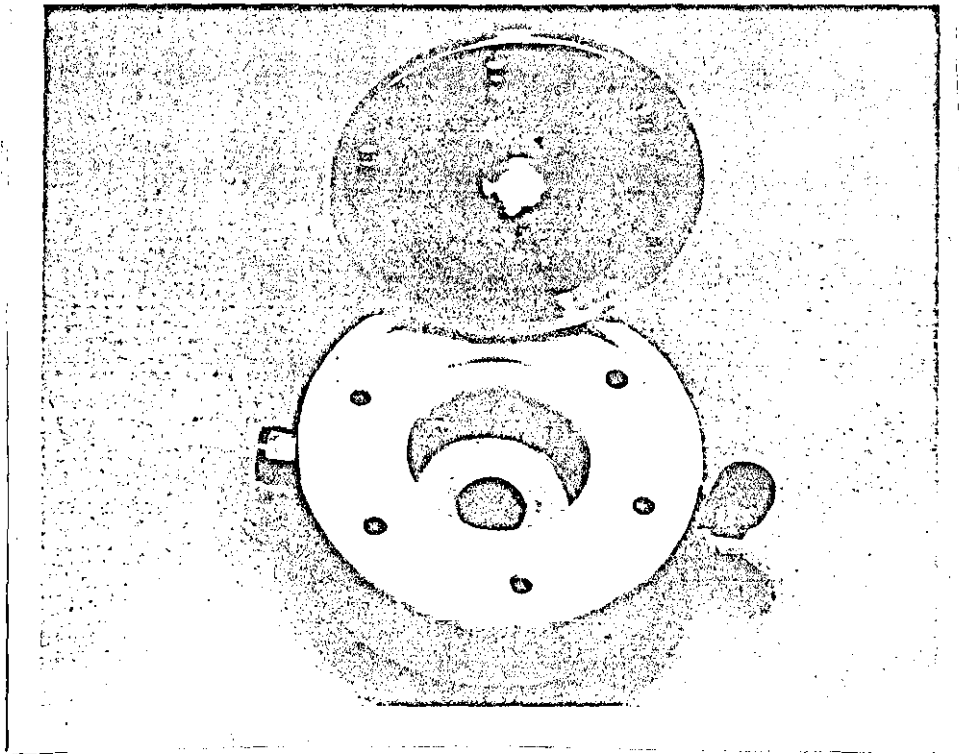


Fig. 5.1.c: A Photograph of the Spark Gap showing the electrodes.

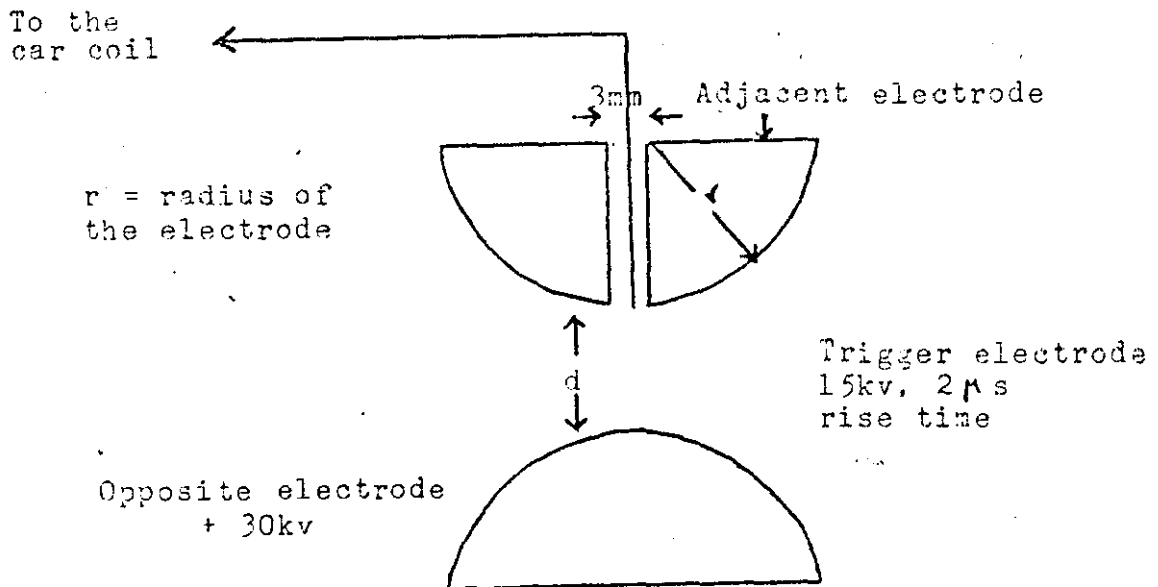
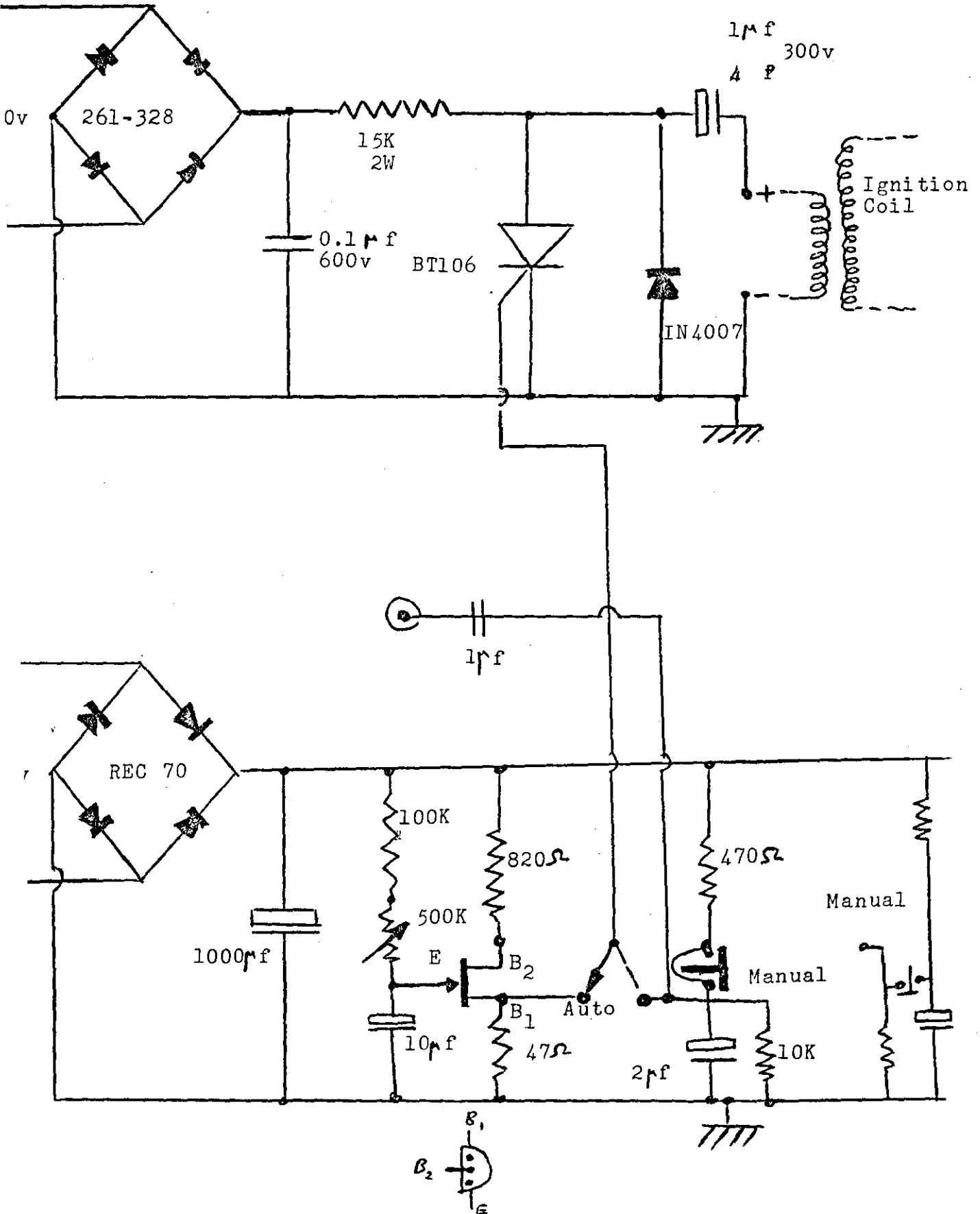


Fig. 5.1.d: Electrodes Polarity Configuration in the Spark Gap

Fig. 5.2.a: Laser Trigger Circuit (Thyristor)



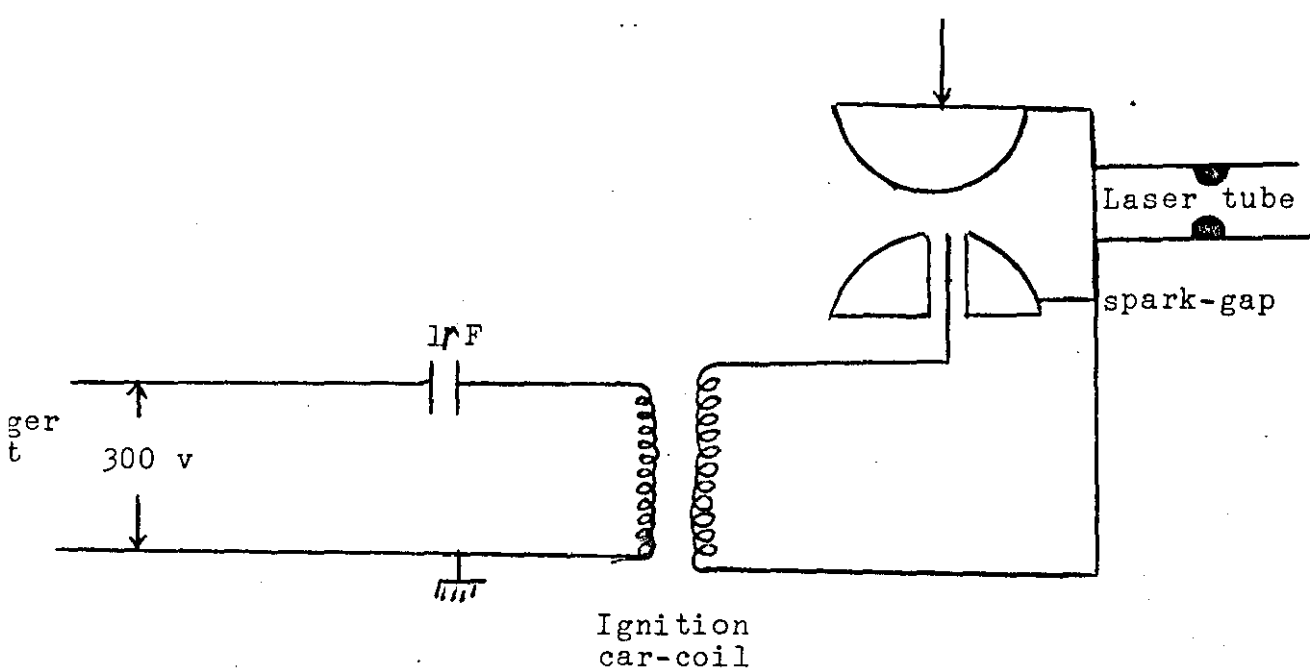


Fig. 5.2.b: The spark-gap, trigger input, and car-coil assembly for the laser firing.

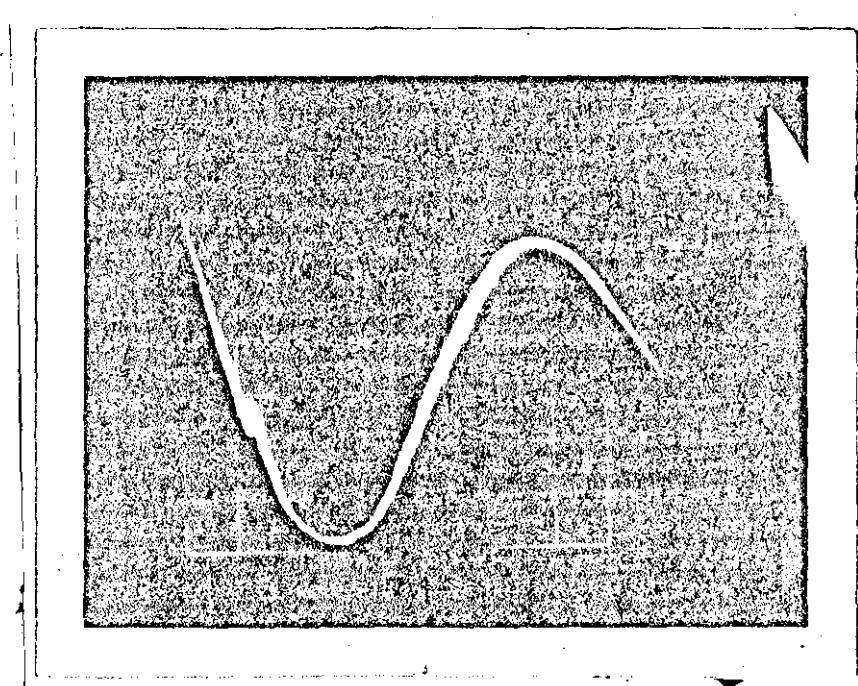


Fig. 5.3: A photograph of the car-coil pulse voltage output. (Horizontal 10 μs/div, vertical 5kv/div.)

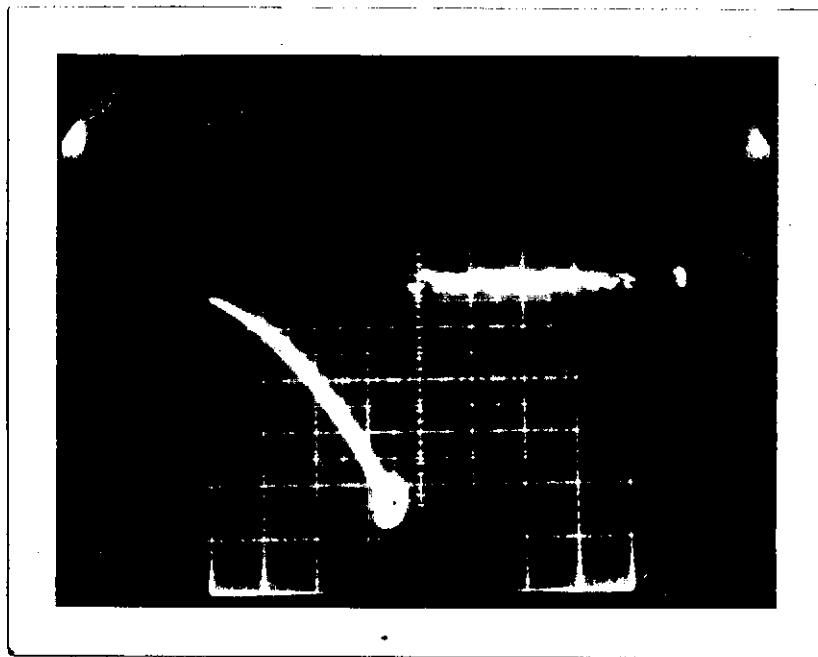


Fig. 5.4: A photograph of trigger electrode gap voltage breakdown giving a jitter time 0.5μ s. (Horizontal 2μ s/div, vertical 1kv/div .)

Table 5.1: The different value of the trigger gap voltage breakdown at different N_2 pressure

N_2 pressure/lbs.	VB/kv.
15	4.5
10	4.2
5	4.0

5.2.4 The Laser Chamber

The walls of the chamber were made of perspex in the form of a box, 40mm height, 220mm width, and 840mm length. A hole of 20mm diameter was drilled in each end of the perspex to mount the mirrors. An O-ring was placed on the upper and lower surfaces to form a seal between the aluminium plates placed above and below the box. These two aluminium plates were used to support the electrodes. A slot of 30mm width, 780mm length was made in the upper aluminium plate in the shape shown in Fig. 5.5.

5.2.5 The Preionizer Electrode

An ordinary saw blade was used as the preionizer electrode, which was placed on the cathode mesh. The length of saw blade was 740mm with 90 sharp points spaced 8mm apart. The uv radiation for ionising the gas before the main discharge was provided from these points. The gap between the preionizer electrode and the cathode was adjustable (see Fig. 5.5).

5.2.6 The Saw Blade Holder

The saw blade was sandwiched between two aluminium plates and held in position by adjustable screws. The saw blade holder was inserted into a slot in a perspex block and held in position by four large screws along its length, each individually sealed by means of O-rings, Fig. 5.5. These screws were also connected to a copper plate running parallel to the saw blade forming the electrical connection between the saw blade and the main storage capacitor. The perspex blade was in turn screwed and O-ringed to the upper aluminium plate, sandwiching the woven mesh between them.

5.2.7 The Main Discharge Electrodes

The cathode was made of a woven mesh with 0.009" hole (50mm width, 740mm length) and 40% light transmission. The woven mesh was placed in the upper aluminium slot mode especially for this purpose, and was supported by the preionizer electrode holder (see Fig. 5.5). The anode was made of aluminium (740 mm long, 65 mm height, and 10mm wide), and was machined to an approximate uniform electric field with radiused edges and end tapering, Fig. 5.6. This was connected to the lower aluminium plate by screws and a seal was formed by means of O-rings. The gap between the cathode (mesh) and the anode was 20mm, giving an active volume of $74 \times 2 \times 1 = 148 \text{ cm}^3$.

5.2.8 The Storage and the Peaking Capacitor

A low inductance 50 nF (Hartley Measurements) capacitor was used as a storage capacitor in which 22J (at 30kv) could be stored. One of the terminals was connected to the power supply (+30kv), and to the upper plate of the spark gap by means of an "L" shaped copper plate. The other terminal was connected to the saw blade by means of an "L" shaped copper plate, Fig. 5.7.a. A series of 8 capacitors (Barium titanate type), each 2.4 nF was arranged between the anode and the cathode mesh. The electrodes were 10cm away from the capacitors. These peaking capacitors were distributed along one side of the electrodes, resulting in a peaking capacitance of 19 nF. The electrical connection between these capacitors and the upper aluminium plate was made through a metal spring attached to each capacitor and pressed by the aluminium plate. The connection to the lower aluminium plate was made by means of screws, see Fig. 5.7.b.

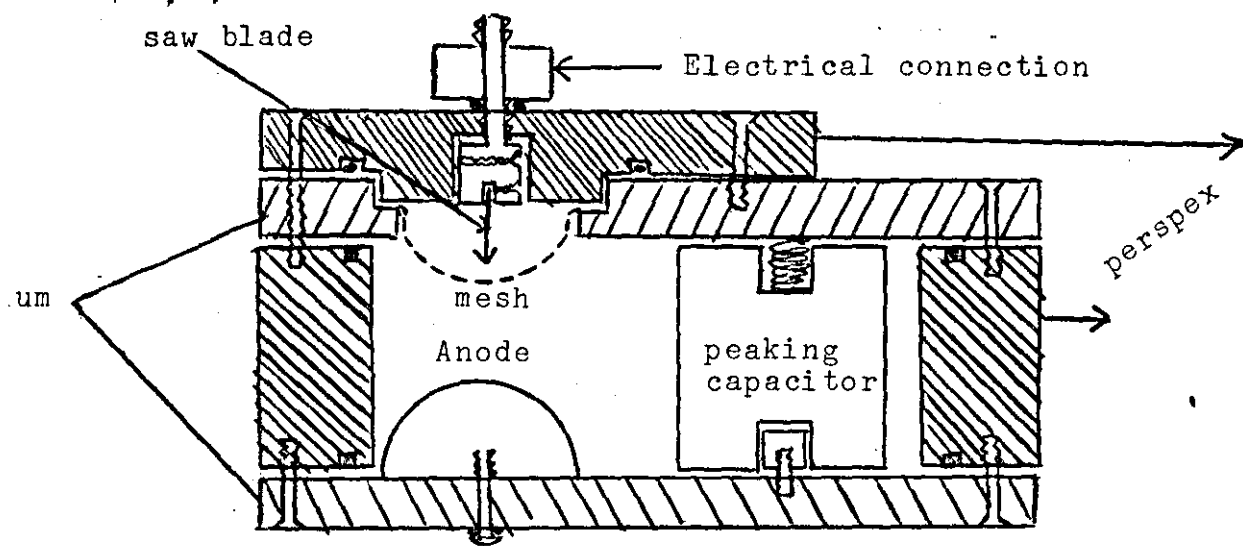
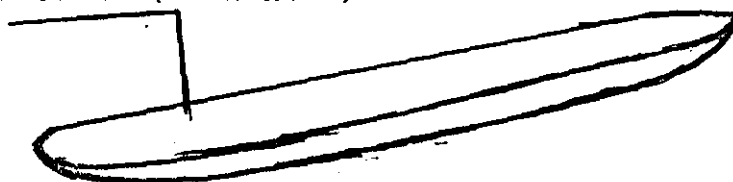


Fig. 5.5: Cross Section of the original laser chamber

Solid Electrode (Aluminium)



Preionizer Electrode

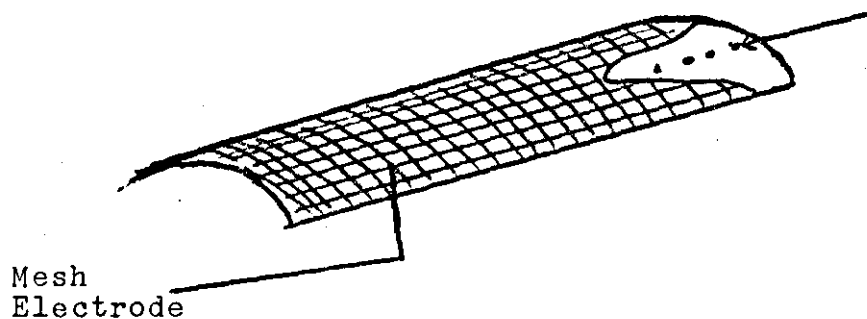


Fig. 5.6: The Electrode Structure of the Laser Discharge Model

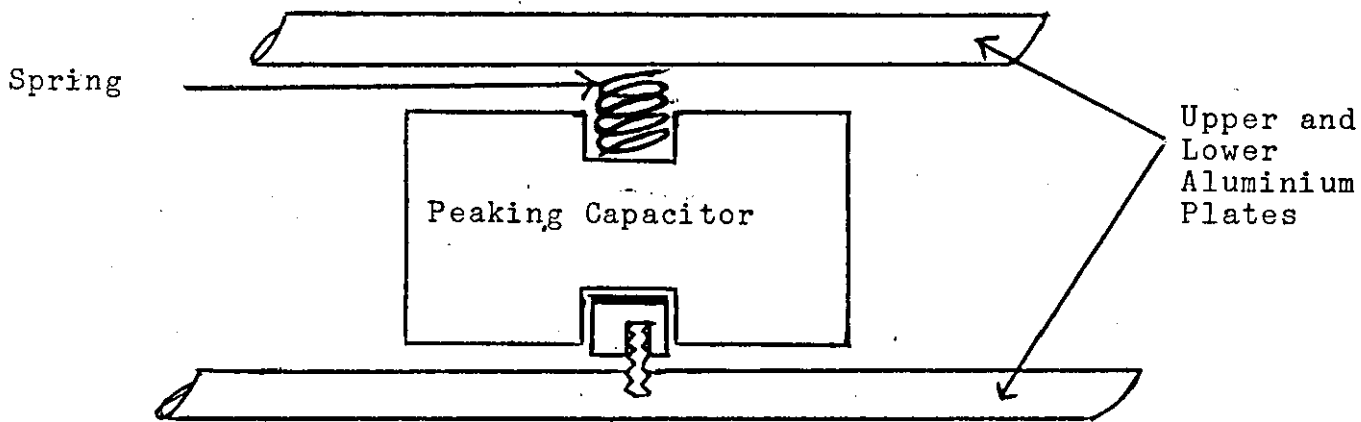
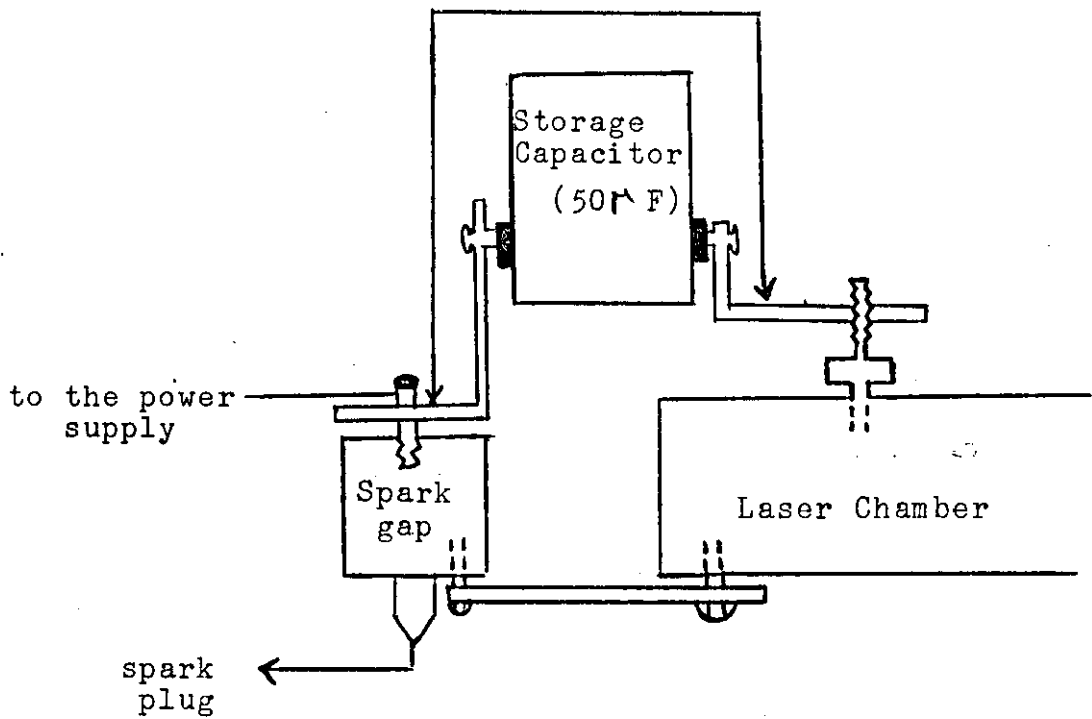


Fig. 5.7: The Electrical Connections of the Capacitor
 (a) The main storage capacitor assembly
 (b) The peaking capacitor

5.2.9 The Power Supply

A Brandenburg model 812 power supply was used to charge the storage capacitor, Fig.5.7.a. Since a positive voltage was required for the circuit operation, the polarity of the power supply was changed. A voltage range of between 15-30kv was provided from this power supply which was suitable for the gas breakdown.

5.2.10 The Operating Principle of the Electrical Discharge Circuit

The electrical discharge circuit is shown in Fig.5.7.c. in which C_s and C_p represent the storage and peaking capacitor respectively, R_1 and R_2 are the charging resistance, R_3 is the stabilizing resistance, A, k are the anode and the cathode respectively, S.G. is the spark gap, and P is the preionizer electrode (saw blade). C_1 is charged to a voltage V_1 (30kv) through R_1, R_2 . As soon as the spark gap is fired by the trigger voltage pulse, C_1 discharges all the stored energy, and therefore a negative voltage appears on the saw blade (P). The uv sparks from the saw blade sharp points will ionize the gas and hence an electron density is produced to initiate the main discharge. After the gap between the preionizer and the cathode mesh breaks down, the peaking capacitors (C_2) start to charge up to voltage (V_2): In the meantime, a high voltage appears on the cathode with respect to the earthed anode electrode. As soon as this voltage reaches a high enough value, the main gap breaks also. Then the peaking capacitors with the main capacitor discharge into the main gap as indicated by the arrows in Fig.5.7.c.

The delay time is measured between the first discharge and the main discharge. It has been found that the optimum time delay between the preionization and main discharge should be in the range of 50-200 ns (Kearsley et al 1979, Sze 1978), depending on the preionizer gap and peaking capacitors. To prevent arcing in the discharge, the energy has to be deposited in a short time compared with the arc formation time. The self inductance of the circuit is minimised by making the system compact.

5.2.11 The Mirror Mounting Construction

A perspex block with 30mm diameter hole drilled in the centre was glued to each end of the laser chamber where a hole was drilled to let the radiation out from the laser chamber. A circular aluminium plate with a clearance hole of 20mm diameter was mounted on the perspex block by means of adjustable screws, Fig. 5.8.

The optical cavity for CO₂ laser (1060 nm) was formed by using an output germanium mirror with 20% transmission and 2m radius of curvature. The total reflector was a flat gold mirror. For the N₂ and excimer lasers, a fused silica output coupler was used, with a total reflector.

The mirrors were aligned by matching the reflection of a cross. The centre of the reflector mirror was adjusted to coincide with the centre of the cross. When the output coupler was situated correctly, the image of the cross centre was found. By adjusting the screws, the cross centre was aligned to the mirror centre.

5.3 The Preliminary Test of the Discharge Uniformity

The chamber was filled with helium gas at 1 atmospheric pressure. The spark was also filled with dry N₂ gas at 1.5 bar for an operational voltage of 20kv and 2 bar for 30kv. When the spark gap was fired, a breakdown occurred between the upper and lower aluminium plates of the spark gap and not across the main gap. This was due to a high electric field concentrated on the non-uniformities of the inner surface of the upper aluminium plate of the spark gap. The problem was overcome by smoothing the surfaces of both the aluminium plates and improving the insulation of the spark gap by applying a silicone rubber

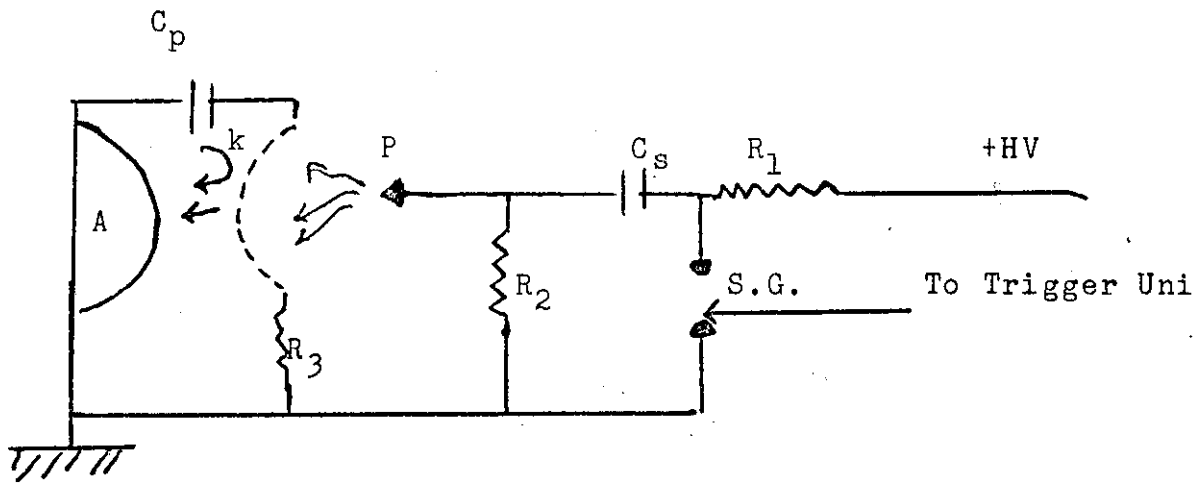


Fig. 5.7.c: The Electrical Circuit of the Laser

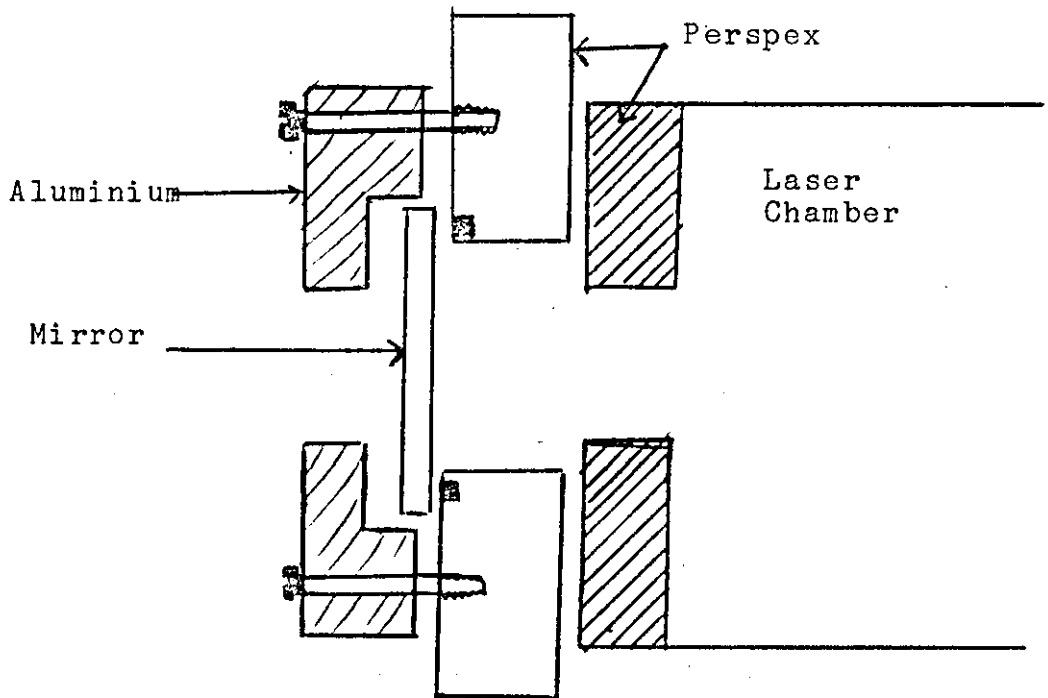


Fig. 5.8: Cross section of the Mirror Mounting

insulator to the top of the upper Al plate. Further testing revealed that the spark gap was firing adequately but that the main discharge was not uniform. Irregularities in the form of arcs occurred directly below the position of the four screws which provided the connection between the main capacitor and the saw blade.

One possible explanation is that due to the large inductance of these screws, the rise time of the current was not fast enough to dump all the stored energy ($\frac{1}{2}cv^2$) passing through the main discharge gap causing the arcs.

The second possibility is that the surface of the woven mesh was not uniform along its length, resulting in a non-uniform electric field between the mesh and the anode.

The third possibility is that the position of the peaking capacitors was 10cm from the main discharge gap. The resulting long path for the current made the charging and discharging processes of the peaking capacitors slow which affected the delay time between the preionization and the main discharge. Thus this affected the uniformity of the discharge.

The same observations were noted when the system was operated at low helium gas pressure (100, 200, 350 torr). The persistent arcing lead to the following modifications of the system.

5.4 The Modification of the Discharge Circuit

To achieve a uniform discharge in the main gap, a fast excitation circuit was needed. Therefore several modifications were made to the system including the electrical connection to the saw blade, peaking capacitors electrical connections, and the use of a different mesh.

The saw blade was inserted and screwed in a slot made in the "T" shaped aluminium block, Fig. 5.9. A slot was also cut into a new perspex block into which the saw blade was inserted. An O-ring was placed between the perspex block and the "T" block to form a seal.

Due to the non-uniformities in the surface of the woven mesh (not being flat, and poor transmission), it has been replaced by a flat perforated nickel mesh with a 0.012" hole and 52% transmission. The mesh was fitted in a slot in the upper aluminium plate and secured by two aluminium bars, Fig. 5.9.

The upper aluminium plate was depressed which in turn flattened a sheet of brass connected to a block of brass by means of a screw. This block of brass was soldered to the peaking capacitor silver layer, Fig. 5.9. With this electrical connection, the inductance was reduced in comparison with the previous connection (spring), which has a large inductance and bad connection. Fig. 5.10 shows some photographs of the whole assembly of the laser.

5.5 The Gas Flow System and Observation of the Discharge Uniformity

Three nylon pipes were supplied from the gas cylinders N_2 , He, CO_2 , to three flow meters. The helium gas flow rate was adjustable between 100 - 800 cc/min. The other two flow rates of N_2 and CO_2 were adjustable between 10-100 cc/min. A nylon pipe was also supplied from the flow meters to transfer the gas mixture to the laser chamber. The gas flow system is shown in Fig. 5.11. The gas mixture entered the chamber through the perspex mirror mounting and passed longitudinally through the chamber. The gas then passed out through an outlet in the other mirror mounting. The discharge was tested using helium gas at

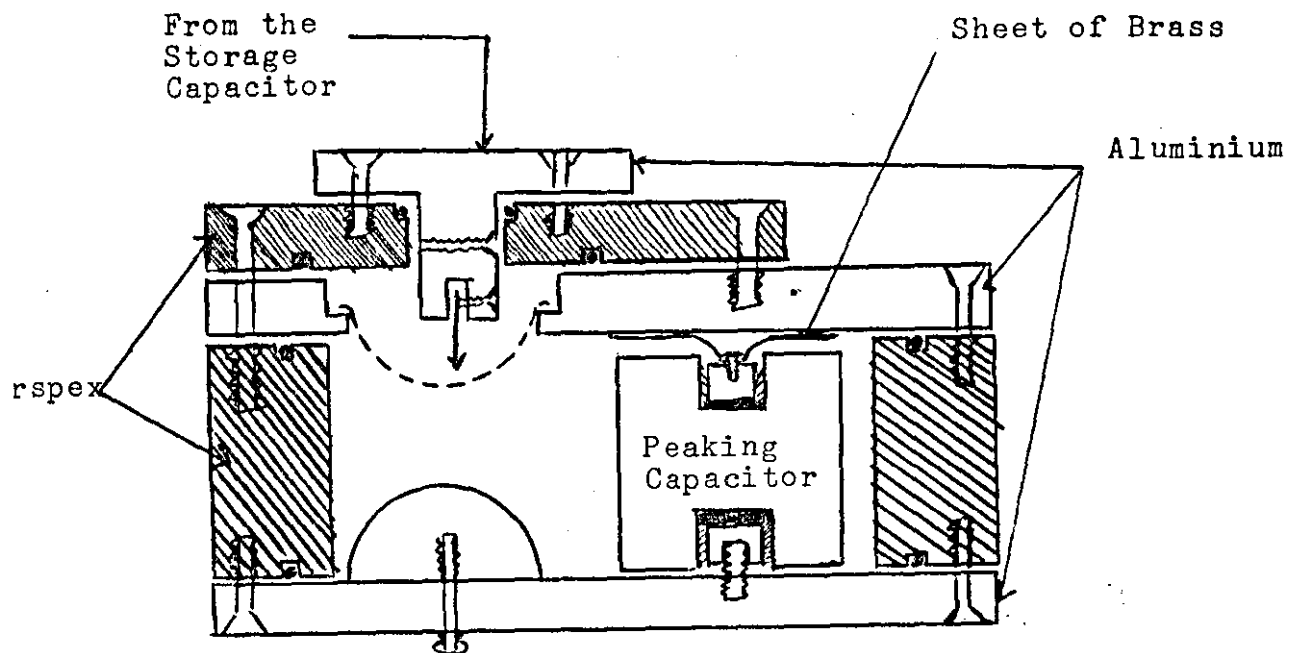


Fig. 5.9.a: The System after Modification

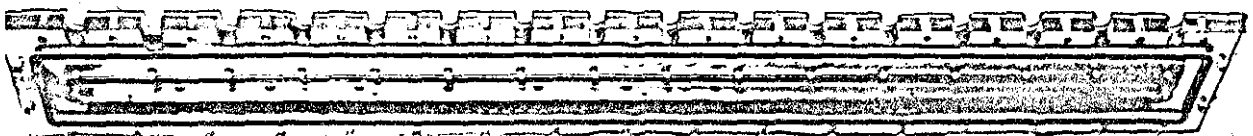


Fig. 5.9.b: A Photograph of the new Perspex Block with the saw blade at its holder

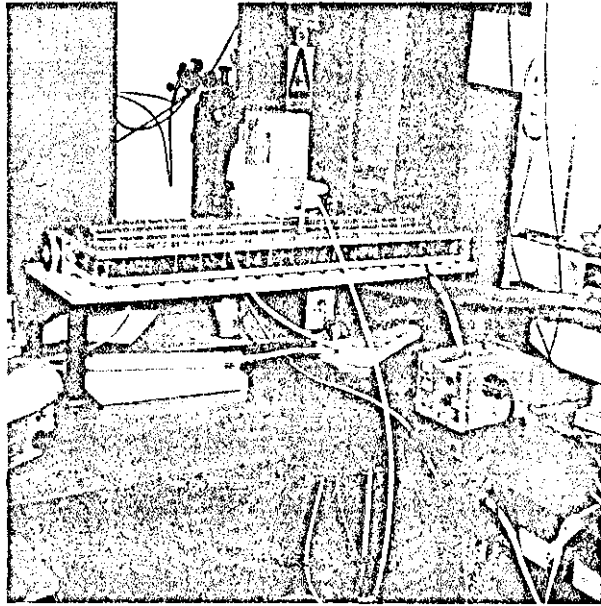


Fig. 5.10.a: A Photograph of the Laser from the front.

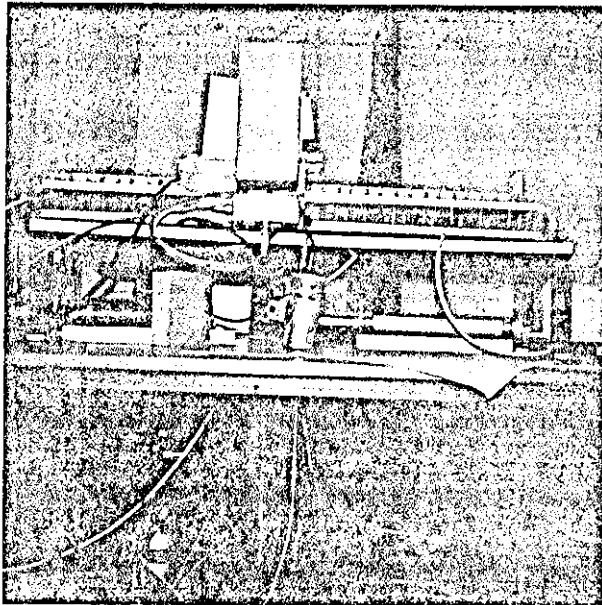


Fig. 5.10.b: A Photograph of the Laser from the rear

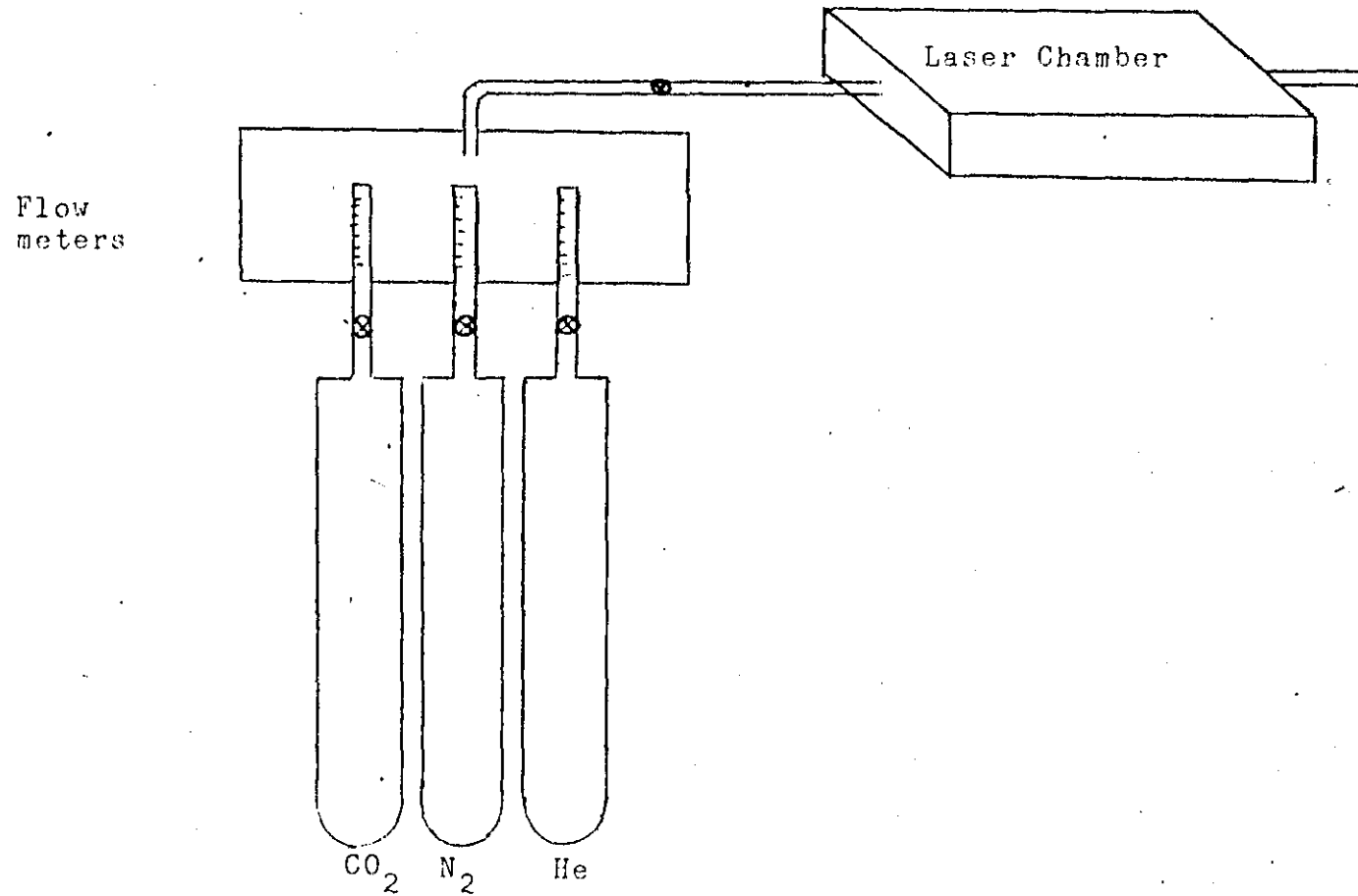


Fig. 5.11: Gas Flow System

800 cc/min. flow rate. A good uniformity in the discharge was found in the range of 16 to 30kv of the operational voltage. Then the discharge was tested with the gas mixture (800 cc/min. He, 100 cc/min. N₂, 80 cc/min. CO₂), and it was found to be uniform in the range of 20 to 30kv of operational voltage. Several photographs of the discharge have been taken using a synchronous camera, Fig. 5.12.a. The discontinuity of the discharge was due to the screws which were threaded through the perspex wall of the chamber. It is clear from this photograph that there is a channel of light (stream) below each point of the saw blade. This means that the uv radiation provided from the saw blade passed through the mesh and then through to the main discharge providing a large volume of gas ionization. The same uniformity of the discharge was observed from the chamber side. Fig. 5.12.b. shows a photograph of the discharge transverse to the electrodes. The same observation was obtained when the chamber was filled with N₂ gas, Fig. 5.13.

5.6 Summary

The requirement of the double discharge TEA CO₂ laser construction, including the spark gap and trigger unit, has been shown.

The uniformity of the discharge test indicated that a low inductance circuit is needed.

Fig. 5.12: A photograph of the CO₂ laser discharge

- (a) Along the axis of the electrodes
- (b) Transverse to the electrodes

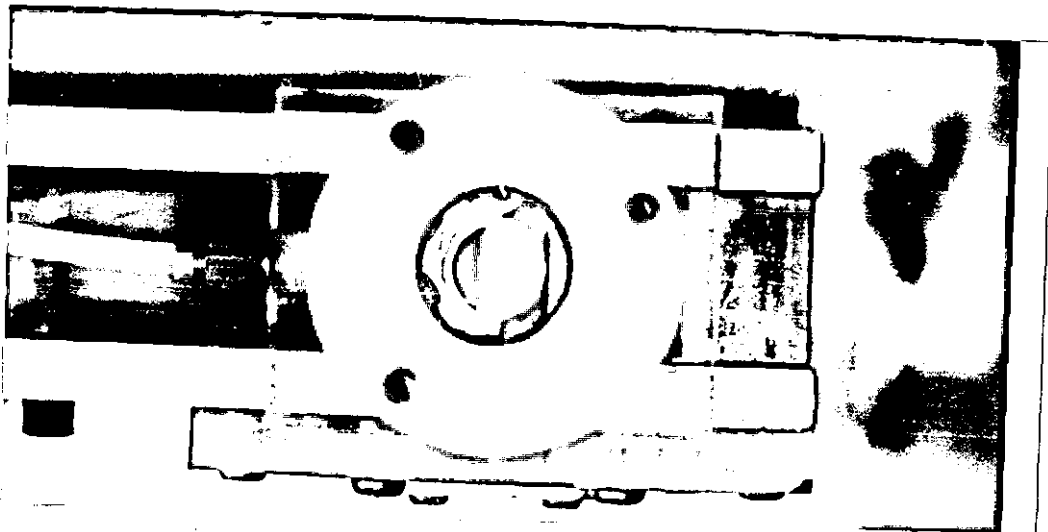
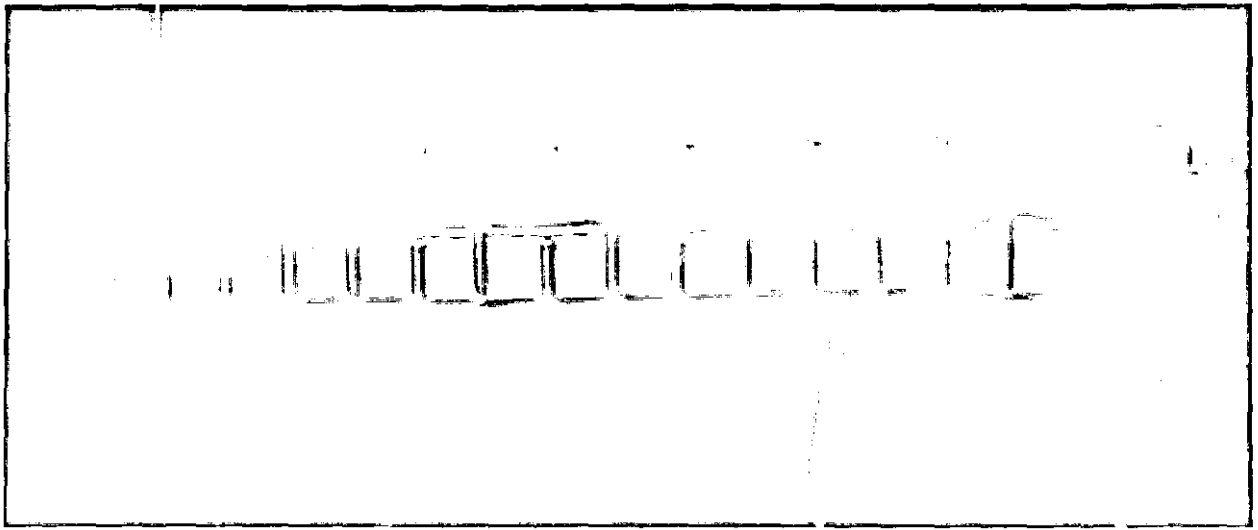
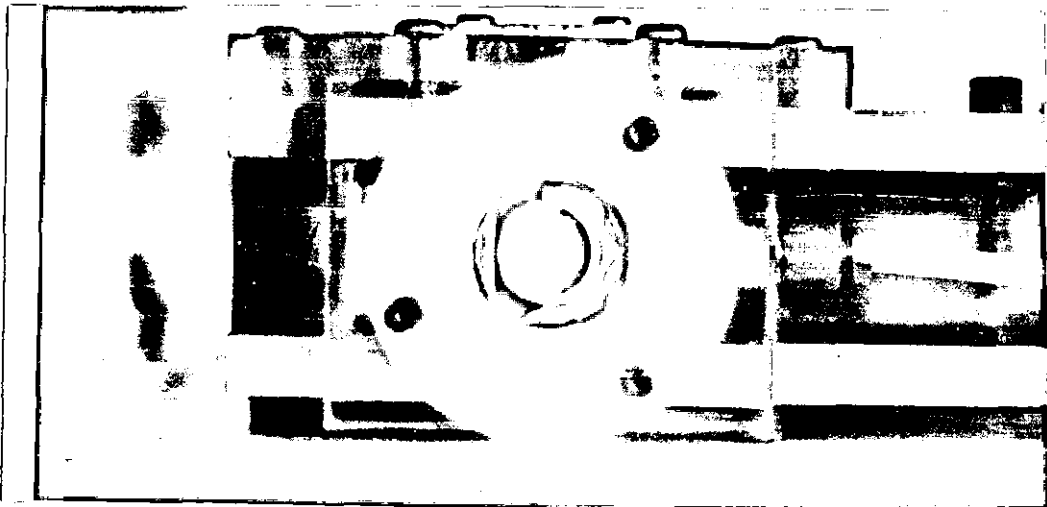
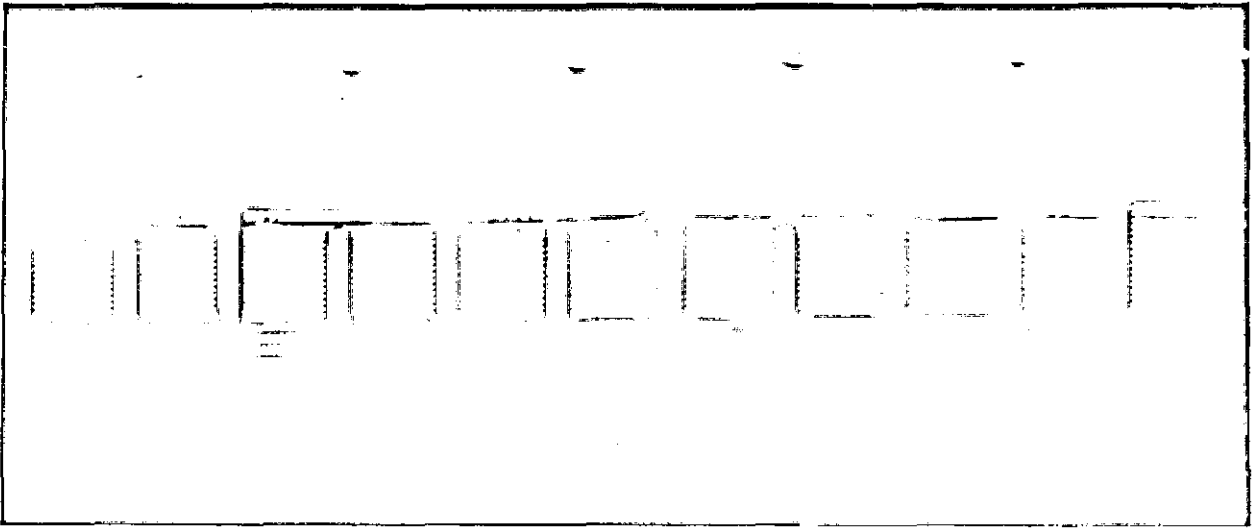


Fig. 5.13: A photograph of the N_2 laser discharge

- (a) Along the axis of the electrodes
- (b) Transverse to the electrodes



Chapter 6

THE OPERATION AND RESULTS OF THE LASER SYSTEM

6.1 Introduction

This chapter describes the operation of the lasers using the double discharge method of excitation. The pulse energy measurement of CO_2 and N_2 lasers are described. Several parameters, such as peaking capacitors, preionization arc length, gas flow rate, electrodes separation, and charging voltage effects on the output energy of the CO_2 laser are investigated. The effect of the gas flow rate of N_2 and CO_2 on the pulse shape of the CO_2 laser is also given.

The effect of the N_2 gas flow rate on the output energy with the input energy effect is studied.

6.2 Single Pulse Measurement

The detector used to measure a single pulse energy was a cone calorimeter which already existed in the laboratory. A slight modification of the circuit was made in order to achieve a high sensitivity. The calorimeter's circuit was operated on the Wheatstone bridge principle, Fig. 6.1.a. One of the bridge resistances was connected in series with a thermistor, (ITT M53 type) which in turn was attached to a brass cone weight 0.975 g. The laser beam entered the cone and heated it, which in turn led to a change in the thermistor resistance (R_t). Hence the balance of the bridge was distorted. The fluctuation R_t of the thermistor, and hence the temperature fluctuation, was observed by a galvano-

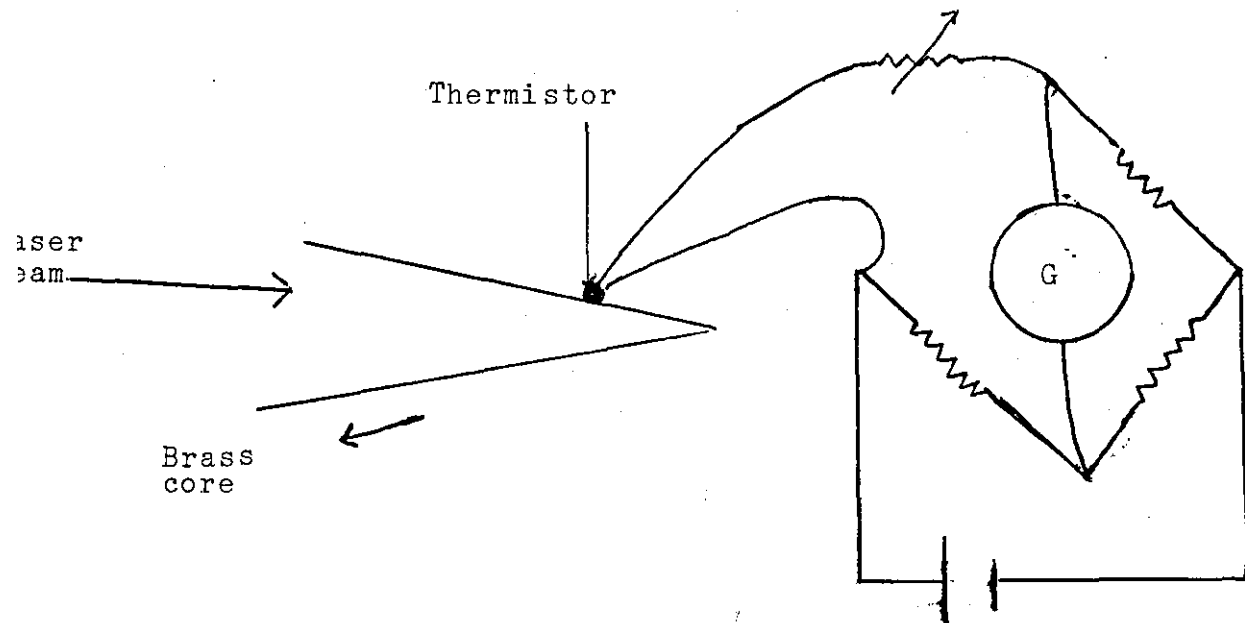


Fig. 6.1.a: Single Pulse Energy Measurement Arrangement

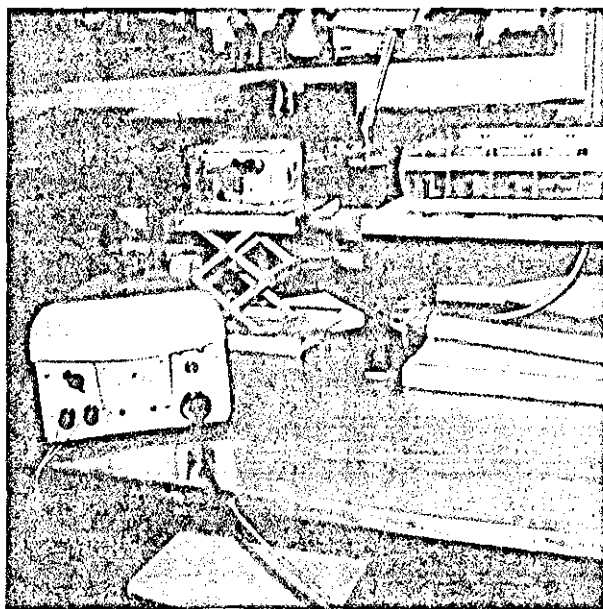


Fig. 6.1.b: A Photograph of the Output Energy Arrangement

meter spot deflection. Therefore the laser energy was calculated from the following formula:

$$E = M.S.\Delta T \quad (6.1)$$

where M, S are the weight and the specific heat of the cone.

The cone calorimeter was calibrated several times at room temperature before it was used. The calibration and calculation of the circuit showed a linearity between the galvanometer current (spot deflection) and the change in the thermistor resistance ($\Delta R, \Delta T$), with a sensitivity of 30mJ/cm.

Fig. 6.1.b shows a photograph which was taken of the pulse energy measurement arrangement when the laser was operated. Care was taken in order to minimise any errors due to the plasma formation on the cone surface.

6.3 The TEA CO₂ (flow rate) Laser Results

This section discusses the results which were obtained when the laser was operated with CO₂, N₂, He gas mixture. The effect of the gas flow rates, peaking capacitor effect, pre-ionizing are length effect, ... etc., on the output energy were also discussed.

6.3.1 Gas Flow Rate Effect

The effect of the gas flow rate of CO₂, N₂, He, was investigated. The CO₂ laser was operated at different flow rate of the helium gas. At low flow rates in the range between 200-400 cc/min, the discharge showed frequent arcs and hence a reduction in the output energy was observed. The discharge showed a good uniformity at high flow rate and hence a maximum output energy was achieved at 800 cc/min. Fig. 6.2.a shows the helium volumetric fraction H effect:

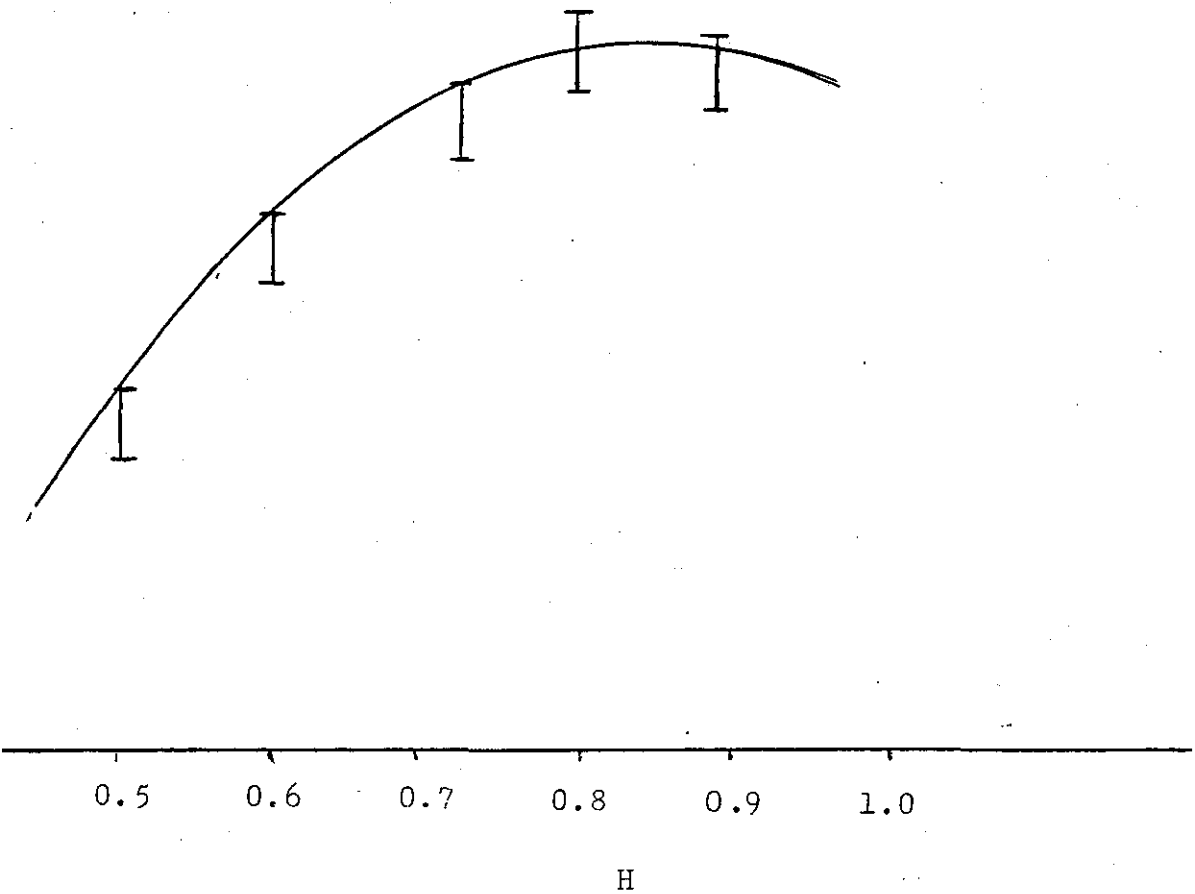


Fig. 6.2.a: Helium volumetric fraction effect on the output energy at
V = 30kv
N₂ = 60 cc/min
CO₂ = 40 cc/min

$$H = \frac{\text{He (flow rate)}}{\text{He (flow rate)} + \text{CO}_2 \text{ (flow rate)} + \text{N}_2 \text{ (flow rate)}}$$

on the laser output energy for different flow rates. The reduction in the output energy was due to a reduction in the helium concentration in the mixture which led to a higher value of E/N, and hence a reduction in the fractional energy going into the relevant molecule levels was expected. More important was the effect on the laser CO₂ level (010) depopulation, (Chapter 2). Since the helium gas acted as a coolant in the mixture and in turn possibly increased the relaxation rates and coupling of the rotational levels. The output energy showed an increase by 0.2J at higher helium concentrations. When the helium flow rates reached 900 cc/min and above, the output energy decreased which was due to the low concentration of the CO₂, N₂ gases in the mixture.

Other version of the gas flow rate effect was the nitrogen flow rate into the mixture. A maximum output energy was obtained at flow rate of 100 cc/min, which corresponded to a volumetric fraction $N = 0.48$ ($N = \frac{\text{N}_2 \text{ (flow rate)}}{\text{N}_2 \text{ (flow rate)} + \text{CO}_2 \text{ (flow rate)}}$)

Fig. 6.2.b.

At low flow rates in the range of 20-40 cc/min, the output energy dropped by a factor 0.3%. This was due to the low N₂ concentration in the mixture which led to the energy transfer process from the nitrogen molecules to the CO₂ molecules being insufficient to excite a large volume of CO₂ molecules.

The laser also was operated at different flow rates of CO₂. The maximum output energy was found at 50 cc/min which corresponded to a volumetric fraction $\gamma = 0.55$;

$$\gamma = \frac{\text{CO}_2 \text{ (flow rate)}}{\text{N}_2 \text{ (flow rate)} + \text{CO}_2 \text{ (flow rate)}} \quad \text{Fig. 6.2.c.}$$

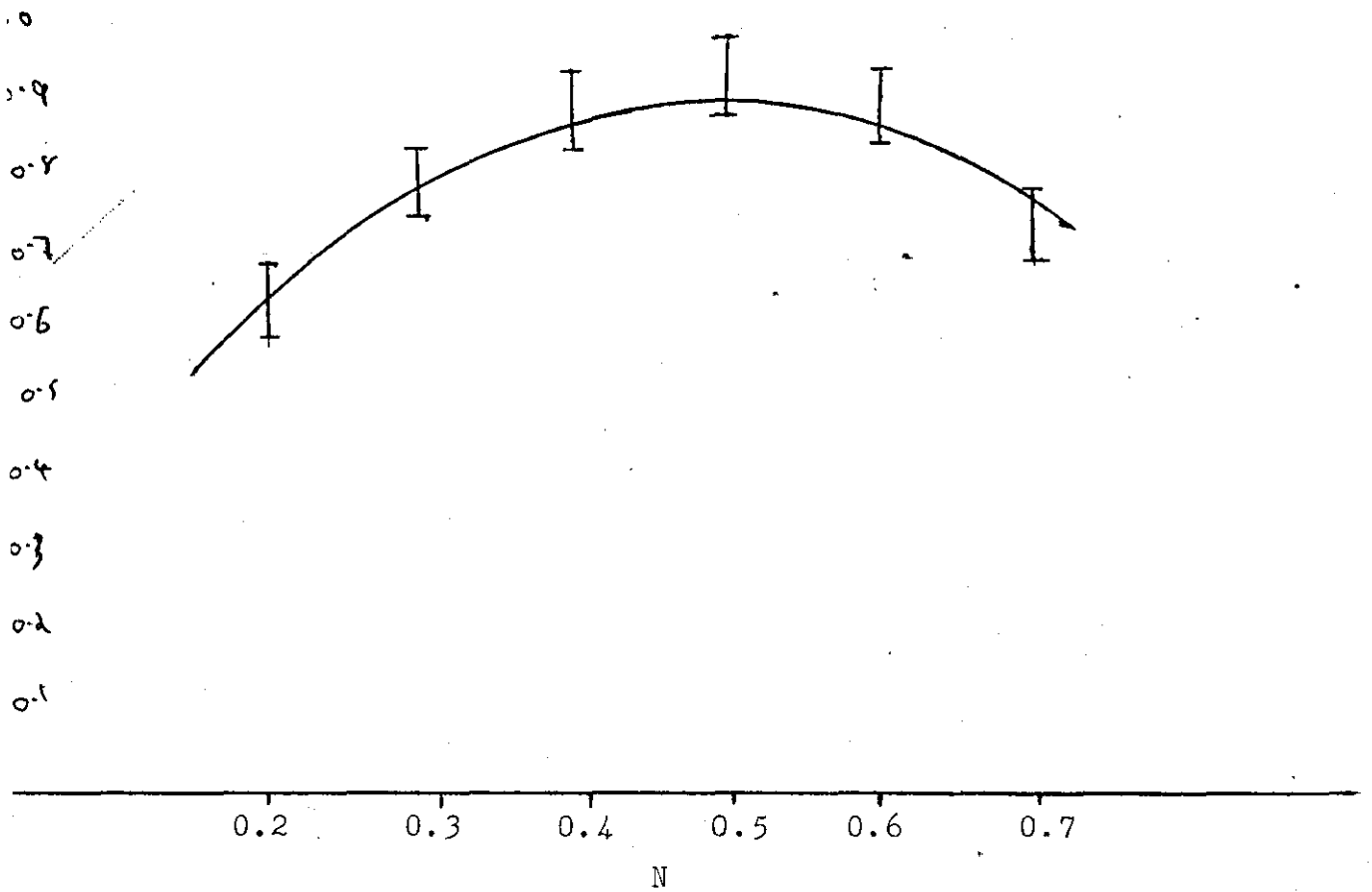
E/b
at

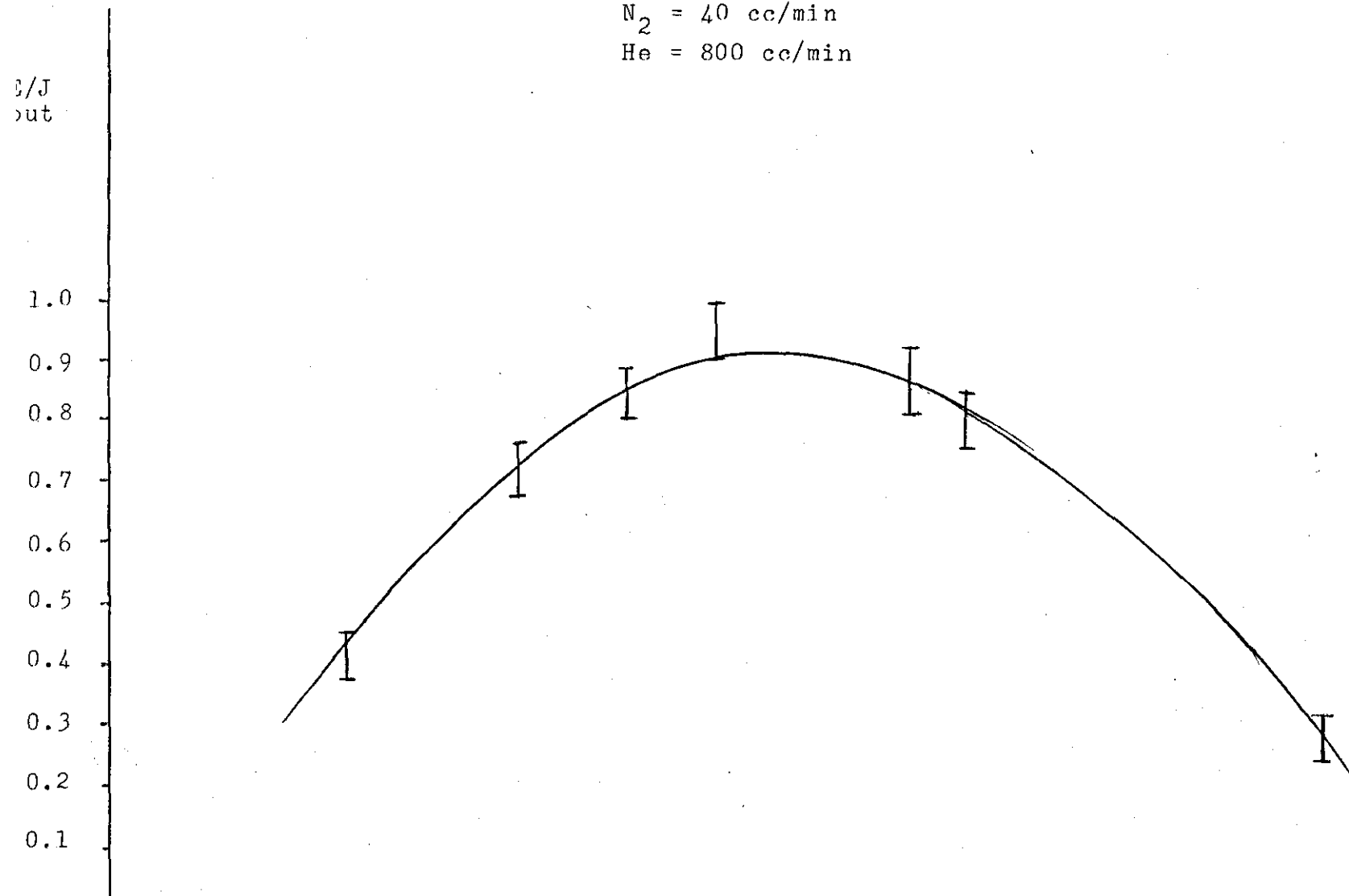
Fig. 6.2.b: Nitrogen Volumetric Fraction N effect
on the Output Energy at
V = 30kv
CO₂ = 40 cc/min
He = 800 cc/min

Fig. 6.2.c: Carbon-dioxide volumetric fraction ϕ
effect on the output energy at

V = 30kv

N₂ = 40 cc/min

He = 800 cc/min



The laser also was operated without nitrogen, but the energy output decreased by a factor 0.5 from the cases when the N_2 was added to the mixture. This was due to the CO_2 molecules being pumped only by direct electrons impact processes (Chapter 2).

6.3.2 Peaking Capacitors Effect

The study of the peaking capacitor effect on the discharge stability and the output energy was investigated. The TEA double discharge CO_2 laser which was developed in the laboratory was used for this purpose. When the laser was operated (at the optimum gas mixture flow rates) without peaking capacitors across the electrodes, frequent arcs were observed at different areas of the discharge region. The electrical circuit of the laser without peaking capacitors is shown in Fig. 6.3a in which the timing between the two discharges was no longer obtained. This led to large inductance of the circuit and in turn led to an increased plasma current which was responsible for the frequent arcs. The output energy was measured within the range of 300-350 mJ. This reduction in output energy was due to the small amount of input energy which was deposited in the discharge, and the ringing in the peak voltage did not occur. When a peaking capacitor of .5 nF was placed between the electrodes, the output energy rose to 600 mJ with better discharge stability. The peaking capacitor slowed the growth of the applied voltage through the preionizer to the main discharge, but sharpened up the current rise time once the main discharge formed. The explanation of the discharge stability was that the peaking capacitors acted as a low impedance source from which a large volume of the plasma was formed.

A higher level of stability of the discharge was obtained when 17 nF peaking capacitors were used. The output energy reached

its maximum value of 1.45 J corresponding to this value. Thus an increase of 25% in the output energy was achieved. The output energy was decreased again when 19 nF peaking capacitors were placed across the electrodes. This possibly was due to the lower peaking voltage, and the longer delay time, Fig. 6.3.b.

6.3.3 The Preionizer Arc Length Effect

The preionizer technique which was described earlier (Chapter 5), provided the system with uv radiation which in turn produced a uniform charge carrier density, both through the photoionization and through photo emission at the cathode surface. Hence a large volume of plasma was expected to be obtained.

The effect of the arc length on the output energy was investigated. The saw blade was placed behind the mesh cathode forming a gap of 8mm. With this arrangement, the maximum energy output was measured as 960 mJ. When the saw blade was placed closer to the mesh with a gap of 6mm, the maximum output energy rose to 1.5 J with an increase of 45% from the previous arc length. Fig. 6.4 shows the result at different charging voltages corresponding to two different arc gaps 6 and 8mm. This increase in the output energy was due to the higher peak current which was limited by the circuit inductance rather than by the arc impedance (few m Ω). The higher peak current led to faster peaking capacitor charging time and hence led to a higher output energy.

6.3.4 Electrodes Separation Effect

Three cathode meshes with different radii of curvature were used in order to study the effect of the discharge gap on the output energy. Fig. 6.5 shows a photograph of the meshes which were used in the laser system. A maximum output energy of 1.5 J was achieved when mesh (b) was used which formed a discharge

E_{out} / J

1.5

1.0

0.5

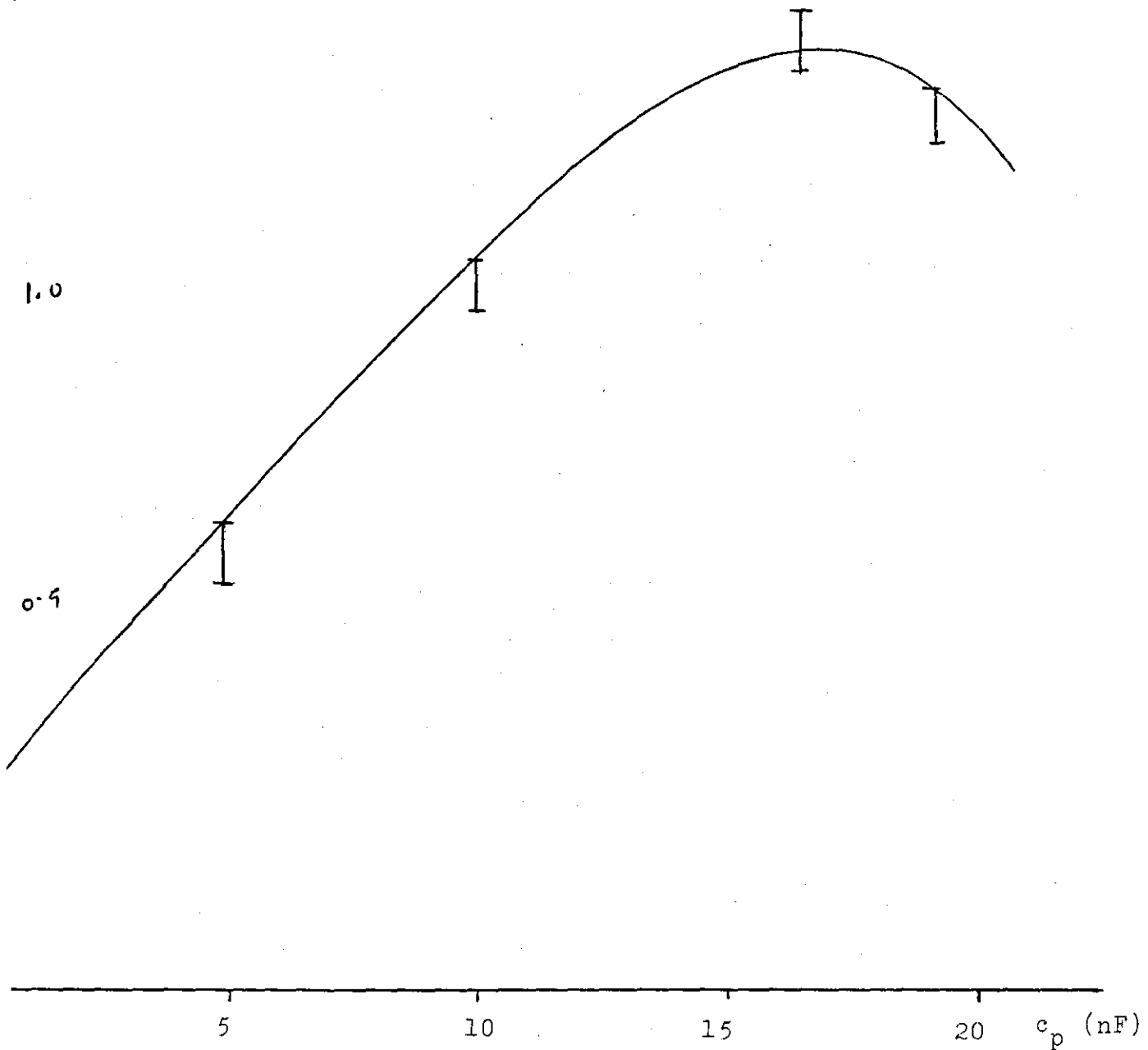


Fig.6.3.b: Peaking capacitors effect on the output energy for

- $\gamma = 0.6$
- $N = 0.4$
- $H = 0.88$
- $V = 30 \text{ Kv}$

E_{out} / J

1.5

0.9

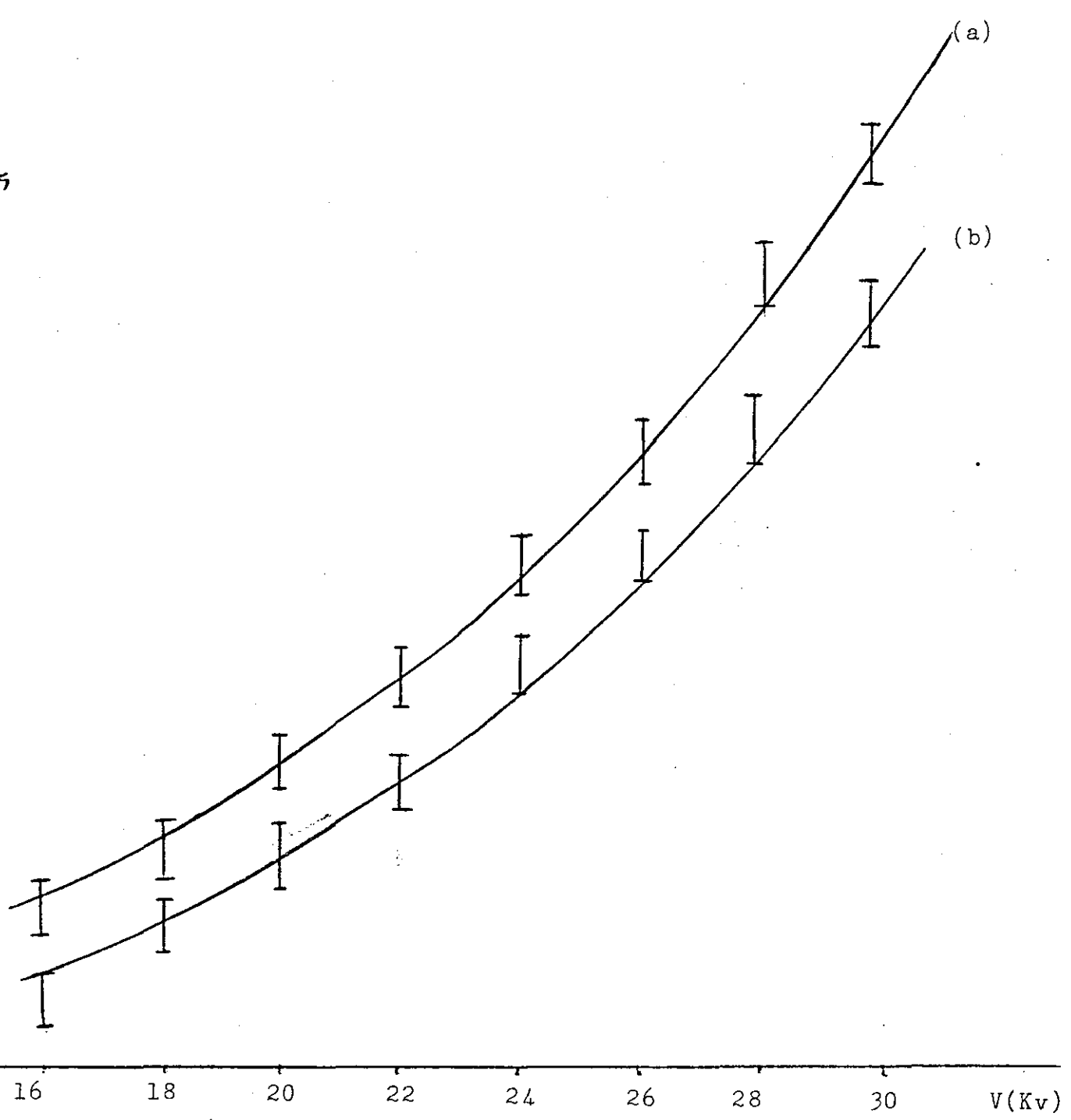


Fig. 6.4: The Preionizer Arc Length Effect on the output energy for:
(a) 6mm V = 50 Kv
(b) 8mm $\phi = 0.44$
 N = 0.55
 H = 0.81

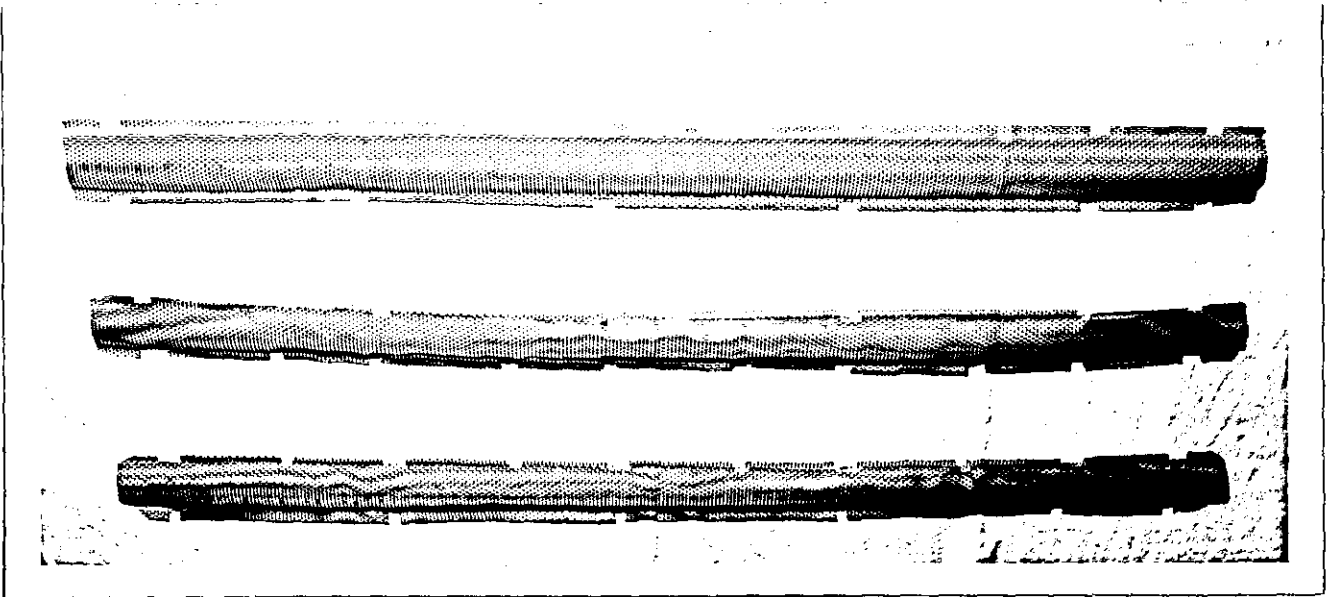


Fig. 6.5: A Photograph of the 3 meshes which were used in the Laser System

- (a) For 15mm electrodes separation
- (b) 20mm
- (c) 22mm

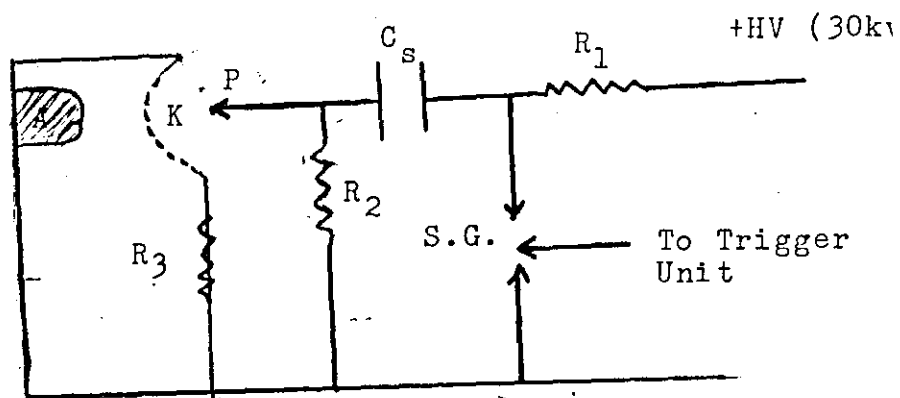


Fig. 6.3.a: The Electrical Circuit of the Laser System without Peaking Capacitor

gap of 20mm with a 6mm preionizer gap. When mesh (a) was used, the main discharge gap was 15mm with a 10mm preionizer gap, the output energy dropped to almost a third of the previous maximum value (≈ 500 mJ). The reduction in the output energy for this discharge gap was due to the reduction in the discharge volume from 148 cm^3 compared to 111 cm^3 for a gap of 15mm. Due to the larger preionizer gap, the preionization effect was not efficient enough to sustain the discharge, hence frequent arcs were formed which led to a reduction in the output energy. Since $E/p = v_d/p\mu_e$, where v_d and μ_e were the drift velocity and mobility of the electron, the higher E/p (21 Kv/cm atm) led to lower electron mobility for the gap 15mm, which resulted in a short path and lowered the number of collisions. When the third mesh (c) was used, a gap of 22mm was formed between the discharge electrodes with a 3mm preionizer gap. Even with this larger active volume, the output energy showed a decrease by a factor of 0.3% from the one obtained when the laser operated with electrodes separation of 20mm. This reduction in output energy with a larger discharge gap was possibly due to the decreased preionizer gap which led to a decrease in the delay time of the circuit between the two discharges from the optimum value, (Section 5.2.9). Also the lower E/p (14.5 Kv/cm atm) could lead to a lower CO_2 dissociation rate from which the CO_2 molecule could be regenerated again in the mixture.

Due to the structure of the preionizer holder, it was not possible to use other meshes to give larger or smaller electrodes separation without touching the saw blade or resulting very large preionizer gap.

6.3.5 The Effect of the Main Storage Capacitor on the Output Energy

The effect of the main capacitor on the output energy was investigated using 50 nF (Hartley measurement), and 80 nF (Maxwell) capacitors. It was found that the maximum output energy corresponding to these values were 1.5 J and 1.75 J respectively. Fig. 6.6 shows the results. It was not expected that the output energy should increase by a factor of 0.25 J, since the energy deposited to the discharge from the main capacitor (80 nF) was 40 J compared with 22 J for 50 nF capacitor. The reason for the increase being no more than 0.25 J was the ratio of the storage capacitors/peaking capacitors was 1/5 as opposed to the optimum ratio of 1/3.

6.3.6 The Charging Voltage Effect

The laser was operated at several values of charging voltage. It was shown that the discharge, and hence the output energy was increased with the increasing of the charging voltage. Fig. 6.7 shows the result.

6.4 Pulse Shape Measurement

The pulse shape was measured using a photon drag detector. Fig. 6.8 shows the arrangement which was used for this purpose. Various pulses were detected for different N_2 and CO_2 concentrations in the mixture. The laser entered and passed through the sensitive element of the detector which was made of a semiconductor crystal. The photons in the laser then transferred this momentum to free carriers in the sensitive element. The free carriers were physically driven down to create a voltage gradient which was amplified and fed to an oscilloscope (Tek

Fig. 6.6: Storage Capacitors Effect on the Output Energy for:

$\gamma = 0.4$

$N = 0.55$

$H = 0.8$

$V = 32Kv$

(a) For $C_s = 80 \text{ nF}$

(b) $C_s = 50 \text{ nF}$

Preionizer gap = 6mm

E_{out}

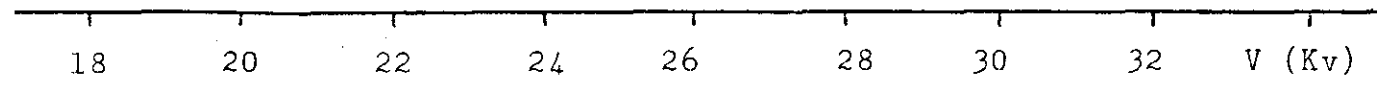
2.0

1.75

1.5

1.0

0.5



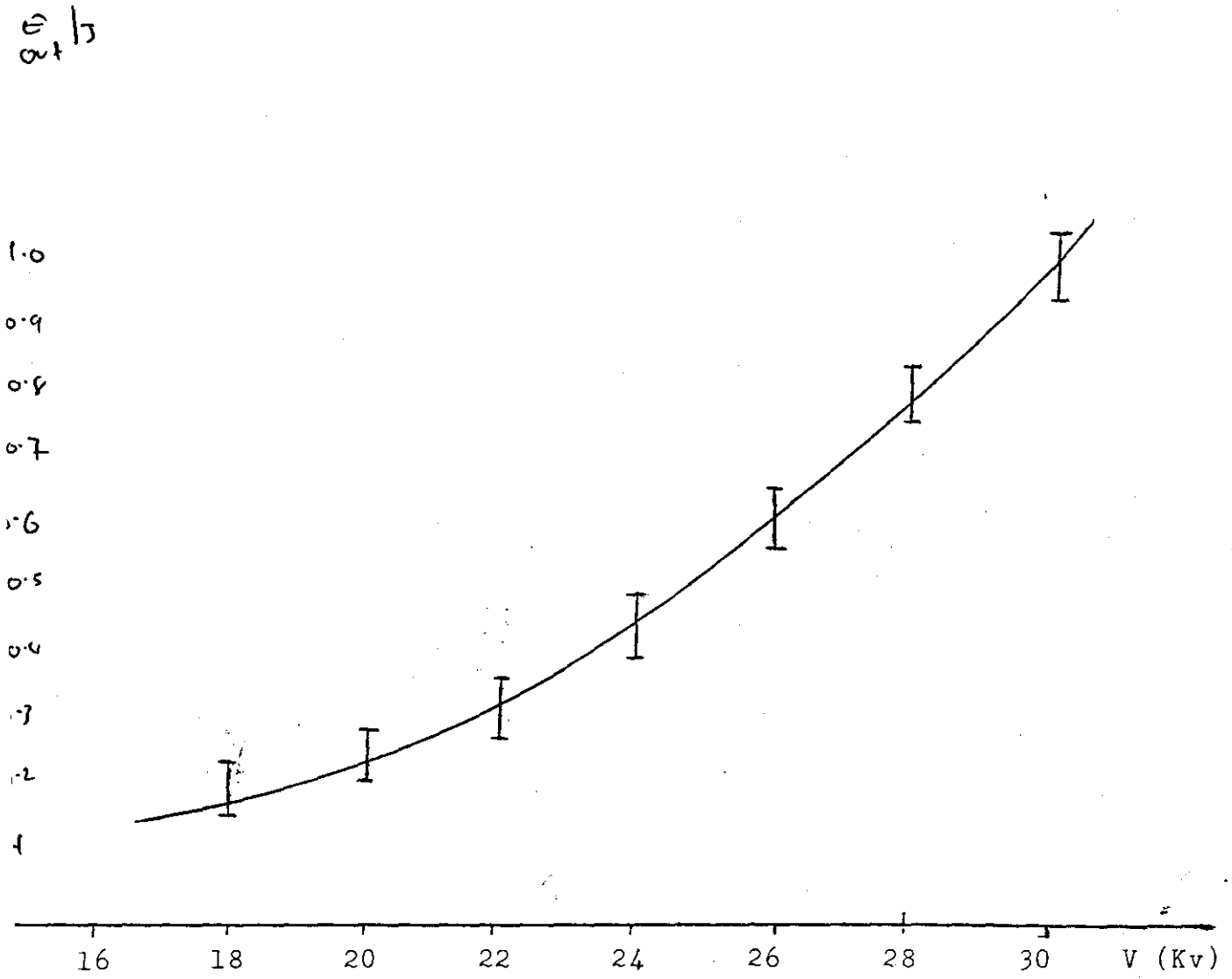


Fig. 6.7: Charging Voltage Effect on the Output Energy

$$\gamma = 0.4$$

$$N = 0.6$$

$$H = 0.88$$

$$C_s = 50 \text{ nF}$$

Preionizer gap = 6mm

Tronix type). Due to the pick up from the surrounding area, the detector was isolated and placed at 4m from the laser in order to get a clean pulse shape.

The pulse shape was detected for different CO_2 volumetric fractions in the mixture, Fig. 6.9. For low δ (Fig. 6.9.a.), the pulse duration was longer, hence a low peak power was obtained. Since the nitrogen molecules acted as an energy reservoir in the mixture, and due to the smaller number of CO_2 molecules compared to that of N_2 molecules in the mixture, the energy transfer process occurred over a long period of time which led to a long tail in the pulse shape. The pulse shape was also measured for different volumetric fractions of N_2 (N) in the mixture, Fig. 6.10. The pulse shape was also measured when the laser chamber was filled only with CO_2 and He gas mixture. Fig. 6.11 shows the photograph that was taken for this gas mixture. No tail on the pulse shape was present due to poor excitation.

6.5 The Nitrogen Laser

The laser was also operated with N_2 gas. A gas mixture of helium and nitrogen in the ratio of 9 : 1 flowed along the axis of the chamber. The optical cavity of the CO_2 laser was replaced by a fused silica output coupler and an aluminium polished flat reflector. The laser was operated at different N_2 flow rates in a range between 10 - 120 cc/min.

6.5.1 Variations of the Output Energy with N_2 Flow Rate and Input Energy

The same measuring single pulse energy arrangement as in section (6.2) was also used. 10 - 20 shots were superimposed on the cone surface for a range of nitrogen flow rate at various applied voltages. The dependence of the output laser energy on

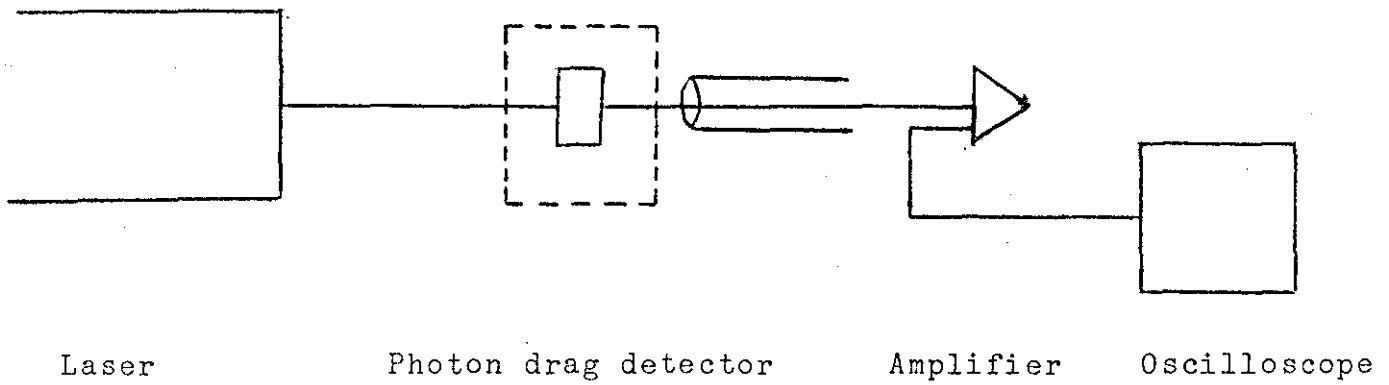
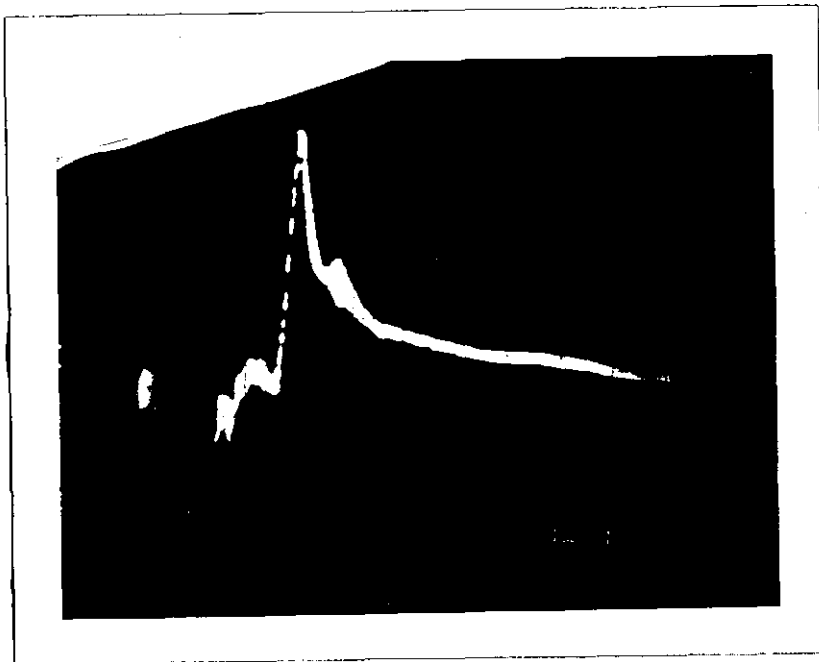


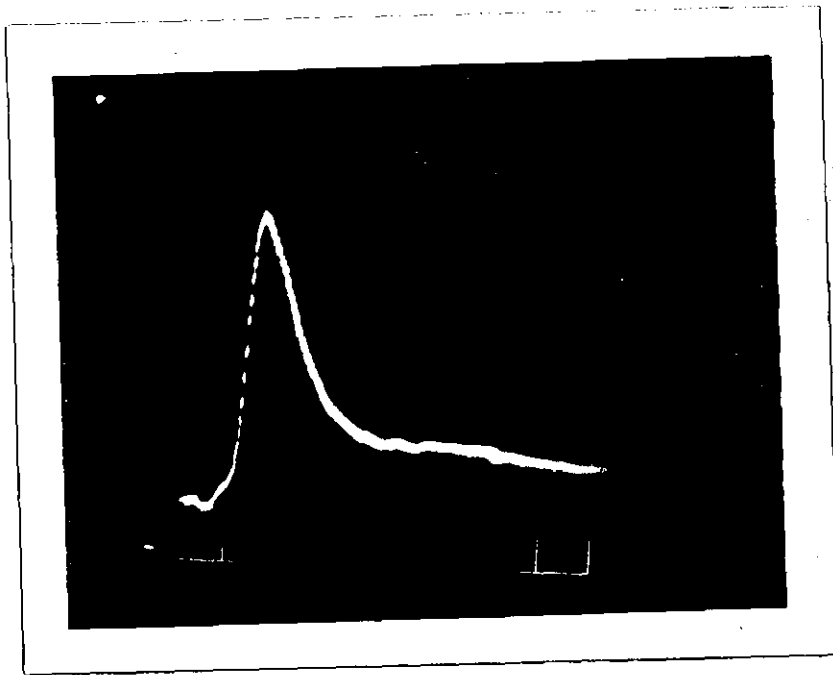
Fig. 6.8: Pulse Shape Measurement Arrangement



(a)

Fig. 6.9: CO_2 Laser Pulse Shape as a Function of CO_2 Concentration in the Mixture.

(a) $\gamma = 0.33$, $V = 30\text{kv}$.
 ($0.5\mu\text{s/div}$, 20mv/div)



(b) $\gamma = 0.5$
 (0.2 μ s/div, 50mv/div).

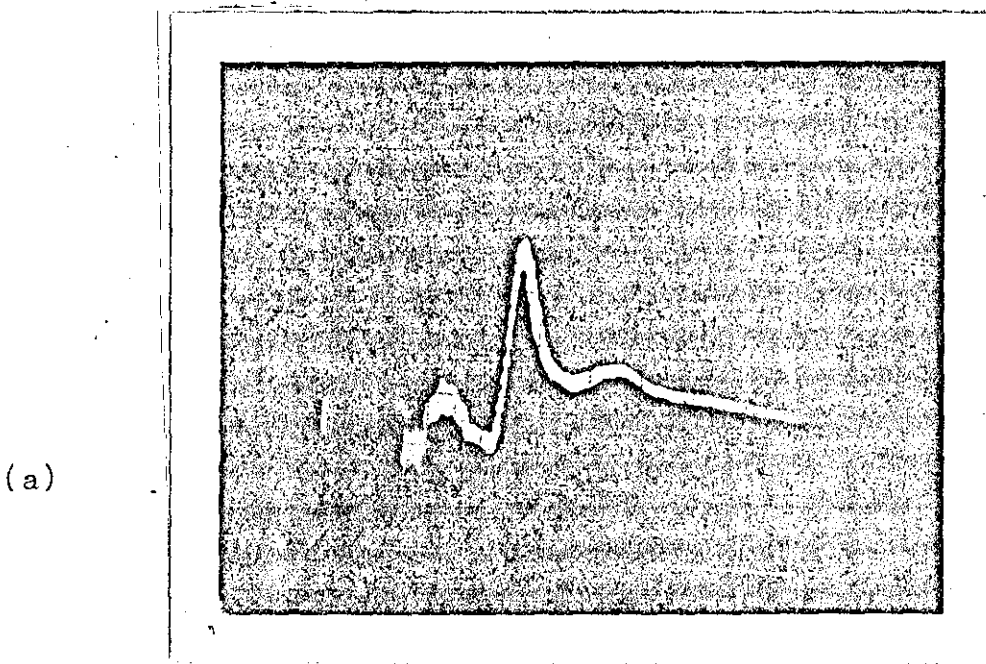
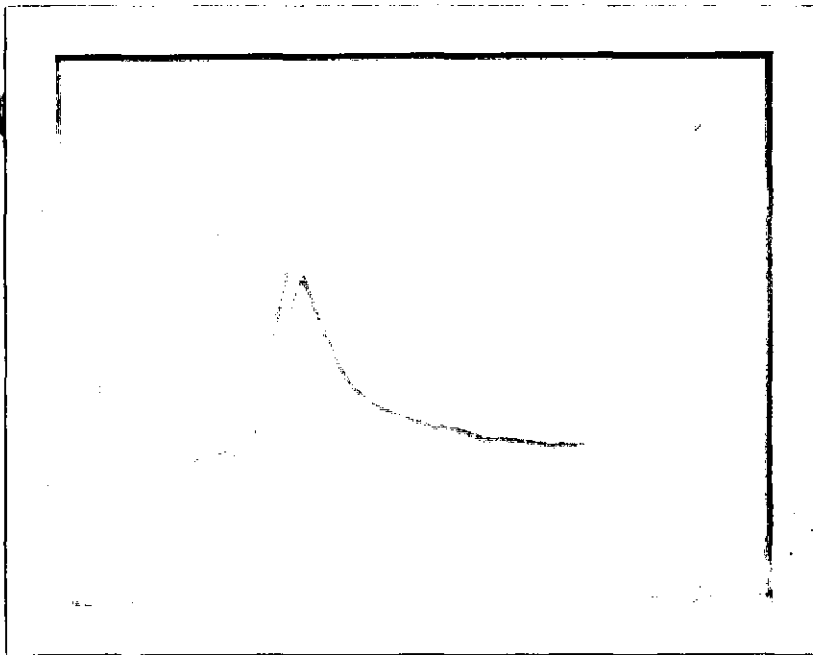


Fig. 6.10: CO₂ pulse shape as a function of nitrogen concentration in the mixture

(a) $N = 0.75$
 (0.5 μ s/div, 20nv/div)



(b) $N = 0.5$
(0.2 μ s/div, 50mv/div)

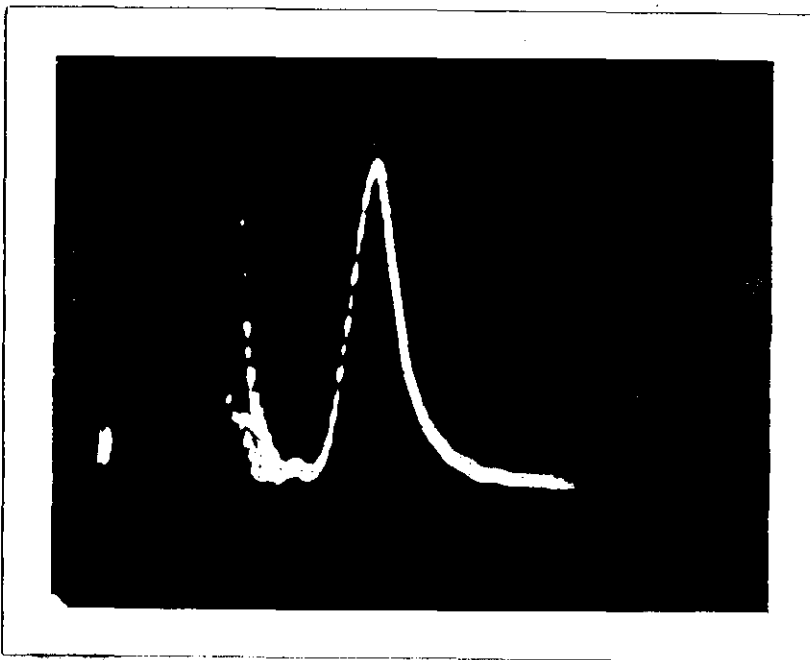


Fig. 6.11: CO_2 pulse shape when the laser was operated without N_2

CO_2 : 40 cc/min

He^2 : 800 cc/min

(0.2 μ s/div, 50mv/div)

the nitrogen gas flow rates is shown in Fig. 6.12, with increasing N_2 flow rates, the output energy increased until a peak of 2.8 mJ was reached at a flow rate of 40 - 60 cc/min. With a further increase of the N_2 flow rates beyond 60 cc/min, the laser output energy fell.

The dependence of the laser energy output on the input energy which was a function of the applied voltage to the storage capacitor ($E = \frac{1}{2} CV^2$) was investigated for different values of N_2 flow rates. Fig. 6.13 shows the variation of the output energy with different values of input energy for a constant N_2 flow rate.

When the laser was operated without the output sampler, a reduction of output energy of 60% was observed.

6.5.2 N_2 Pulse Shape Measurement

A fast rise time Si detector was used for measuring the pulse shape. The detector was screened by tin plated boxes, while the cables were running in copper pipes in order to make the signal displayed on the oscilloscope measurable and free from superimposed interference. The signal was displayed on a Phillips PM 3262 oscilloscope (100 MHz), each end of the cable was terminated in 50 Ω . The pulse was observed on the screen and photographed simultaneously. Fig. 6.14 shows the pulse shape. The half width of the pulse was measured as 6 ns, a variation in the output peak power of the laser beam from shot to shot was 0.50 kw.

6.6 Rare Gas Halide Excimer Laser

Since it was very difficult to get perfect seal of the laser system, and due to some mechanical problems which led to slight cracks in the perspex, it was unwise to operate the laser with rare gas halides such as Xe Cl, Xe F, since halogen gases are poisonous when free in the atmosphere.

000
λ.8

Fig. 6.12: The output energy as a function of the nitrogen flow rate, measured at various applied voltage.

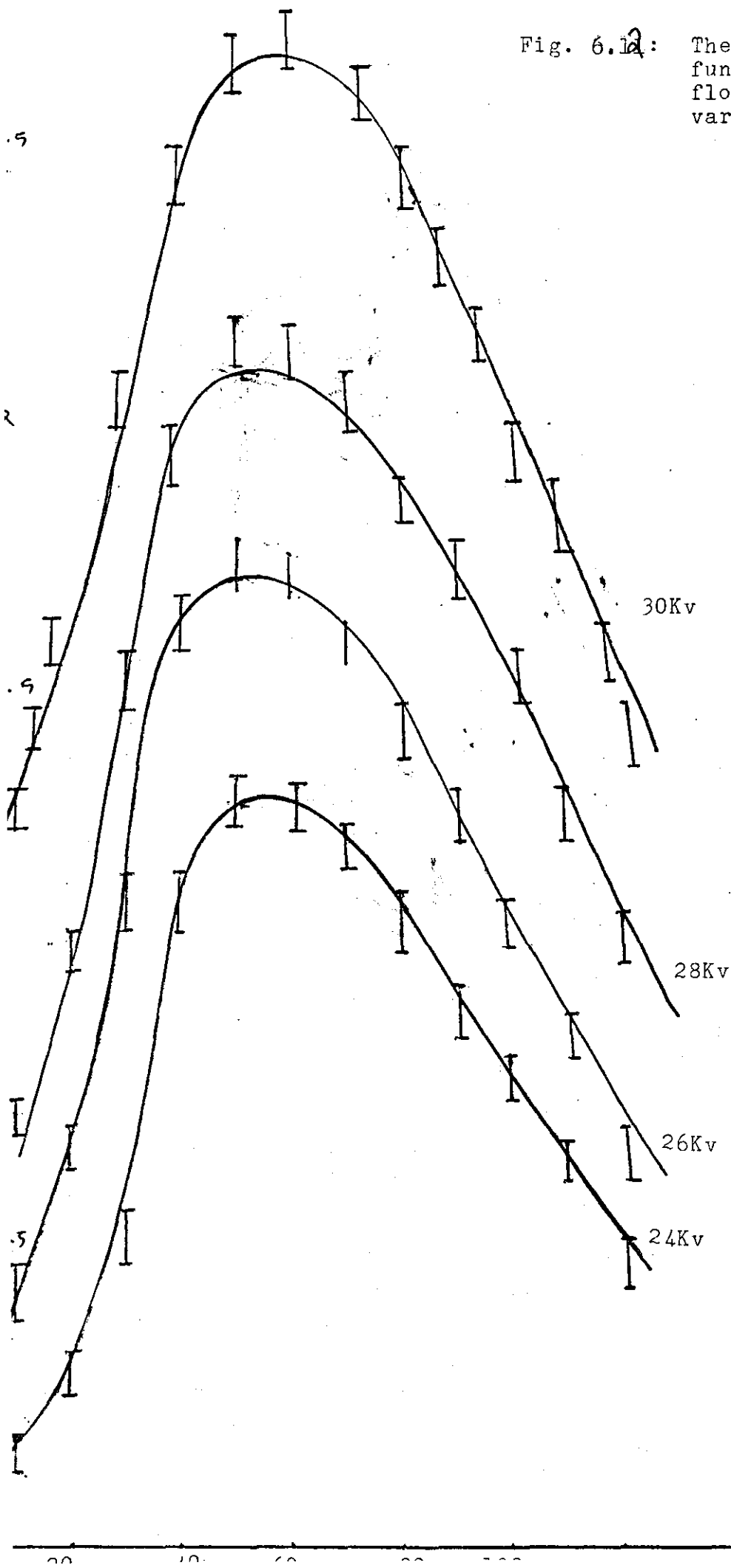
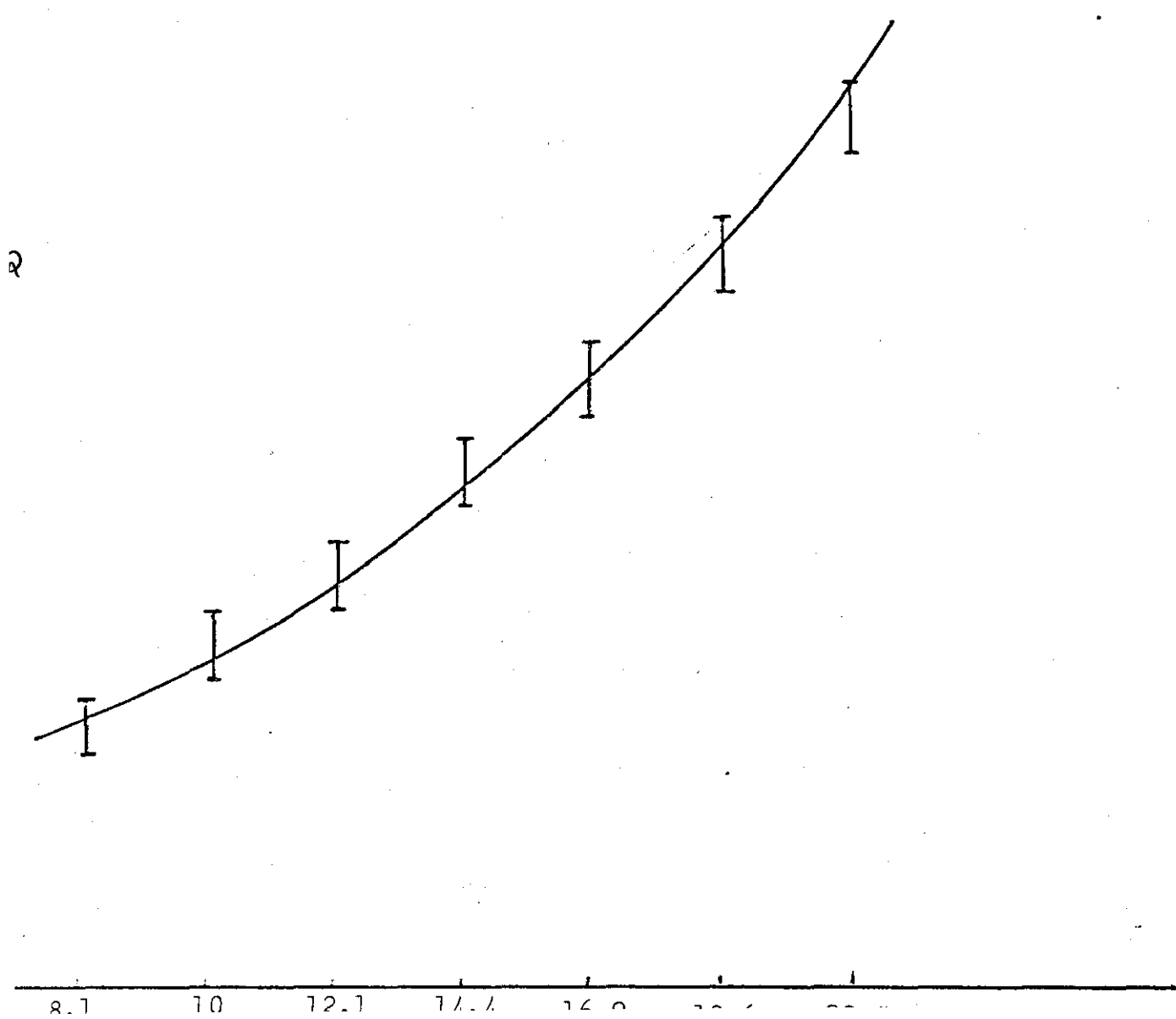


Fig. 6.13: The output energy as a function of stored energy at a fixed N_2 flow rate of 30 cc/min

E_{out}/mJ



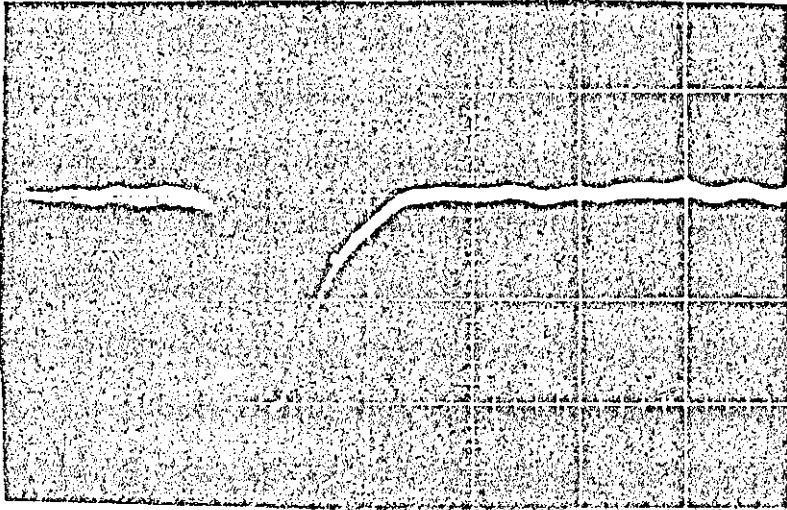


Fig. 6.14: N_2 Pulse Shape.

A photo copy from the original
photograph at 28 kv,
 N_2 : 40 cc/min,
time base 10 ns/cm.

6.7 Summary of the Results

The double discharge excitation method of the $\text{CO}_2 - \text{N}_2 - \text{He}$ gas mixture, and the $\text{N}_2 - \text{He}$ gas mixture has been successfully applied to an axial flow transverse discharge laser system, with 15 mm, 20 mm, and 22 mm discharge gaps.

A large uniformity of the discharge has been achieved when the laser system was operated with peaking capacitors across the discharge gap. An increase of 25% in the output energy was achieved when 17 nF peaking capacitors were placed between the electrodes.

Maximum output energy has been obtained when the preionizer arc length was changed from 8 mm to 6 mm with an increase of 45%. Maximum output energy has been achieved (1.5 J) with a 20 mm discharge gap with an increase of 35% from the 15 mm gap.

The output energy of the N_2 laser increased by 60% when the laser operated with two mirrors.

Chapter 7

THE COMPUTATION MODELLING OF THE ELECTRICAL DISCHARGE CIRCUIT OF THE LASER SYSTEM

The Theoretical Modelling of the Discharge Circuit

The electrical circuit of the discharge model is shown in Fig. 7.1, in which:

V_0 is the initial voltage

C_1, C_2 , are the stored and peaking capacitors respectively

L_1 is the inductance of the preionizer and slow circuit

R_1, R_2 , are the preionizer and discharge impedances

L_2 is the laser head

R_{ch1}, R_{ch2} , are the charging resistances.

Since the preionizer discharge is generally an unsteady arc, in which the gas is highly ionized (electron-electron collisions are important) and the gas is strongly heated. The preionizer impedance R_1 is usually quite low and the current is limited by the circuit inductance more than the arc impedance. Therefore, R_1 is ignored in this model, and the new circuit is shown in Fig. 7.2.

The current i_1 represents the preionizer current, i_2 is the current which charges C_2 after the first discharge occurs, and i_3 is the discharge current.

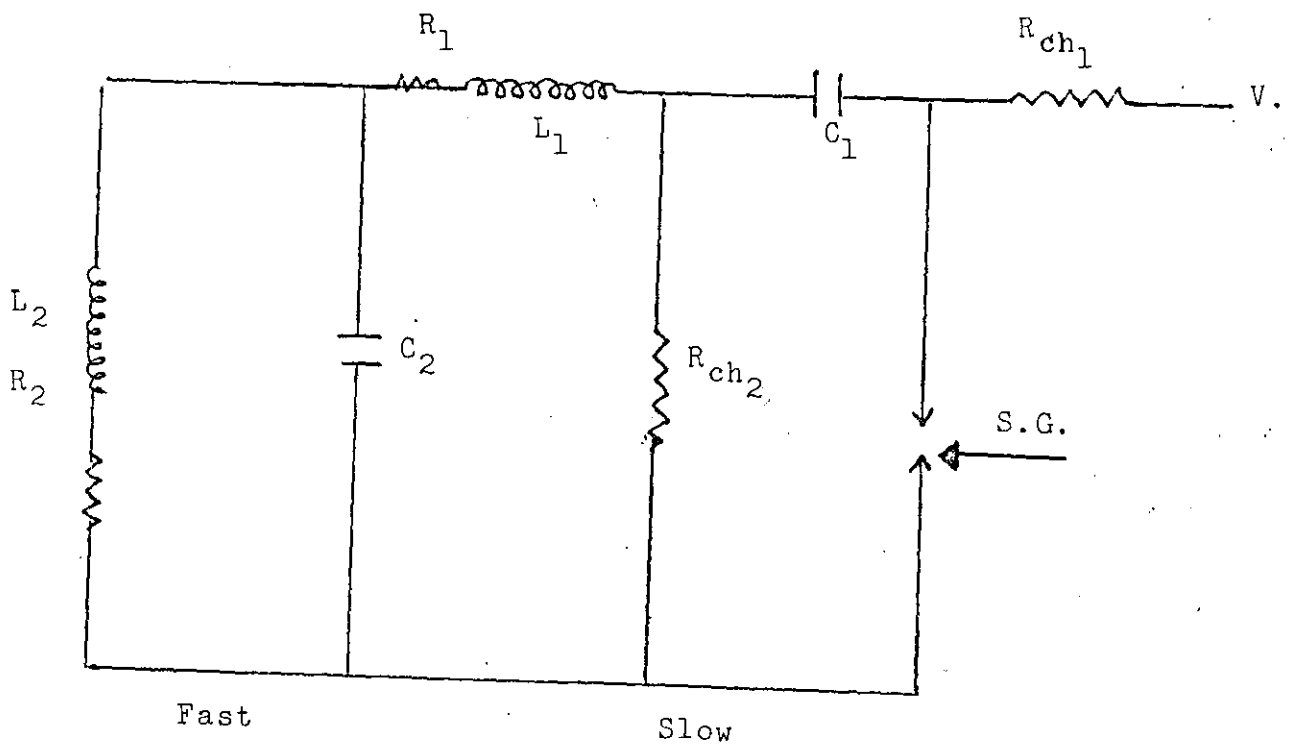


Fig. 7.1: The discharge circuit model

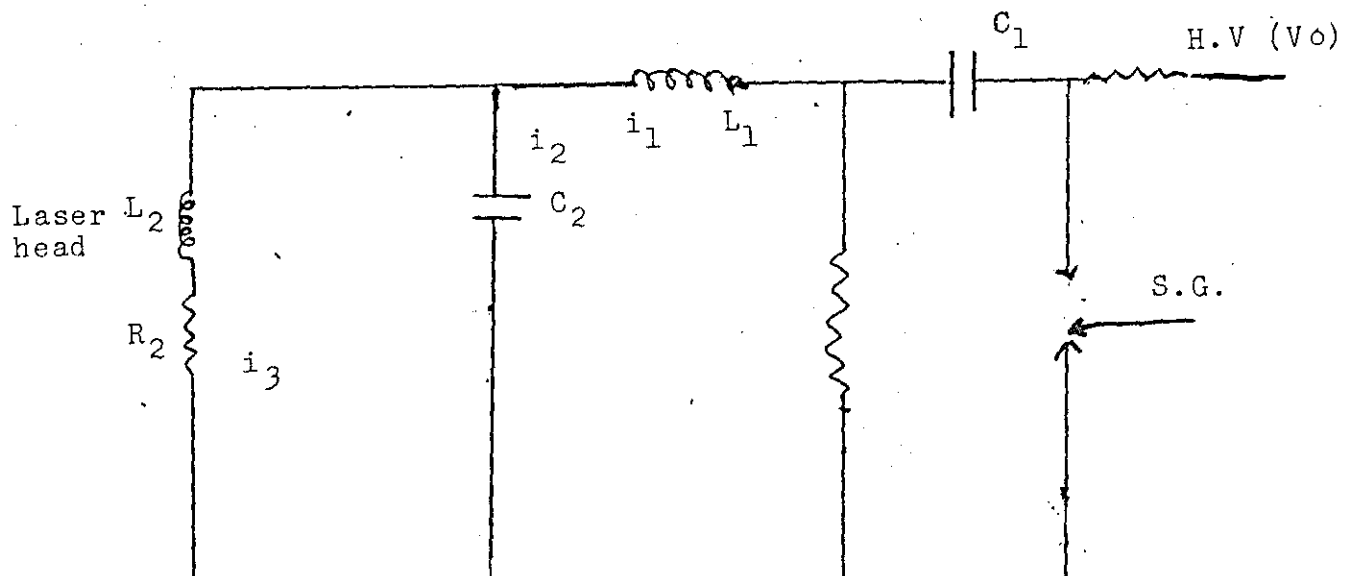


Fig. 7.2: The discharge circuit model without a preionizer resistance

The equations of this model can be written as:

$$V_o = \frac{1}{C_1} \int i_1 dt + L_1 di_1/dt + \frac{1}{C_2} \int i_2 dt \quad \text{Slow circuit} \quad (7.1)$$

$$\frac{1}{C_2} \int i_2 dt = L_2 di_3/dt = R_2 i_3 \quad \text{Fast circuit} \quad (7.2)$$

$$i_1 = i_2 + i_3 \quad (7.3)$$

Substitute (7.3) into (7.1), this will give:

$$V_o = \frac{1}{C_1} \int i_2 dt + \frac{1}{C_1} \int i_3 dt + L_1 di_2/dt + di_3/dt + \frac{1}{C_2} \int i_2 dt \quad (7.4)$$

$$V_o = \left(\frac{1}{C_1} + \frac{1}{C_2} \right) \int i_2 dt + \frac{1}{C_1} \int i_3 dt + L_1 di_2/dt + L_1 di_3/dt \quad (7.5)$$

From (7.2) and by differentiating twice, it becomes:

$$\frac{1}{C_2} di_2/dt = L_2 d^3 i_3/dt^3 + R_2 d^2 i_3/dt^2 \quad (7.6)$$

Substituting (7.6) in (7.5), equation 7.5 becomes

$$V_o = \frac{1}{C} (C_2 L_2 di_3/dt + R_2 C_2 i_3) + \frac{1}{C_1} \int i_3 dt + L_1 L_2 C_2 d^3 i_3/dt^3 +$$

$$L_1 C_2 R_2 d^2 i_3/dt + L_1 di_3/dt \quad (7.7)$$

$$\text{where } \frac{1}{C} = \frac{1}{C_1} + \frac{1}{C_2}$$

Applying Laplace-Transformer method, where \int changes to $\frac{1}{S}$, and

$\frac{d}{dt}$ changes to S . Thus equation (7.7) becomes:

$$\frac{V_o}{S} = \frac{C_2 L_2}{C} S i_3(S) + \frac{R_2 C_2}{C} i_3(S) + \frac{1}{C_1 S} i_3(S) + L_1 L_2 C_2 S^3 i_3(S) +$$

$$L_1 C_2 R_2 S^2 i_3(S) + L_1 S i_3(S) \quad (7.8)$$

or

$$\frac{V_o}{S} = i_3(S) \left(L_1 L_2 C_2 S^3 + L_1 C_2 R_2 S^2 + \frac{C_2 L_2}{C} S + L_1 S + \frac{1}{C_1 S} + \frac{R_2 C_2}{C} \right) \quad (7.9)$$

$$\frac{V_o}{s} = \frac{i_3(s)}{CC_1s} \left(L_1L_2C_2C_1C s^4 + L_1C_1C_2CR_2s^3 + C_2L_2C_1s^2 + L_1C_1Cs^2 + C + R_2C_2C_1s \right) \quad (7.10)$$

From this equation $i_3(s)$ can be written in the following form:

$$i_3(s) = \frac{V_o}{L_1L_2C_2} \frac{1}{s^4 + \frac{R_2}{L_2}s^2 + s^2 \frac{1}{L_1C} + \frac{1}{L_2C_2} + \frac{R_2s}{L_2L_1C} + \frac{1}{L_1L_2C_1C_2}} \quad (7.11)$$

$$\text{or } i_3(s) = \frac{V_o}{L_1L_2C_2} \frac{1}{(S+a)(S+b)(S+c)(S+d)}$$

$$i_3(s) = \frac{V_o}{L_1L_2C_2} \frac{1}{(S+a)(S+b)(S+c)} \cdot \frac{1}{(S+d)} \quad (7.12)$$

The use of Laplace Transform time table helped to transfer $i_3(s)$ to $i_3(t)$. Therefore equation (7.12) becomes:

$$i_3(t) = \frac{V_o}{L_1L_2C_2} \underbrace{\frac{e^{-at}}{(b-a)(c-a)} \frac{e^{-bt}}{(a-b)(c-b)} \frac{e^{-Kt}}{(a-c)(b-c)}}_{f_1(t)} \underbrace{e^{-d}}_{f_2(t)} \quad (7.13)$$

However, the use of $f_1(t)$, $f_2(t)$ convolution is necessary in which:

$$\int f_2(t-u) f_1(t) du = f_1 * f_2$$

By applying this rule to equation (7.13), the discharge circuit i_3 becomes:

$$i_3(t) = \frac{V_o}{L_1L_2C_2} \frac{e^{-dt} \frac{d(d-a)t - 1}{(b-a)(c-a)(d-a)} + \frac{e^{(d-b)t} - 1}{(a-b)(c-b)(d-b)} + \frac{e^{(d-e)t} - 1}{(d-c)(b-c)(a-c)}}{(7.14)}$$

The same method was used to calculate the discharge voltage. It was found that it has the following form:

$$V_2(t) = \frac{V_0}{L_1 C_2} e^{a_4 t} \frac{(a - a_1) (e^{t(a_4 - a_1)} - 1)}{(a_2 - a_1) (a_3 - a_1) (a_4 - a_1)} + \frac{(a - a_2) (e^{(a_4 - a_2)t} - 1)}{(a_1 - a_2) (a_3 - a_2) (a_4 - a_2)} + \frac{(a - a_3) (e^{t(a_4 - a_3)} - 1)}{(a_2 - a_3) (a_4 - a_3) (a_1 - a_3)} \quad (7.15)$$

where a , a_1 , a_2 , a_3 , a_4 , V_0 , L_1 , and C_2 are constants, and have the values of the electrical circuit.

The inductances L_1 , and L_2 were estimated using the following assumptions:

The inductance of the slow circuit L_1 was estimated using the picture of the discharge voltage which was taken by the scope Fig. 7.3.a. The voltage can be written as:

$$V = V_0 e^{(-R/2L_1)t} \cos wt \quad (7.16)$$

$$\text{where } W^2 = \frac{1}{L_1 c} - \left(\frac{R}{2L_1}\right)^2 \quad (7.16a)$$

For two peaks of the voltage form, the equation (7.16) becomes:

$$\frac{V_1}{V_2} = \frac{e^{-Rt_1/2L_1} + \cos wt_1}{e^{-Rt_2/2L_1} + \cos wt_2} = e^{-R/2L_1 (t_1 - t_2)}$$

But $\cos wt_1 = \cos wt_2 = 1$ at the peaks, and $t_2 - t_1 = \Delta t = \frac{1}{f} = \frac{2K}{W}$

$$\text{Therefore } \frac{V_1}{V_2} = e^{R/2L_1 (t_2 - t_1)} = \delta$$

$$\text{in which } \frac{V_1}{V_2} = \delta \quad (7.17)$$

practically V_1 and V_2 can be measured from the pictures and therefore $\frac{V_1}{V_2} = 1.4$, thus δ is calculated.

$$\text{From (7.16a), one can write } R = 2L_1 \left(\frac{1}{L_1 C} - W^2 \right)^{\frac{1}{2}} \quad (7.18)$$

Therefore $\delta = \frac{KR}{L_1 W}$, and hence using equation (7.18),

$$\delta = \frac{K}{L_1 W} \cdot 2L_1 \left(\frac{1}{L_1 C} - W^2 \right)^{\frac{1}{2}} \quad (7.19)$$

Or
$$\delta = \frac{\pi}{W} \left(\frac{1}{L_1 C} - W^2 \right)^{\frac{1}{2}}$$

Since $\Delta t = \frac{2\pi}{W}$, therefore equation (7.19) becomes

$$\delta = \Delta t \left(\frac{1}{L_1 C} - W^2 \right)^{\frac{1}{2}}$$

or the inductance L_1 becomes

$$L_1 = \frac{1}{C} \left(\frac{1}{\left(\frac{\delta}{\Delta t} \right)^2 + W^2} \right) \quad (7.20)$$

or
$$L_1 = \frac{1}{CW^2} \left(\frac{1}{1 + \left(\frac{\delta}{2\pi} \right)^2} \right) \quad (7.21)$$

Since $\left(\frac{\delta}{2\pi} \right)^2 \ll 1$, therefore $L_1 = \left(\frac{\Delta t}{2\pi} \right)^2 \cdot \frac{1}{C} \quad (7.22)$

From the picture, Δt is the time between two successive peaks and is $\Delta t = 240$ ns, and $C = 13.78$ nF, therefore

$$L_1 = 106 \text{ nh.}$$

The laser head inductance L_2 was estimated using equation (7.22), with $t = 75$ ns, $C = 17$ nF. The fast circuit voltage form is shown in Fig. 7.3.b. Thus the inductance L_2 is ≈ 9 nh.

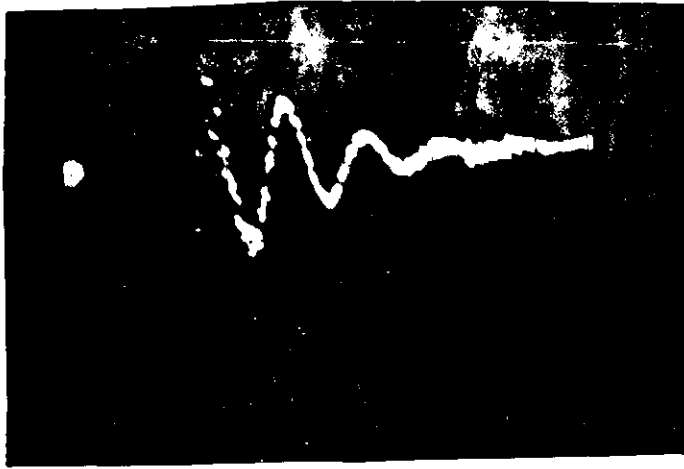


Fig. 7.3.a: A photograph of slow circuit voltage form
(0.2 s/div, 0.2c/div)

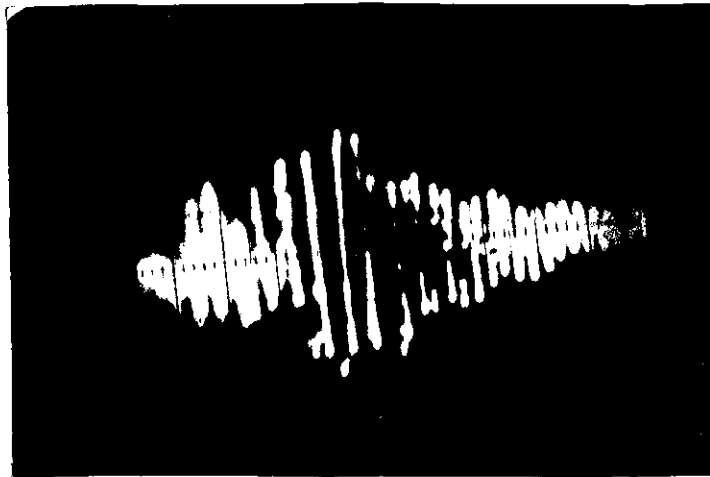
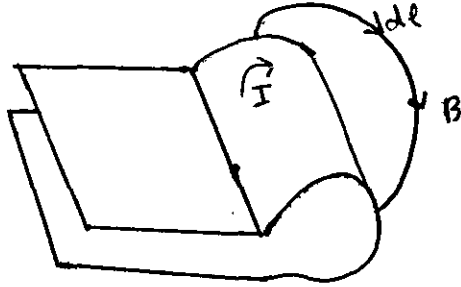


Fig. 7.3.b: A photograph of fast circuit voltage
(ringing voltage)
(0.2 s/div, 0.5v/div)

Theoretically, the laser head inductance was estimated as follows: the laser head is assumed to be a length of selenoid having one turn.



From Ampere's Law, the line integral of the B field around a closed loop enclosing the current I, satisfies the equation:

$$\oint \vec{B} \cdot d\vec{l} = \mu_0 I \quad (7.23)$$

Since the B field is concentrated inside the selenoid of length l , the field is given by the formula: (MKs units)

$$B \cdot l = \mu_0 I \quad (7.24)$$

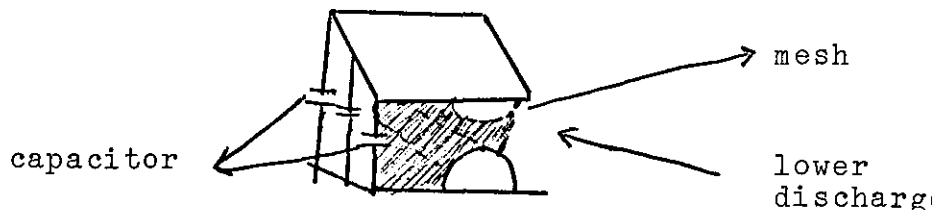
But the voltage (V), around a loop generated by a changing flux $\frac{d\phi}{dt}$ through the loop is:

$$V = d\phi/dt = A \frac{dB}{dt} = L \frac{dI}{dt} \quad (7.25)$$

According to Faraday's Law, where A is the loop area, L is defined as the inductance. Combining (7.24) and (7.25) the inductance then is given by the formula:

$$L = \mu_0 A/l \quad (7.26)$$

To estimate A, l , we look at the laser geometry:



The length of the electrodes was 74 cm, and the selenoid area (shown shaded) was of the order of 60 cm^2 . Substitute into (7.26) gives an inductance of 10 nh.

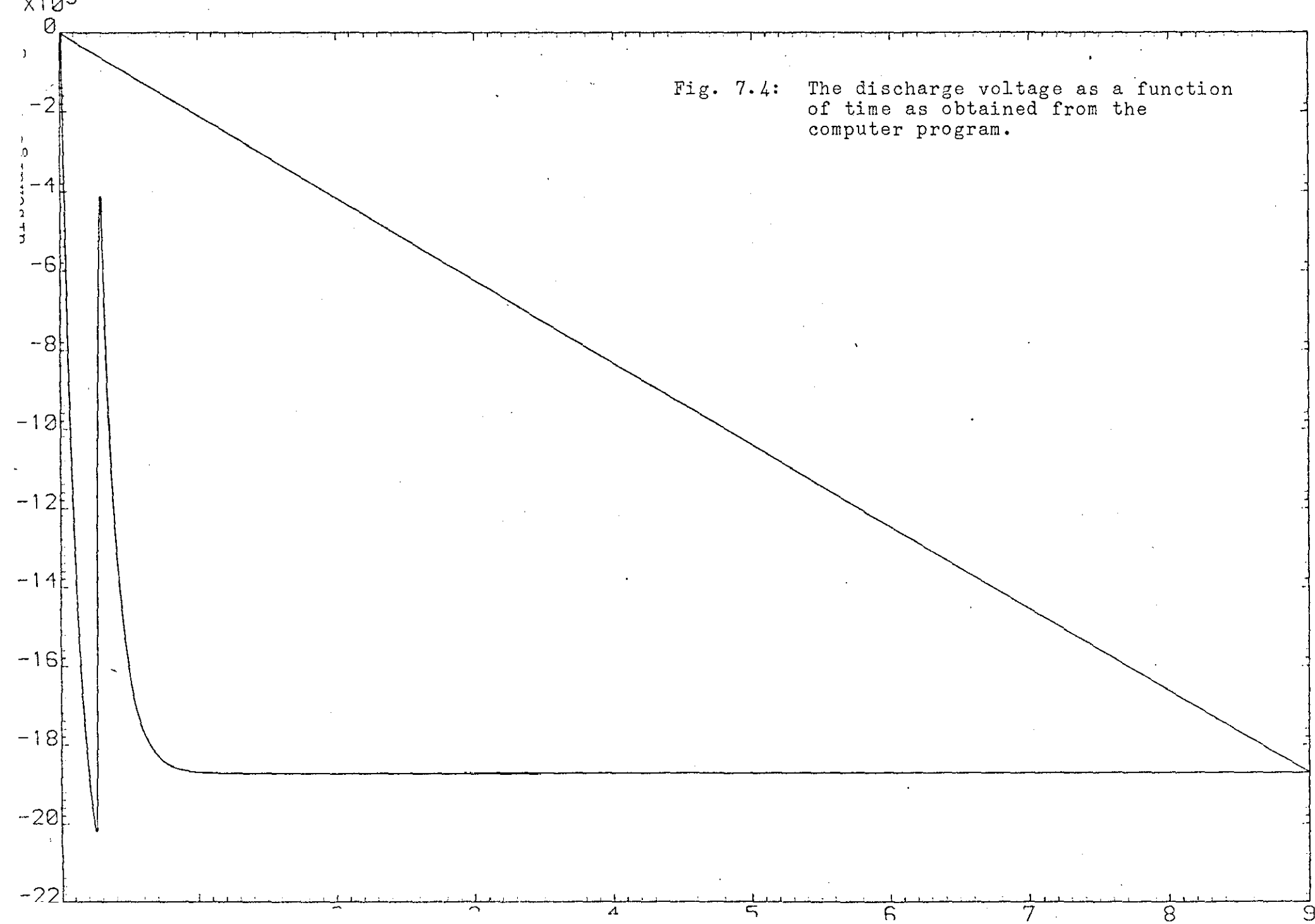
The values of L_1 and L_2 were used in a computer program in order to calculate the voltage discharge. Fig. 7.4 shows the results which were obtained from the computer. Since a negative voltage appears on the preionizer electrode, and as soon as the preionizer gap breaks down, the voltage between the electrodes increase (discharge voltage) up to a point at which the main discharge starts. Then the voltage drops down to a minimum value which was determined by the circuit constant.

The fast circuit voltage (ringing voltage) was also calculated from another computer program as a function of the peaking capacitors and the circuit inductance. Fig. 7.5.a,b. shows the results.

It is clear from the figure that the peak of the voltage decreases as the peaking capacitors increased which agrees with the practical results which were obtained in section 6.3.2, and led to a higher output energy.

The effect of the circuit inductance L_1 on the ringing voltage was also studied using the computer program, and the results are shown in Fig. 7.5.c,d. It is clear that as the inductance increased the ringing voltage of the fast circuit was slower, which may have led to frequent arcs.

Fig. 7.4: The discharge voltage as a function of time as obtained from the computer program.



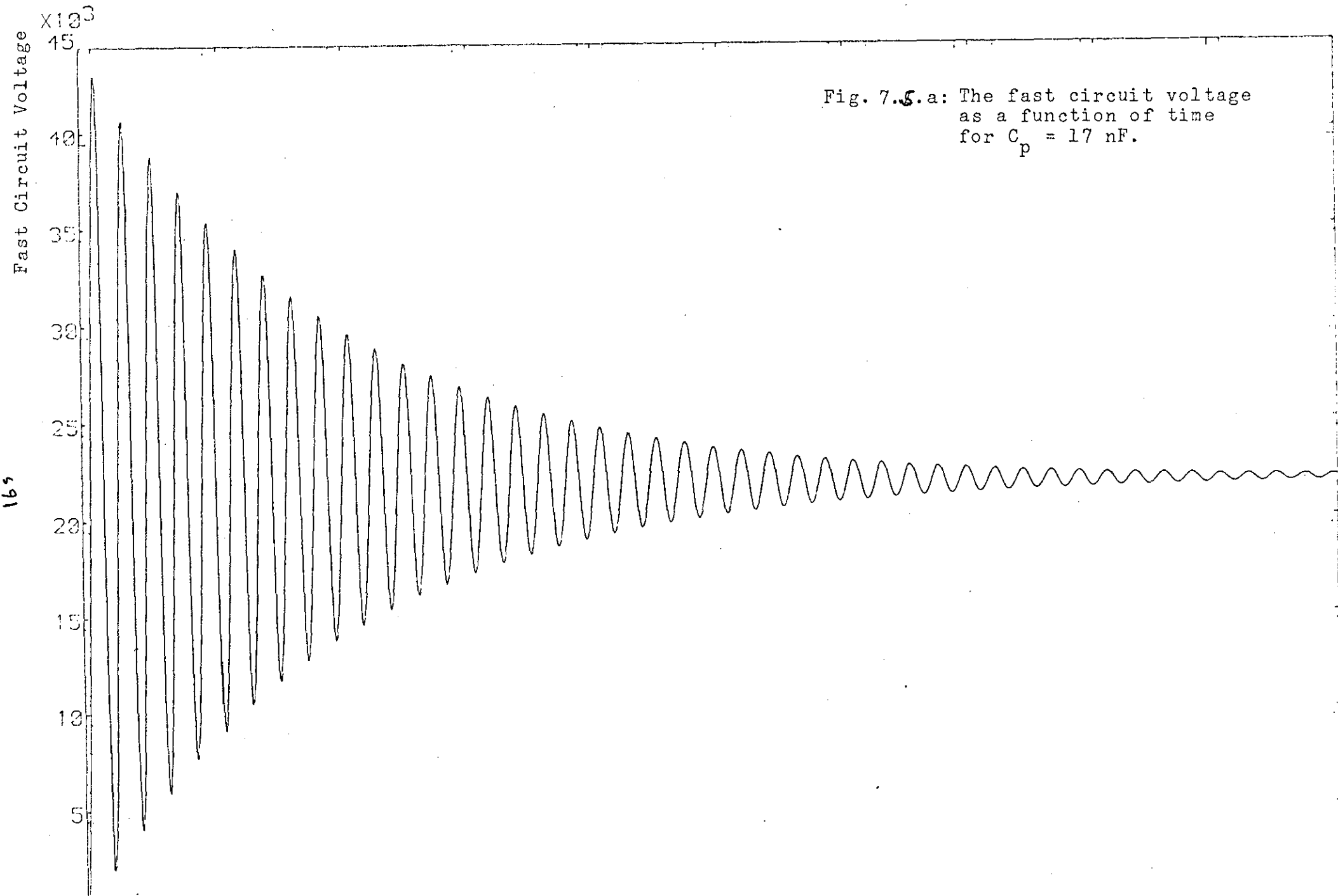


Fig. 7.5.a: The fast circuit voltage as a function of time for $C_p = 17$ nF.

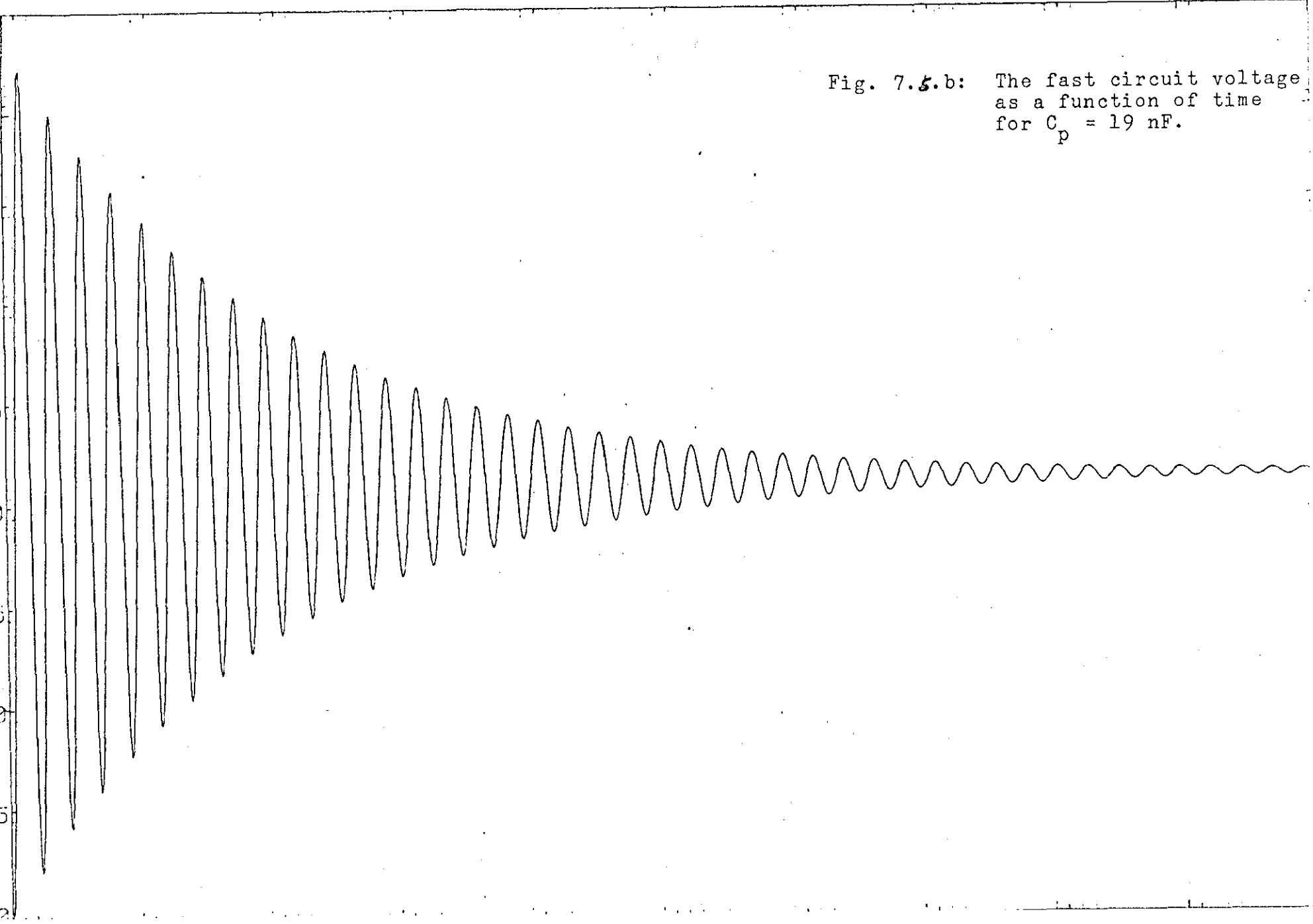
X10³
45

Fast Circuit Voltage

Fig. 7.5.b: The fast circuit voltage as a function of time for $C_p = 19$ nF.

166

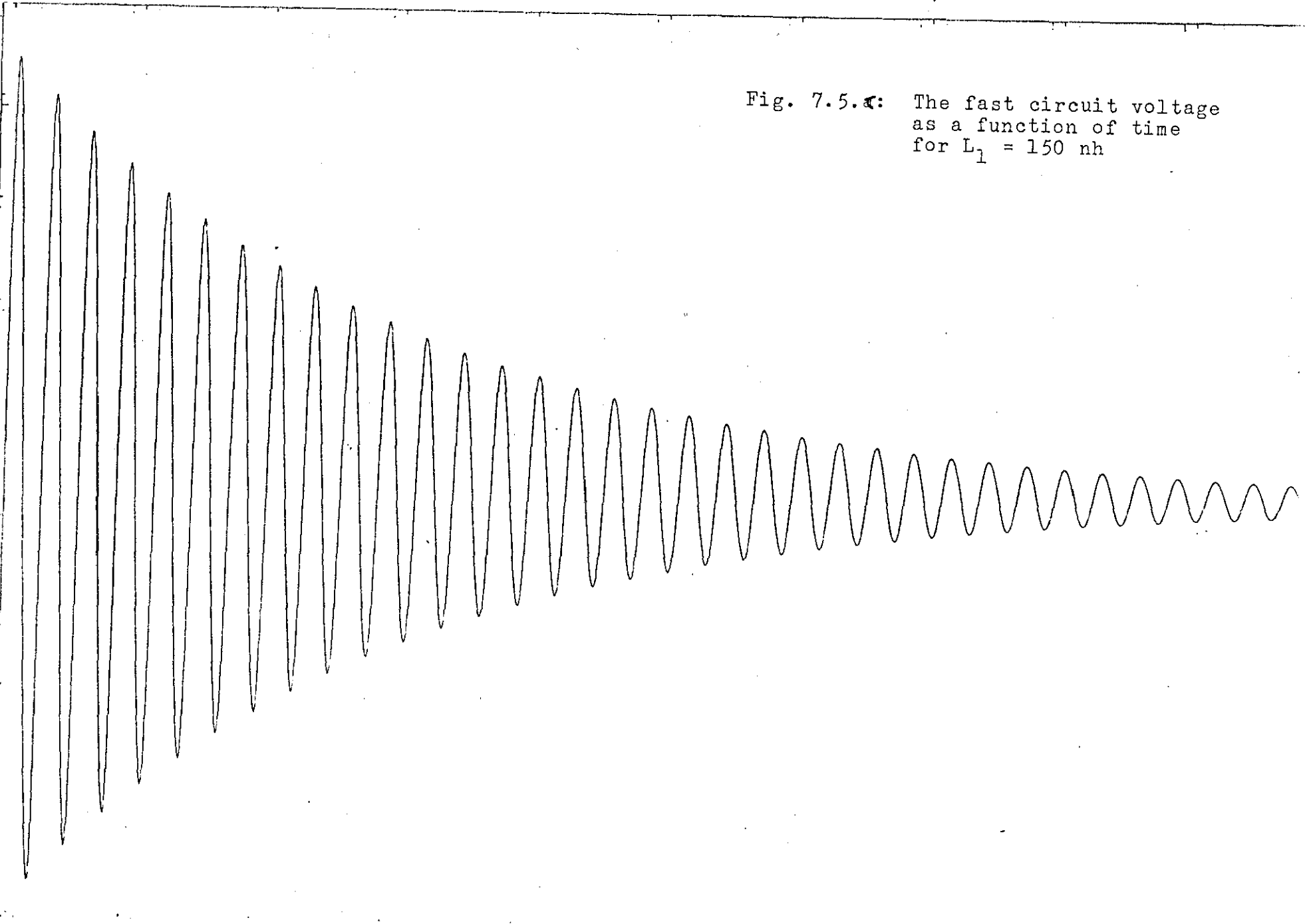
40
35
30
25
20
15
10
5
0



X10⁻⁴
45

Fast Circuit Voltage
40
35
30
25
20
15
10
5
0

Fig. 7.5.4: The fast circuit voltage as a function of time for $L_1 = 150$ nh



Fast Circuit Voltage

45
40
35
30
25
20
15
10
5

168

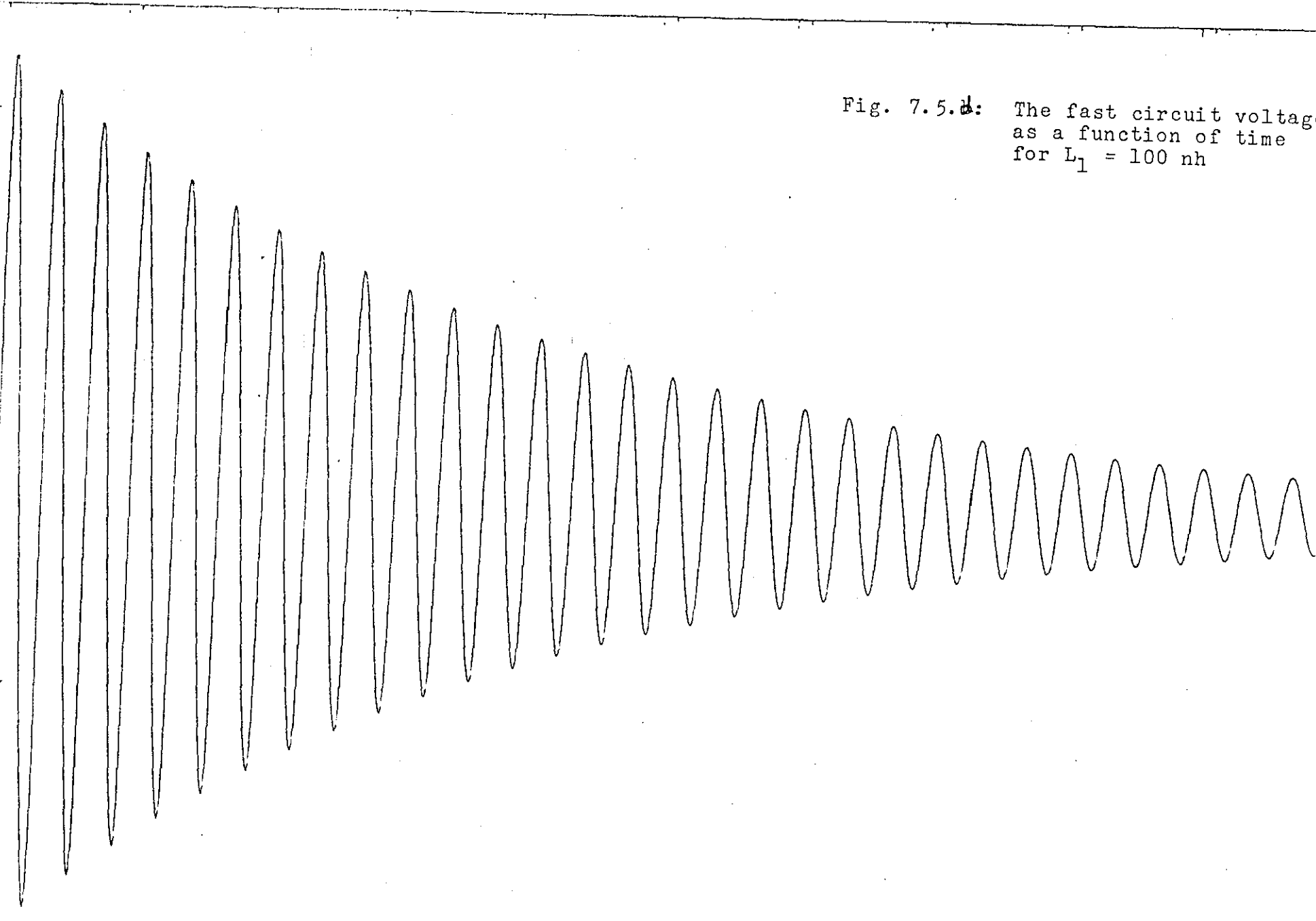


Fig. 7.5.d: The fast circuit voltage as a function of time for $L_1 = 100$ nh

LUGHBOROUGH UNIVERSITY COMPUTER CENTRE GEORGE 2L MK4F STREAM B

RUN ON 04/09/81 AT 13:58

```

JOB THREE.IT,PHRS,YN7848
JOBTIME 250
FORTRAN ,.PDS
DOWN 22
JOBCONF 4AK
VOL 1000
RUN
****

```

FORTRAN COMPILATION BY JXFAT MK AC DATE 04/09/81 TIME 13:58/24

```

0001 SEND TO (ED,SEMCOMPUSER,AXXX)
0002 DUMP ON (ED,PROGRAM USER)
0003 WORK (ED,WORKFILEUSER)
0004 RUN
0005
0006 LIBRARY(ED,SUBGROUPPAGE)
0007 LIBRARY(ED,SUBGROUPG1NO)
0008 PROGRAM(SPCH)
0009 COMPACT
0010 COMPRESSINTEGERANDLOGICAL
0011 INPUT 1=CR0
0012 OUTPUT 2=LPO
0013 TRACE 2
0014 END

```

```

0015 MASTER POL
0016 DIMENSION A(10),R(10),AI(10)
0017 DIMENSION X(1000),Y1(1000),Y2(1000)
0018 COMPLEX Y(1000)
0019 COMPLEX A1,A2,A3,A4,EX,XXX
0020 REAL L1,L2
0021 T=1E-9
0022 C1=50E-9
0023 C2=17E-9
0024 L2=13E-9
0025 C=67E-9
0026 R2=0.2
0027 V0=30000
0028 L1=100E-9
0029 A0=(L1*L2)
0030 AA=V0/(A0*C2)
0031 A(1)=1
0032 A(2)=(R2/L2)
0033 A(3)=(1/(L1*C)+1/(L2*C2))
0034 A(4)=(R2/(1+L2*C))
0035 A(5)=1/(1+L2*C1+C2)
0036 P=0.1
0037 PI=P*X01AAF(P)
0038 TOL=X02AAF(PI)
0039 IFAIL=0
0040 CALL C02AFF(A,5,R,AI,TOL,IFAIL)

```

```

0041 WRITE(2,1)IFAIL
0042 1 FORMAT(1H,15)
0043 DO 3 I=1,5
0044 WRITE(2,2)(R(I),AI(I))
0045 2 FORMAT(1H,2(F20.5,4X))
0046 3 CONTINUE
0047 A1=-CMPLX(R(1),AI(1))
0048 A2=-CMPLX(R(2),AI(2))
0049 A3=-CMPLX(R(3),AI(3))
0050 A4=-CMPLX(R(4),AI(4))
0051 DO 5 I=1,1000
0052 X(I)=1
0053 Y(I)=((EX*(-(A4-A1)+(I-1)*T))-1)/((A2-A1)*(A3-A1)*(A4-A1))
0054 Y(I)=Y(I)+((EX*(-(A4-A2)+(I-1)*T))-1)/((A3-A2)*(A1-A2)*(A4-A2))
0055 Y(I)=Y(I)+((EX*(-(A4-A3)+(I-1)*T))-1)/((A1-A3)*(A2-A3)*(A4-A3))
0056 Y(I)=(AA)*Y(I)*EX(-A4*(I-1)*T)
0057 Y1(I)=REAL(Y(I))
0058 Y2(I)=AIMAG(Y(I))
0059 5 CONTINUE
0060 CALL LP120
0061 CALL GRAF(X,Y1,1000,0)
0062 CALL PICCLE
0063 CALL GRAF(X,Y2,1000,0)
0064 CALL DEVFND
0065 STOP
0066 END

```

Chapter 8

CONCLUSIONS AND RECOMMENDATION

8.1 Conclusions

A study of the use of the double discharge technique as a method for excitation of CO_2 , N_2 , and excimer lasers has been made. The results have been applied to:

- (a) Carbon-dioxide laser
- (b) Nitrogen laser

The results indicated that in the case of the CO_2 laser, the energy output increased with increase in helium flow rate in the mixture and reached a peak of around 930 mJ corresponding to a helium volumetric fraction of 0.8. The output energy also increased with an increase in the nitrogen flow rate and reached a peak of 1 J corresponding to nitrogen volumetric fraction of 0.48. When the laser was operated without nitrogen, the output energy decreased by a factor of a half. These results were in agreement with the previous materials which have been reported. The behaviour of the discharge was improved when the peaking capacitors were placed across the electrodes. The energy output reached the peak of 1.45 J when the ratio of peaking to main capacitors was 1 : 3, and when the delay time between the pre-ionization and the main discharge was optimized of the order of 100 ns. The behaviour of the discharge and variation of the output energy of CO_2 laser have been investigated as a function of the preionizer arc length, electrodes separation, and charging voltage. The output energy reached the peak of 1.5 J corresponding to an arc length of 6 mm. This result has not been reported before.

The output energy of the N_2 laser was studied as a function of the N_2 flow rate. It was found that the energy reached the peak of 2.8 mJ corresponding to N_2 flow rate of 40 - 60 cc/min. The pulse shape of a CO_2 laser was measured as a function of CO_2 , and N_2 volumetric fraction (ϕ, N). It was found that at lower 0.33, the pulse duration was longer. No tail on the pulse shape

was present when the CO_2 laser was operated without N_2 in the mixture due to pure excitation.

A survey of the various excitation methods of CO_2 , N_2 , and rare gas halide excimer lasers, some of their applications were also made with published materials.

8.2 Recommendation for further work:

The present work has demonstrated the principles of double discharge laser operation.

1. It was not easy to optimize the delay time between the pre-ionizer and main discharge by changing the preionizer gap, therefore more investigation should be carried out in this field.
2. Further work should be carried out by using more than one preionizer electrode (saw blade) in order to achieve an efficient preionization effect.
3. Further investigations for materials which have a high resistance for operating rare gas fluoride excimer lasers.

Appendix 1

The solution of the population densities equations on page 65 . One can write the sum of eqs. (3.4) and (3.5) in Section (3.6) as:

$$(d/dt)(N_2 + N_3) = X_{13}N_1 \quad (1.1)$$

which can be readily integrated to yield:

$$N_3 + N_2 = X_{13}N_1 t \quad (1.2)$$

Here it is assumed that N_1 and the pumping rates are constants. Equations (1.2) and (3.3) modified according to conditions stated in Section (3.6) will be:

$$dN_3/dt = X_{13}N_1 + (X_{13}N_1 t - N_3)X_{23} - \beta N_3 \quad (1.3)$$

where

$$\beta = (\tau_{32}^{-1} + Y_{32})$$

Equation (1.3) can be reformulated as:

$$\frac{dN_3}{dt} + \alpha N_3 = X_{13}N_1 + X_{13}N_1 t + X_{13}X_{23}N_1 t \quad (1.4)$$

where

$$\alpha = (\beta + X_{23})$$

$$\text{or } (D + \alpha)N_3 = X_{13}N_1 + X_{13}X_{23}N_1 t \quad (1.5)$$

The solution of equation (1.5) is:

$$N_3 = N_3' + N_3''; \quad \text{where } N_3' = \text{General solution and} \\ N_3'' = \text{Particular solution.}$$

$$\text{The General solution } N_3' = Ke^{-\alpha t} \quad (\text{from } (D + \alpha)N_3 = 0) \quad (1.6)$$

where K is a constant to be evaluated from the boundary condition stated in Section (3.6):

$$K = - (N_1 X_{13} \alpha^{-2}) (Y_{32} + \tau_{32}^{-1}) \quad (1.7)$$

the particular solution is:

$$\begin{aligned}
 N_3'' &= \frac{(D/\alpha + 1)^{-1}}{\alpha} (X_{13}N_1 + X_{13}N_1 + X_{13}X_{23}N_1t) \\
 &= \frac{1}{\alpha} (1 - D/\alpha + D^2/\alpha^2 + \dots)(X_{13} + X_{13}X_{23}N_1t) \\
 &= \frac{1}{\alpha} (X_{13}N_1 + X_{13}X_{23}N_1t - 0 - \frac{X_{13}X_{23}N_1}{\alpha} + 0 \dots) \\
 &= \frac{X_{13}N_1}{\alpha} + \frac{X_{13}X_{23}N_1t}{\alpha} - \frac{X_{13}X_{23}N_1}{\alpha^2} \\
 &= \frac{\alpha X_{13}N_1 + \alpha X_{13}X_{23}N_1t - X_{13}X_{23}N_1}{\alpha^2} \\
 &= \frac{\beta X_{13}N_1 + X_{13}X_{23}N_1 + \alpha X_{13}X_{23}N_1t - X_{13}X_{23}N_1}{\alpha^2} \\
 &= \frac{\beta X_{13}N_1}{\alpha^2} + \frac{X_{13}X_{23}N_1t}{\alpha}
 \end{aligned}$$

Therefore

$$N_3 = \frac{\beta X_{13}N_1}{\alpha^2} + \frac{X_{13}X_{23}N_1t}{\alpha} + Ke^{-\alpha t} \quad (1.8)$$

For small times one can expand $e^{-\alpha t}$ up to terms in t^2 as

$$e^{-\alpha t} = (1 - \alpha t + \frac{\alpha^2 t^2}{2!} \dots)$$

$$\therefore Ke^{-\alpha t} = -\frac{\beta N_1 X_{13}}{\alpha^2} + \frac{\beta X_{13}N_1t}{\alpha} - \frac{\beta N_1 X_{13}t^2}{2} \quad (1.9)$$

Substituting (1.9) in (1.8) as:

$$\begin{aligned}
 N_3 &= \frac{\beta X_{13}N_1}{\alpha^2} + \frac{X_{13}X_{23}N_1t}{\alpha} - \frac{\beta N_1 X_{13}}{\alpha^2} + \frac{\beta X_{13}N_1t}{\alpha} - \frac{\beta N_1 X_{13}t^2}{2} \\
 &= X_{13}N_1t \frac{(X_{23} + \beta)}{\alpha} - \frac{\beta N_1 X_{13}t^2}{2} \\
 &= X_{13}N_1t - S_{13}N_1 (Y_{32} + \frac{-1}{32}) t^2/2 \quad (1.10)
 \end{aligned}$$

Equations (1.10) and (1.2) yield:

REFERENCES:

- ALLAN, R., "Laser in the factory", IEEE spec., 42-49, May 1979.
- AULT, E.R., BRADFORD, R.S.Jr., BHAUMIK, M.L.: Appl. Phys. Lett. 27, 413 (1975).
- ALI, A.W., KOLB, A.C., and ANDERSON, A.D., Appl. Opt., 6, 2115-2119, 1967.
- ANDREWS, A.J., KEARSLEY, A.J., WEBB, C.E.,: Opt. Commun. 20 265 (1977).
- BABCOCK, R.V., LIBERMAN, I., PARTLOW, W.D.,: IEEE J. QE-12, 29 (1976).
- BASTING, D., SCHAFER, F.P., and STEYER, B., Opto. Elec., 4, 43-49, 1972.
- BEAULIEN, A.J., Appl. Phys. Letts., 16, 504-505, 1970.
- BERGMAN, E., Rev. Sci. Inst. 48, 545-46, 1977.
- BASOV, N.G., DANILYCHEV, V.A. and POPOV, Y.M., Sov. J. Quantum Electron. 1, 18 (1971).
- BENNETT, R.G., DALBY, F.W., J. of Chem. Phys. 31, 434-441 (1959).
- BHAUMIK, M.L., BRADFORD, R.S. JR., AULT, E.R.: Appl. Phys. Lett. 28, 23 (1976).
- BRAU, C.A., in Excimer Lasers, Topics in Appl. Phys. Vol. 30, ed. by C.K. Rhodes, Springer Verlag, Berlin, 1979.
- BRAU, C.A., and EWING, J.J., Appl. Phys. Lett. 27, 435 (1975).
- BURNHAM, R., POWEEL, F.X., DJEU, N.,: Appl. Phys. Lett. 29, 39 (1976).
- BURNHAM, R., DJEU, N.,: Appl. Phys. Lett. 29, 707 (1976).
- BURNHAM, R., HARRIS, N.W., DJEU, N.,: Appl. Phys. Lett. 28, 86 (1976).
- BURNHAM, R., EDEN, G., and DJEU, N., IEEE Spectrum, April, 50-59, 1979.

- BUGAEV, S.P., MESYATS, G.A., PROSKUROVSKII, D.I.,: Sov Phys. -
Dolk. 14, 605 (1969).
- CHEO, P.K., J. Appl. Phys. 38, 3567-681, 1967.
- CHRISTIANSEN, W.H., and HERTZBERG, A., "Gas dynamic lasers and
photon machines", proc. IEEE, 61, 1060, 1973.
- DEMANIA, A.J., proc. IEEE, 61, 731-48, 1973.
- DJEU, N., BURNHAM, R.,: Appl. Phys. Lett. 30, 473 (1977).
- DUMANCHIN, R., and ROCCA-SERRA, C.R. Acad. Sci. Paris B.
269, 916-17m 1969.
- DYER, P.E., J. phys. E. Sci. Inst. 11, 1094, 1978.
- EWING, J.J., BRAU, C.A.,: Appl. Phys. Lett. 27, 350 (1975).
- FORTIN, R., and GRAVEL, M., Con. J. phys. 49, 1783-93, 1971.
- FOX, A.G., and LI, T., Proc. IEEE, 51, 80-89, 1963.
- GELLER, M., ALTMAN, D.E., and DETENPLE, T.A., J. Appl. phys.,
37, 3639-3640, 1966.
- GERRY, E.T., Appl. Phys. Let., 7, 6-8 (1965).
- GREEN, J.M., Optics and Laser Technology, Dec. 1978.
- HARRY, J.E., "Industrial Lasers and their Applications".
McGraw-Hill, London, 1974.
- HARTMANN, B., and KLEMAN, B., Con. J. phys., 44, 1609-12, 1966.
- HERZBERG, G.H., "Spectra of diatomic molecules".
Van Nostrand, Princetown, N.J. 1963.
- HERZBERG, G.H. "Molecular spectra and molecular structure.
1- Spectra of diatomic molecules", second edition.
Van Nostrand Reinhold Co., New York (1950).
- HILL, A.E., Appl. phys. letts. 18, (5), 194-97, 1971.
- HOFF, P.W., SWINGLE, J.C., and RHODES, C.K.,: Appl. Phys. Lett.
23, 245 (1973).

- HOFFMAN, J.M., HAYS, A.K., TISONE, G.C.,: Appl. Phys. Lett. 28, 538 (1976).
- HOCKER, L.O., KOVACS, M.A., RHODES, C.K., FLYNN, G.W. and JARAN, A.,: Phys. Rev. Lett. 17 (8), 233-35, 1966.
- HOUTERMANS, F.G., Helv. Phys. Acta 33, 933 (1960).
- HUGHES, N.M., SHANNON, J.S. and HUNTER, R., Appl. Phys. Lett. 24, 448 (1974).
- HUNTER, R.O., OLDENETTEL, J., HOWTON, C., McCUSKER, M.V., J. Appl. Phys. 49, 549 (1978).
- HUTCHINSON, M.H.R., App. phys. 21, 95-114, 1980.
- JOHNSON, P.C., IEEE J. Quan. Elec., QE-7(5), 185-89, 1971.
- KOGEŁNIK, H., and LI, T., Appl. Opts., 5(10), 1550-67, 1966.
- KOHLER, H.A., FERDERBER, L.J., REDHEAD, D.L., and EBERT, P.J., Appl. Phys. Lett. 21, 198 (1972).
- KRUPKE, W.F., GEORGE, E.V., and HAAS, R.A., Laser Handbook Vol. 3, p. 627, North-Holland, Amsterdam (1979).
- KURWEG, L., EGBERT, G.T., and BURNS, D.J., J. of Chem. Phys. 59, No. 5, 2641-2645 (1973).
- LAFLAMME, A.K., Rev. Sci. Inst. 41(11), 1578-61, 1970.
- LAMBERTON, H.M., and PEARSON, P.R., Electr. Letts. 7, 141-42, 1971.
- LANGMUIR, I., Phys. Rev. vol. 11-6, 455 (1913).
- LAWRINE, K.A., and HALE, M.H., IEEE J. Quan, Elec., QE-6, 530-31, 1971.
- LEGLER, W., Z-Physik, 173, 169-183 (1963).
- LENGEL, B.A., "Lasers". John Wiley, 1971.
- LEONARD, D.A., Laser focus, February, 26-32 (1967).
- LEONARD, D.A., Appl. Phys. Letts., 7, 4-6, (1965).

- LIVINGSTONE, M.S., BLEWETT, J.P.,: Particle Accelerators,
(McGraw-Hill, New York 1962).
- LOCKE, E.V., and HELLA, R.A., IEEE J. Quan. Elect., QE-10(2),
179-85, 1974.
- LOREE, T.R., SZE, R.C., BARKER, D.L.,: Appl. Phys. Lett. 31,
37 (1977).
- LORENTS, D.C.,: Physica 82c, 19 (1976).
- MAIMAN, T.H., Nature 187, 493 (1960).
- MATHIAS, E.S., and PARKER, J.T., Appl. Phys. Letts., 3,
16-18, (1963).
- McFARLANE, R.A., Phys. Rev., 140, A1070-A1071, (1965).
- McKEE, T.J., STOICHEFF, B.P., WALLACE, S.C., Appl. Phys. Letts.
30, 278-80, 1977.
- McKEE, T.J., et al, IEEE J. QE-15, 332, 1979.
- MAELLER, G., and RIGDEN, J.D., Appl. phys. letts., 7(10).
274-76, 1965.
- MOORE, C.B., WOOD, R.E., and YARDLEY, T.J., J. Chem. phys.,
46(11), 4222-31, 1967.
- NIGHAN, W.L., Phys. Rev, A (5), 1989-2000, 1970.
- NIGHAN, W.L., and WIEGAND, W.J., Appl. phys. letts., 25(11),
633-36, 1974.
- NICHOLLS, R.W., Ann. Geophys. T20, face 2, 144-181 (1964).
- PARKS, J.A., in: High Power Lasers and Applications
(Ed. by K.L. Kompa and H. Walther) Springer Verlag,
Berlin, 1978, p. 37.
- PATEL, C.K.N., Phys. Rev. Letts., 12(25), 588-90, 1964 a.
- PATEL, C.K.N., Phys. Rev. Letts., 136A, 1187-91, 1964 b.
- PATEL, C.K.N., Phys. Rev. Letts., 13(23), 617-19, 1964 c.

- PATEL, C.K.N., Appl. phys. Letts., 7(1), 115-17, 1965.
- PEARSE, R.W.B., GAYDON, A.G., "The identification of molecular spectra", second edition. Chapman and Hall Ltd., London (1950).
- PEARSON, P.R., and LAMBERTON, H.M., IEEE J. Quan. Elec., QE-8, 145-49, 1972.
- POLANYI, J.C., J. Chem. Phys., 34, 347-48, 1961.
- ROBINSON, A.M., IEEE J. Quan. Elec., QE-7, 199-200, 1971.
- READY, J.F., "Industrial application of Lasers", Academic Press, 1978.
- RICHARDSON, M.C., ALCOCK, A.J., LEOPOLD, K., and BYRTY, N.P., IEEE J. Quan. Elec., QE-912, 236-43, 1973.
- ROKNI, M., MANGANO, J.A., JACOB, J.H., and HSIA, J.C., IEEE J. of Quantum Electron. QE-14, 464 (1978).
- ROKNI, M., JACOB, J.H., MANGANO, J.A.,: Phys. Rev. A16, 2216 (1977).
- SALEH, S.N., Ph.D. Thesis, Loughborough University, 1981.
- SARJEANT, W.J., ALCOCK, A.J., LEOPOLD, K.E.,: IEEE J. QE-14, 177 (1978).
- SCHWARTZ, R.N., SLAVESKY, Z.I., and HERZFELDT, K.F., J. Chem. Phys., 20(10), 1591-99, 1952.
- SEARLES, S.K., and HART, G.A., Appl. Phys. Lett. 27, 350 (1975).
- SHIPMAN, J.D., and KOLB, A.C., IEEE J. Quantum Electron. QE-2, 298, (1966).
- SHIPMAN, J.D., Appl. Phys. Letts., 10, No. 1, 3-4, (1967).
- SMALL, J.G., and ASHARI, R., Rev. Sci. Inst., 43, 1205-1206, (1972).
- SUTTON, D.G., SUCHARD, S.N., GIBB, O.L., WANG, C.P.,: Appl. Phys. Lett. 28, 522 (1976).
- SZE, R.C., SCOTT, P.B., J. Appl. Phys. 47, 5492 (1976).

- SARJEANT, W.J., ALCOCK, A.J., LEOPOLD, K.E.: Appl. Phys. Lett. 30, 635 (1977).
- SZE, R.C., LORE, T.R., IEEE J. Quant. Electr. QE-14 944 (1978).
- TALLMAN, C.R., Los Alamos Labs., LA-UR, 79:1630, Excimer Laser meeting of Optical Society of America.
- Triggered spark gap application notes, EC eG.
- TYTE, D.C., and NICHOLLS, R.W., University of Western Ontario, Ontario.
- VELAZCO, J.E., and SETZER, D.W., J. Chem. Phys. 62, 1990 (1975).
- WANG, C.P., Appl. Phys. Lett. 29, 103 (1976).
- WILKINSON, P.G., J. of Chem. Phys. 30, No. 3, 773-776 (1959).
- YARIV, A., and GORDON, J.P., "The Laser", Procs. IEEE, 51 (Jan), 4-29, 1963.
- YARIV, A., "Quantum electronics", John Willey, 1967.
- YOUNG, R.A., J. Chem. Phys. 40, 1848-1853, 1964.

